FINAL TECHNICAL REPORT

Project A-1164

TECHNIQUES FOR GENERATING GUIDANCE SIGNALS FROM BODY-FIXED SENSORS

L. D. HOLLAND AND R. D. WETHERINGTON

Contract DAAH01-69-C-1390

9 February 1971

Prepared for
Systems Dynamics Branch
Advanced Sensors Laboratory
Research and Engineering Directorate
U. S. Army Missile Command
Redstone Arsenal, Alabama

Engineering Experiment Station
GEORGIA INSTITUTE OF TECHNOLOGY
Atlanta, Georgia

GEORGIA INSTITUTE OF TECHNOLOGY
Engineering Experiment Station
Atlanta, Georgia

FINAL TECHNICAL REPORT

PROJECT A-1164

TECHNIQUES FOR GENERATING GUIDANCE SIGNALS FROM BODY-FIXED SENSORS

By

L. D. HOLLAND AND R. D. WETHERINGTON

CONTRACT DAAH01-69-C-1390

9 February 1971

Prepared For

SYSTEMS DYNAMICS BRANCH
ADVANCED SENSORS LABORATORY
RESEARCH AND ENGINEERING DIRECTORATE
U. S. ARMY MISSILE COMMAND
REDSTONE ARSENAL, ALABAMA

FOREWORD

This report was prepared by the Electronics Division of the Georgia Institute of Technology under Contract DAAH01-69-C-1390. The work described was performed under the general supervision of D. W. Robertson, Head, Communications Branch, and R. D. Wetherington, Project Director. The authors are L. D. Holland and R. D. Wetherington. The contributions of J. L. Birchfield and G. W. Spann to the project are acknowledged. Overall technical guidance was provided by R. H. Farmer of the Advanced Sensors Laboratory.

ABSTRACT

The feasibility of using a relatively simple guidance technique and a strapdown sensor for guidance of a small tactical missile has been investigated. The principal method investigated was Dynamic Lead Guidance (DLG). Theoretical analyses were carried out to determine workable system parameters, to determine the required sensor characteristics, and to investigate the performance of DLG for sampled data input. Simulation runs were used to examine the dependence of system performance on the sensor characteristics, sampled data operation, cross-feed between channels, gyro gain, and gravity bias. Both constant velocity and maneuvering targets were simulated.

Dynamic Lead Guidance was found to be a practical technique provided a strapdown sensor with the proper characteristics can be developed.

TABLE OF CONTENTS

LIST OF FIGURES

LIST OF FIGURES (Continued)

LIST OF FIGURES (Continued)

LIST OF TABLES

I. INTRODUCTION

This report describes the results of the second phase of an investigation of the use of strapdown seekers for missile guidance. The first phase of the program dealt specifically with air-intercept type missiles and linear sensors used in conjunction with proportional navigation. In that phase of the program two methods were found for implementing a proportional navigation system using a strapdown sensor. One of these required a sensor that had a steerable beam, as available in such sensors as inertialess scan radars. Such a system would closely approximate the performance of a system using a gimbaled seeker with the major difference being that the beam would be electronically steered rather than mechanically steered.

The other implementation discovered in Phase I did not require a steerable beam but required a seeker control loop at the front of the guidance package with a high natural frequency (several hundred radians per second). Although the system performed well in simulation runs using ideal signals, the high frequency of the seeker loop would make the system quite susceptible to angular noise effects such as those produced by target glint and minor atmospheric perturbations. The results of the Phase I investigation are described in detail in Interim Technical Report No. 1 under the contract [1].

During the second phase of the program, emphasis has been placed on guidance systems for use against lower speed surface targets such as vehicles. With a lower speed target the intercept problem becomes simpler. The possibility that a simpler (and less costly) guidance system might be adequate to insure a high probability of intercept against such targets needed investigating.

An extensive literature survey was made for information on strapdown seekers and guidance schemes. No new information was found on strapdown seekers and associated guidance methods, but the survey did reveal a number of interesting papers on general guidance techniques. A summary of the findings from the literature survey is given in the Appendix.

Effort was then directed to studying and analyzing a recently proposed simple guidance scheme designated Dynamic Lead Guidance (DLG). DLG is intended for use with a strapdown sensor, and utilizes feedback from an

attitude gyroscope in such a manner that the missile heading develops a lead angle when operating against a moving target. The lead angle that DLG can develop is less than that required for a collision course, so the method would probably not be satisfactory for guidance against high speed airborne targets; it does appear to offer a practical guidance technique for use against surface targets.

Most of the effort under the program was devoted to the study and analysis of DLG and the results are presented in the following sections. Some analysis of pursuit guidance was done for comparison, but pursuit guidance was found to be unsatisfactory against surface targets moving at nominal speeds.

The investigation of DLG consisted of both theoretical analyses and simulated missile flights using a modification of the digital simulation developed during the first phase of the program. Throughout the program theoretical analysis and simulation studies were carried out more or less concurrently.

The major areas in which theoretical studies were made were in the selection of DLG parameters, the definition of sensor requirements, and the determination of DLG performance for a sampled data sensor. Each of these studies is discussed in the following sections.

Section II summarizes the analysis and the results in the choice of the DLG parameters. To facilitate this work, digital programs were developed to compute and automatically plot both Nyquist and Bode plots. These programs proved to be valuable tools in carrying out the analyses, and FORTRAN listings of the two subroutines as well as the calling program are given in the Appendix.

The parameter choice analysis provided a workable set of parameters in addition to providing considerable insight into the performance of DLG. The parameter choices were verified with simulation runs, and variations in their values were tested. These runs demonstrated that except for the sensor, the values of the guidance loop parameters are not critical. Simulation runs indicated satisfactory performance for a range of values for system gain, time lag, and gyro gain.

Section III summarizes the results of simulation studies. For these studies the digital simulation developed during the first phase of the program was modified to simulate DLG; included in the program are provisions

for simulating sensor characteristics, missed pulses, sampled data input, gravity bias, and variations in gyro gain. A listing of the complete simulation program is included in the Appendix. Performance characteristics studied by simulation included DLG parameter variations, sensor characteristics (linearity, field-of-view, limiting, and boresight error), sampled data operation, gyro gain, cross-feed between pitch and yaw guidance signals, and the effect of gravity upon pitch axis performance. Both constant-velocity and maneuvering targets were simulated.

Section IV discusses in detail the sensor requirements for DLG, and these turn out to be rather stringent. A hard limiting or saturating sensor will not work; the sensor must provide an output which is sensitive to the angle of the line-of-sight over the entire field of view. It is not necessary that the sensor characteristic be perfectly linear, but the permissible deviation from linearity is limited. It is shown in Section IV that the degree of saturation in the sensor must be sufficiently low that the "equivalent gain" (slope) does not drop below about 0.85 as the target approaches the edge of the field of view.

Section V discusses the use of sampled data sensors. It was found that DLG performs well with sampled data if the sampler is properly located; the performance was verified with simulation runs using data rates of 10, 20, and 30 samples per second. Simulation showed that missing up to 10% of the samples did not significantly degrade the performance of the system.

The conclusions, presented in Section VI, can be summarized as follows: DLG offers a practical technique for guidance against surface targets provided a sensor with only mild saturation and with a field of view of around $\pm 10^{o}$ can be developed.

Page intentionally left blank

II. DYNAMIC LEAD GUIDANCE PARAMETER CHOICE

Dynamic Lead Guidance (DLG) is a guidance technique well-suited to the use of strapped-down sensors in small tactical missiles. In addition to a body-mounted (non-gimbaled) sensor which determines the angular location (pitch and yaw) of the target with respect to the missile center line, DLG uses a position gyro (free gyro) which determines the angular attitude of the missile with respect to a reference attitude. For this report, the missile is assumed to have a separate roll control system; a single axis (pitch or yaw) of the system will be studied.

Figure 1 shows the geometry of the missile-target relationship, while Figure 2 gives a block diagram of the DLG system. As shown in Figure 2, the sensor output, σ_m, is summed with the attitude gyro output, θ, to estimate the angle (σ_R') between the missile-target line-of-sight (LOS) and the inertial reference direction. The gyro signal, θ', is fed through a lag circuit with time constant τ_L and subtracted from σ_R' to form the error signal for the guidance loop. A lead network with corner frequencies ω_1 and ω_2 is available for cascade compensation of the guidance loop if

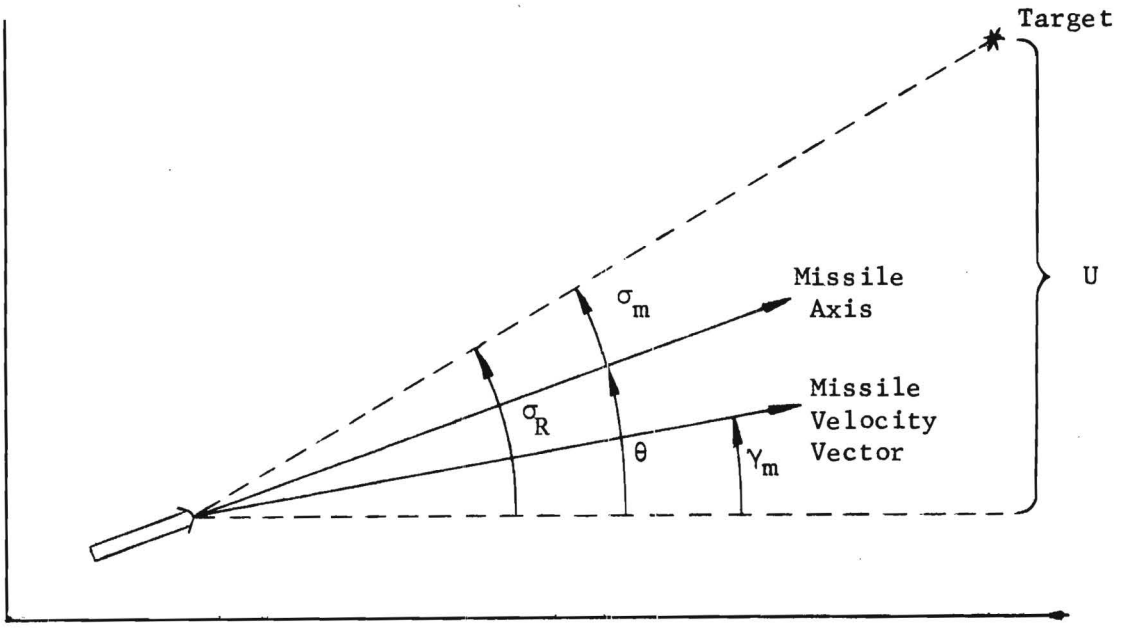

Figure 1. Missile-Target Geometry.

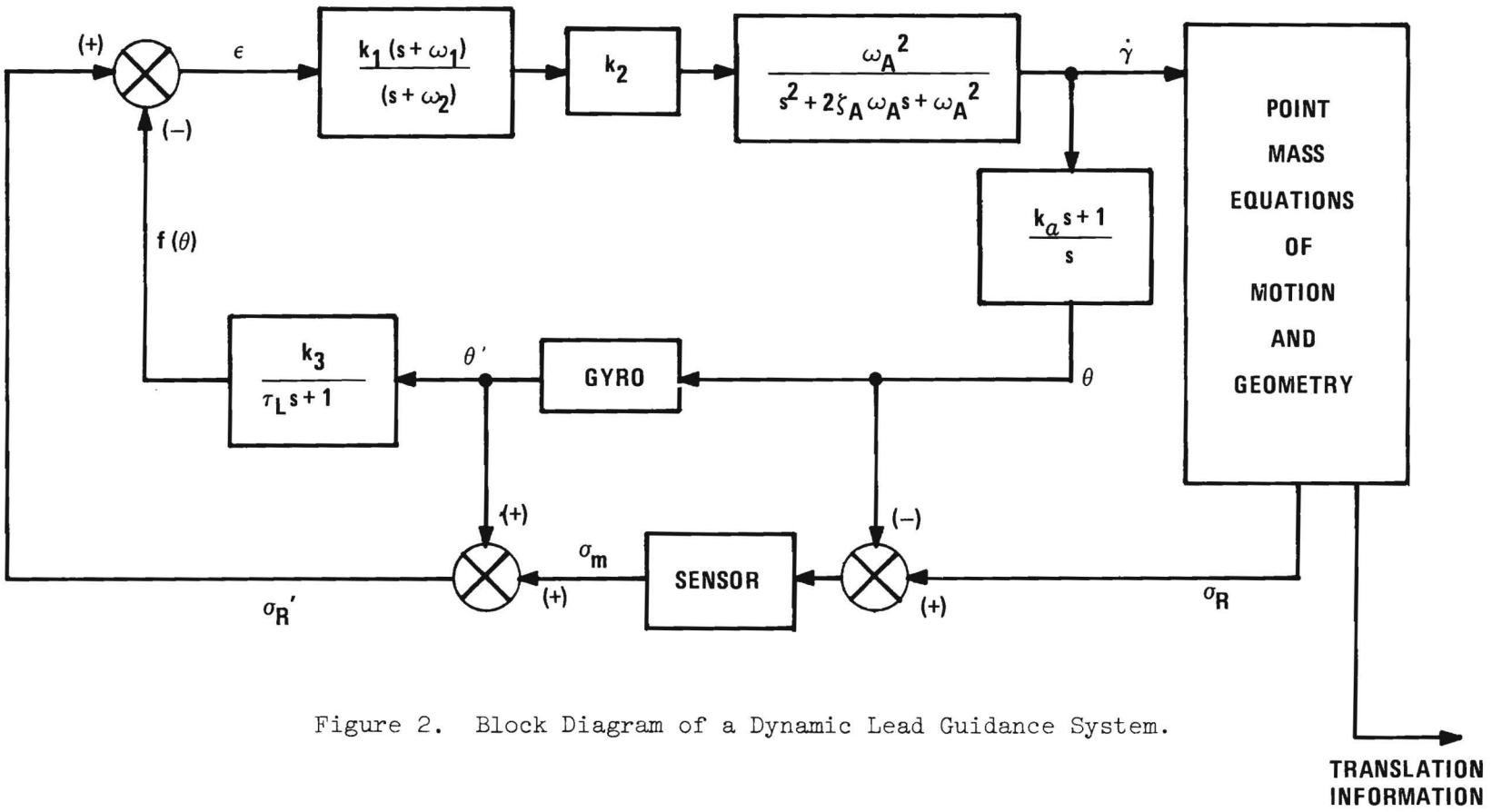

Figure 2. Block Diagram of a Dynamic Lead Guidance System.

required. The remainder of the block diagram in Figure 1 represents the missile actuator and airframe dynamics and missile-target geometry. The variable γ represents the angle between the missile velocity vector and the inertial reference.

Before getting involved with the analysis and design of a DLG system, it is interesting to compare its makeup with well-known guidance techniques such as pursuit and proportional navigation. First, observe that as the lag time constant τ_L approaches zero (for $k_3 = 1$), DLG approaches pursuit guidance since the driving signal, ε, approaches σ_m. As τ_L is increased from zero, the lag in $f(\theta)$ produces a driving signal, ε, which behaves very much as if there were a lead in the inertial LOS angle, σ_R'. Proportional navigation corresponds to 90^o lead, or pure differentiation, in the σ_R' path in that it commands a missile turning rate ($\dot{\gamma}$) proportional to the time-rate-of-change of the LOS angle as measured from an inertial reference.

The digital computer simulation program developed earlier for the study of strapdown guidance methods [1], has been modified to incorporate DLG and is included in the Appendix. The techniques used to determine reasonable values for the parameters τ_L, k_1k_2, ω_1 and ω_2 for the first group of simulation runs is described in the following.

A linear model for the geometric portion of the system diagram is required for application of the classical control analysis and design techniques. From the geometry of Figure 1 it can be seen that the time rate of change of the cross-range distance between the missile and the target is

$$\dot{U} = -V_y + gt = -V \tan \gamma + gt \ , \tag{1}$$

where g is the gravitational acceleration for the pitch axis and is zero for yaw axis analysis. Assuming a small angle γ, then

$$\dot{U} = -V \gamma + gt \ , \tag{2}$$

and for constant missile speed and negligible target speed one has

$$\ddot{U} = -V \dot{\gamma} + g \ , \tag{3}$$

or

$$U = \iint (-V \dot{\gamma} + g) \, dt \, dt \ . \tag{4}$$

But,

$$\sigma_R \doteq \sin^{-1}\left(\frac{U}{R}\right) \approx U/R$$

$$\sigma_R \doteq \frac{1}{R}\iint (-V\,\dot{\gamma} + g)\,dt\,dt\ , \tag{5}$$

which is expressed in Laplace transform notation for block diagram form as shown in Figure 3.

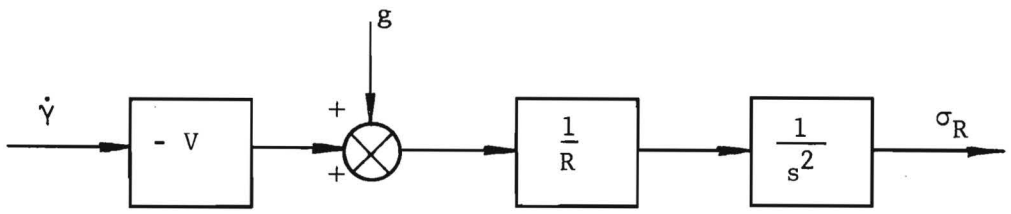

Figure 3. Model of Geometric Portion of System.

The substitution of this result into Figure 2 results in the linear block diagram of Figure 4.

It is desired to determine values of the four DLG parameters τ_L, k_1k_2, ω_1, and ω_2 (by analysis of the linearized model) which will give a stable guidance loop. The values of these parameters will then be further refined by trial and error in the digital simulation to improve DLG performance. In order to use the classical stability analysis tools, the system of Figure 4 will be treated as time-invariant and stability will be investigated for several representative values of range, R, using fixed-point analyses. Note from Figure 4 that three of the four parameters to be chosen are associated with the lead network driven by the error signal, ϵ; i.e., if τ_L were known, the only unknowns would be together in the classical location for cascade compensation. The search for suitable parameters will thus be made by choosing a "best guess" for the lag time constant, τ_L, and choosing k_1k_2, ω_1, and ω_2 by the standard control system design techniques utilizing Bode diagrams. An alternate procedure would be to use the Routh-Hurwitz stability criteria with the closed-loop characteristic equation; however, the resulting inequalities in four variables would be very difficult to handle. Note that the desired or nominal values of the gains at the sensor, gyro, and lag network are known to be unity; i.e., $k_s = k_G = k_3 = 1$.

The lag circuit time constant, τ_L, will be chosen as if it alone determined the amount of dynamic lead to be provided; i.e., τ_L will be chosen initially as the desired guidance system time constant. For the test case being used for evaluation of DLG, the nominal flight time is ten seconds and the airframe natural frequency is 10 rad/sec ($f = \omega/2\pi = 1.6$ Hz; $T = 0.63$ sec); a reasonable choice for τ_L might be in the range $0.1 < \tau_L < 0.5$ sec. Arbitrarily, $\tau_L = 0.3$ was chosen as a starting point. The design technique using Bode and Nyquist plots will now be used to determine whether or not values of k_1k_2, ω_1, and ω_2 exist such that the guidance loop can be stabilized for the assumed value of τ_L.

For nominal values of k_s, k_G, and k_3, the linearized DLG block diagram can be redrawn as shown in Figure 5. The open-loop transfer function, exclusive of the lead network (compensation) is seen to be

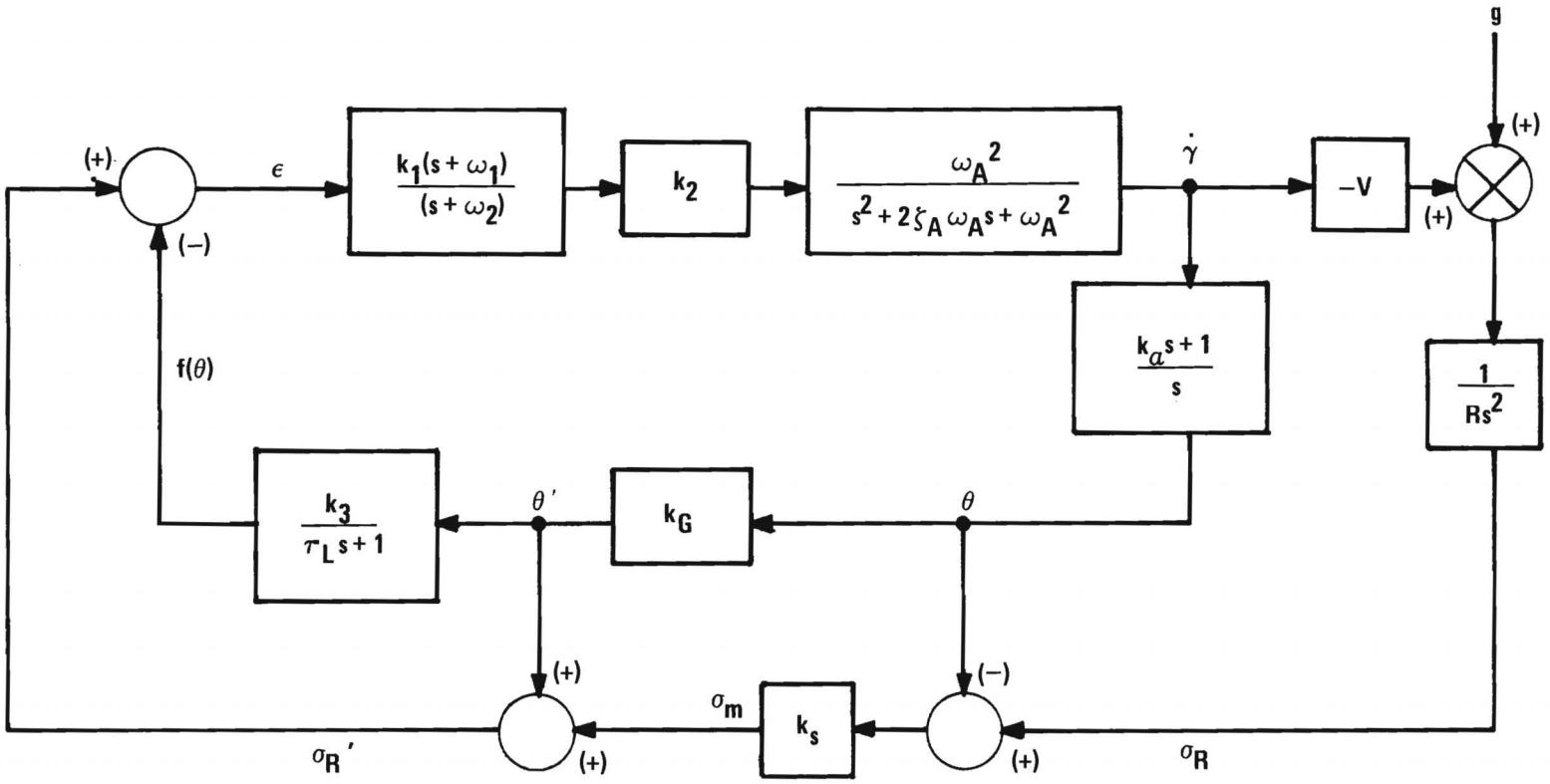

NOTE:

g = 0 for yaw axis analysis

Figure 4. Block Diagram of Dynamic Lead Guidance System with Geometry Model Included.

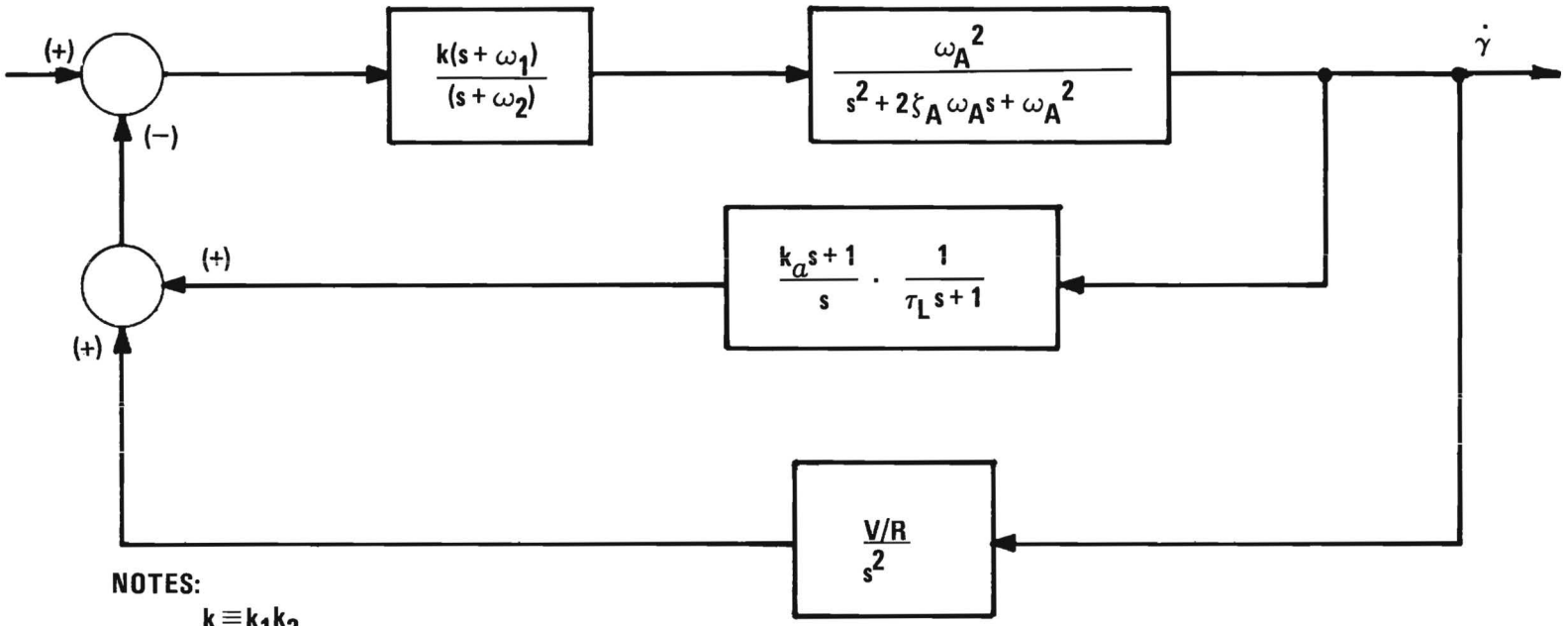

NOTES:

$k \equiv k_1 k_2$

Nominal values assumed for k_s, k_G, and k_3.

Yaw axis assumed.

Figure 5. Linearized Block Diagram of DLG.

$$HG(s) = \left[\frac{\omega_A^2}{s^2 + 2\zeta_A\omega_A s + \omega_A^2} \right] \cdot \left[\frac{k_\alpha s + 1}{s} \cdot \frac{1}{\tau_L s + 1} + \frac{V/R}{s^2} \right], \quad (6)$$

or

$$HG(s) = \left\{ \frac{\omega_A^2 (k_\alpha s^2 + s + [\tau_L s + 1]\, V/R}{s^2(\tau_L s + 1)(s^2 + 2\zeta_A\omega_A s + \omega_A^2} \right\} . \quad (7)$$

While one could manually sketch Bode and Nyquist plots for this open loop transfer function by the asymptotic method, the anticipated large number of such plots required for various values of R and τ_L led Georgia Tech to develop a computerized automatic plotting procedure using a CALCOMP plotter. The program evaluates the open-loop transfer function for a specified range (4 decades) of frequency and calls subroutines which cause the CALCOMP plotter to plot the data in the forms of Bode and Nyquist plots. The program and subroutines are written in FORTRAN V and listings of these programs are included in the Appendix.

For the parameters given in Table I, Bode and Nyquist plots of the open loop transfer function were made for several representative values of range, R. These plots are for the assumed time-constant value of $\tau_L = 0.3$ sec and are shown in Figures 6 through 10. (Note that the unit circle is drawn as a reference magnitude on the Nyquist plots.) Since the open loop transfer function contains no poles in the right-half-plane (for $\tau_L > 0$ and the air-frame-actuator second order system assumed stable), the stability condition is simply zero encirclements of the critical point (-1 + j0) on the Nyquist plot.

TABLE I

SYSTEM PARAMETER VALUES FOR BODE AND NYQUIST PLOTS OF FIGURES 6 THROUGH 10

$\tau_L = 0.3$	$k_3 = 1$	$k_s = 1$
$k_2 = 1$	$\zeta_A = 0.7$	$k_\alpha = 0.5$
$\omega_A = 10$		

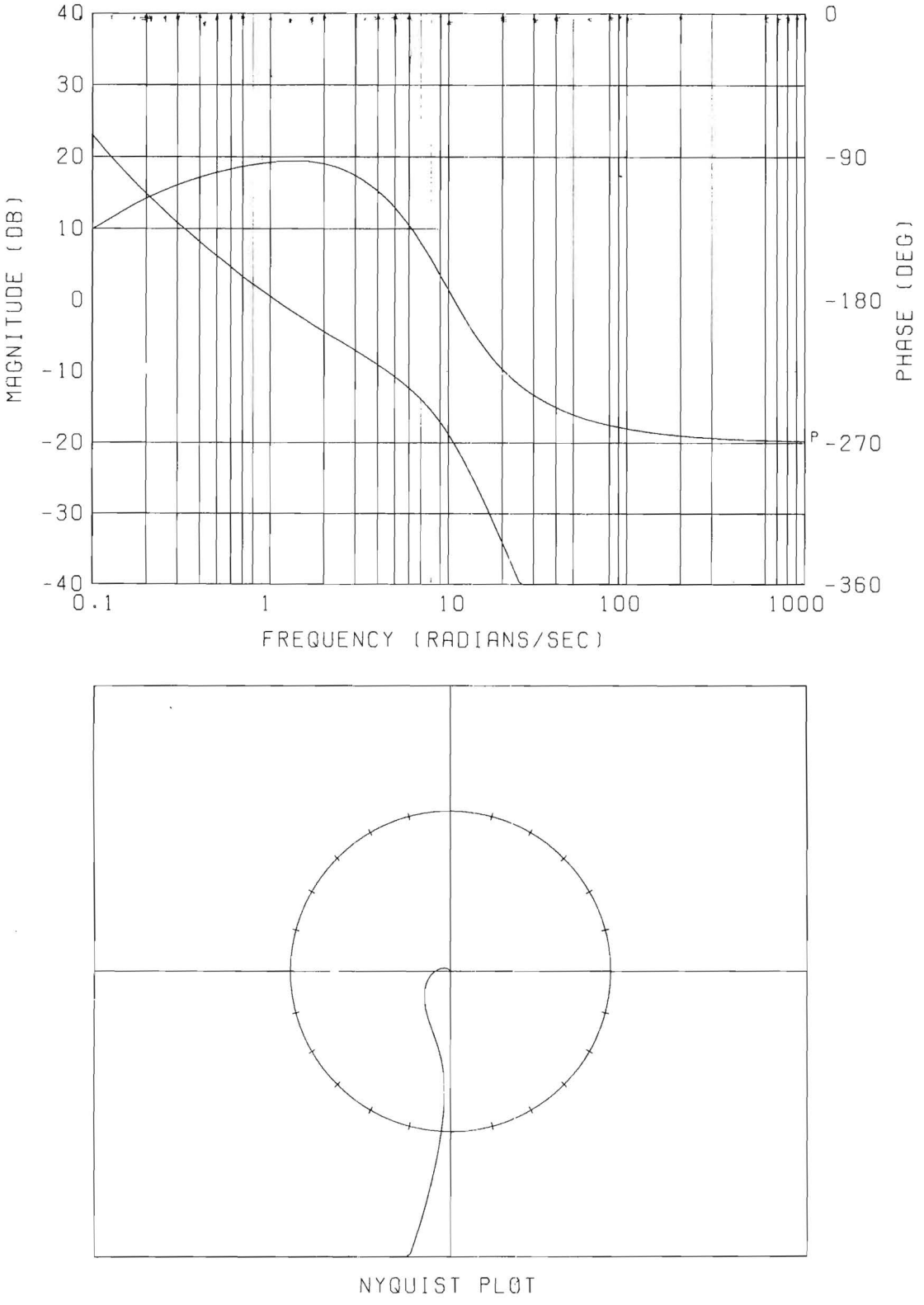

Figure 6. Nyquist and Bode Plots for Linear, Continuous DLG Model with $\tau_L = 0.3$, $k_2 = 1.0$, and R = 10,000 feet.

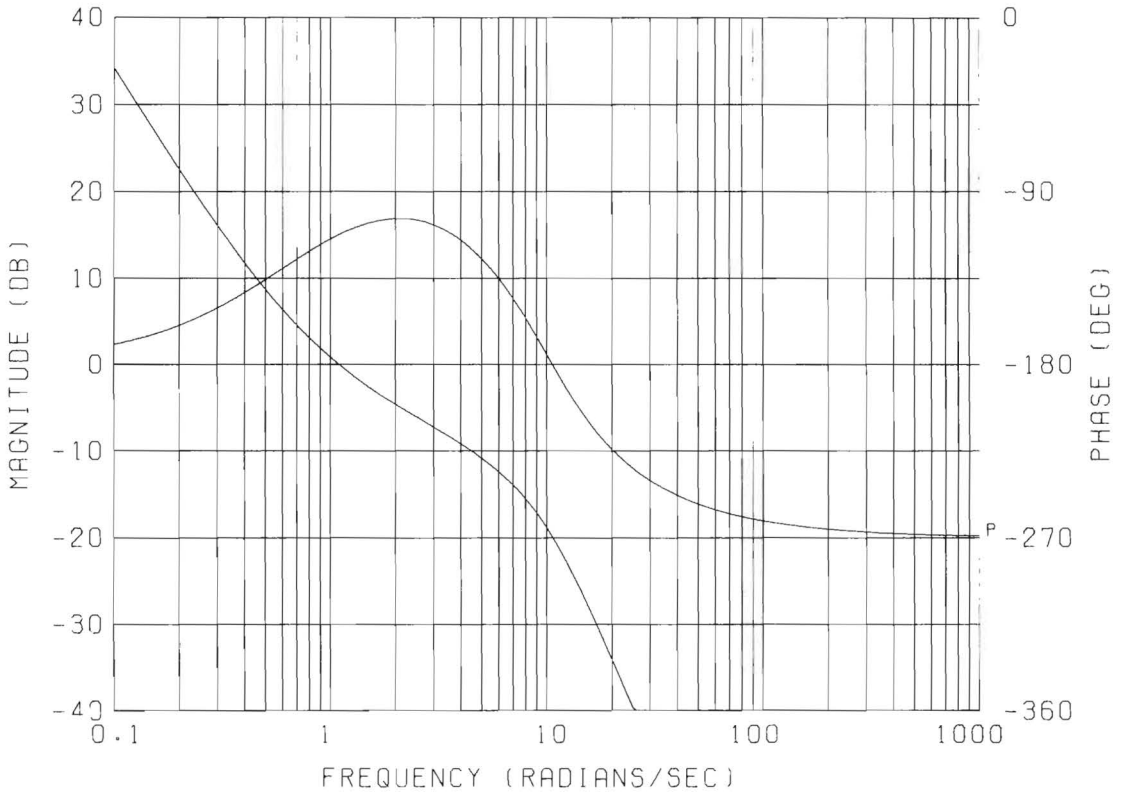

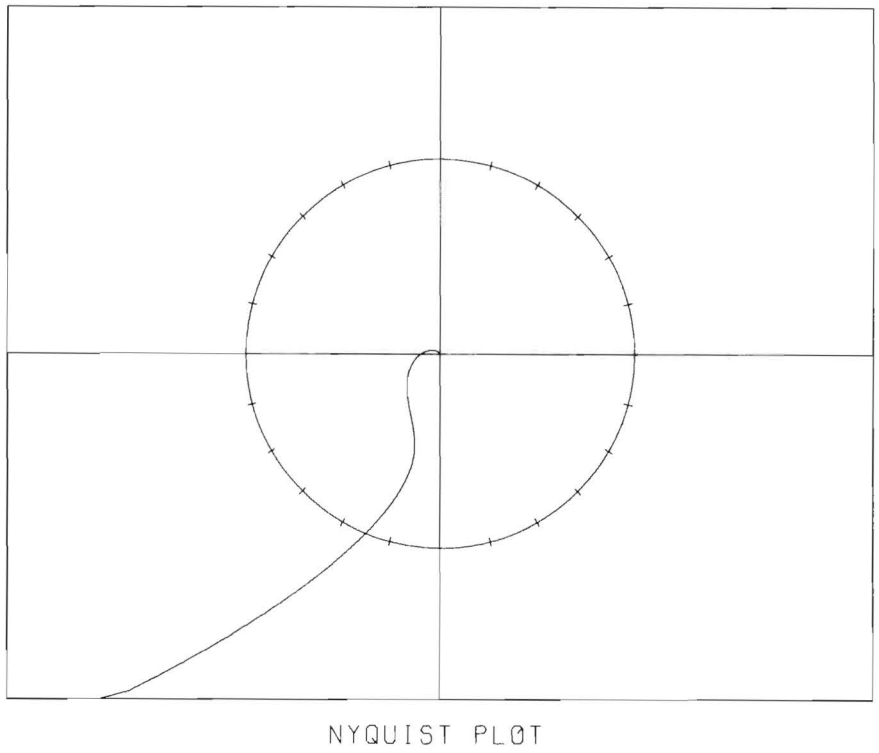

Figure 7. Nyquist and Bode Plots for Linear, Continuous DLG Model with $\tau_L = 0.3$, $k_2 = 1.0$, and R = 2,000 feet.

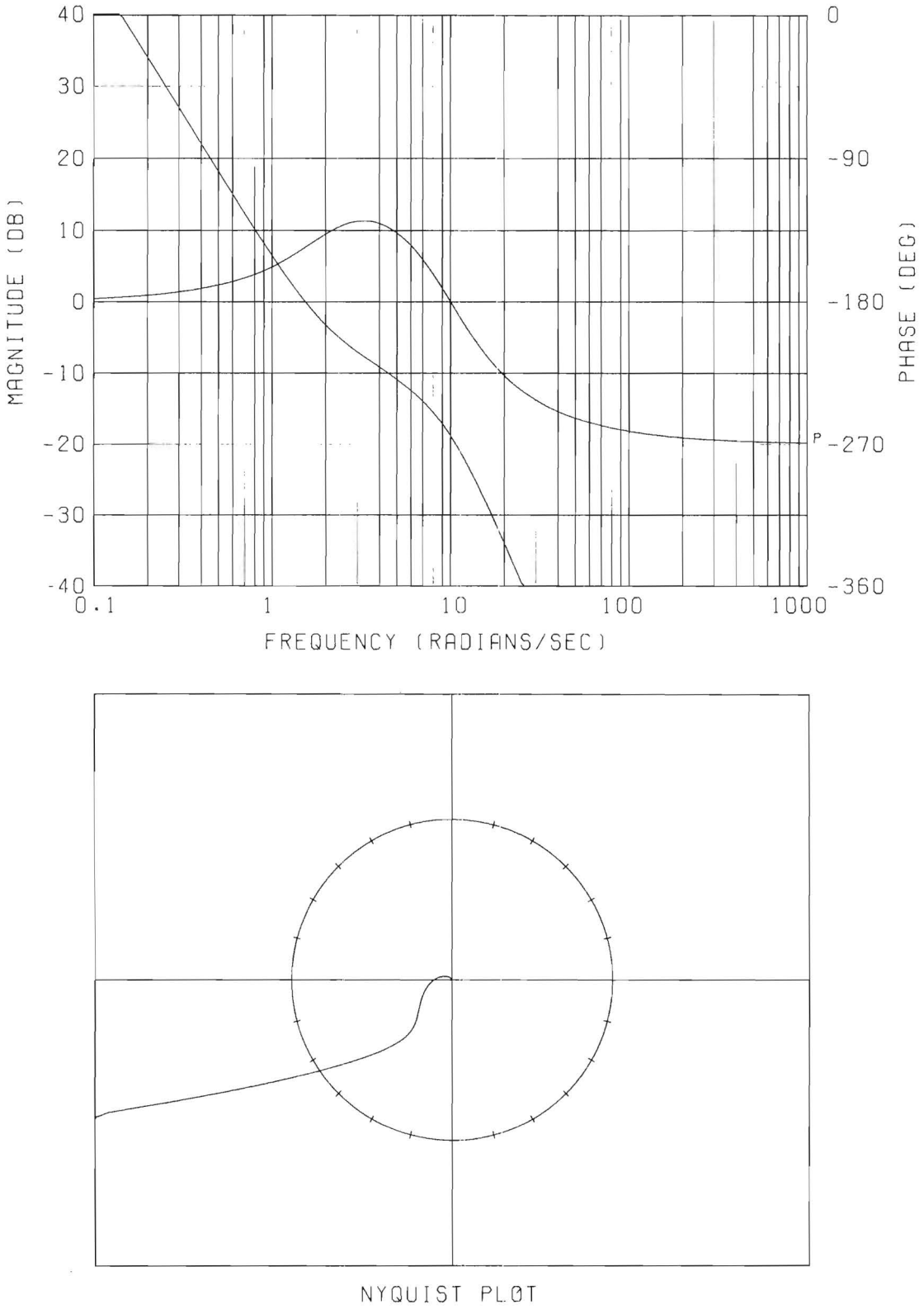

Figure 8. Nyquist and Bode Plots for Linear, Continuous DLG Model with $\tau_L = 0.3$, $k_2 = 1.0$, and R = 500 feet.

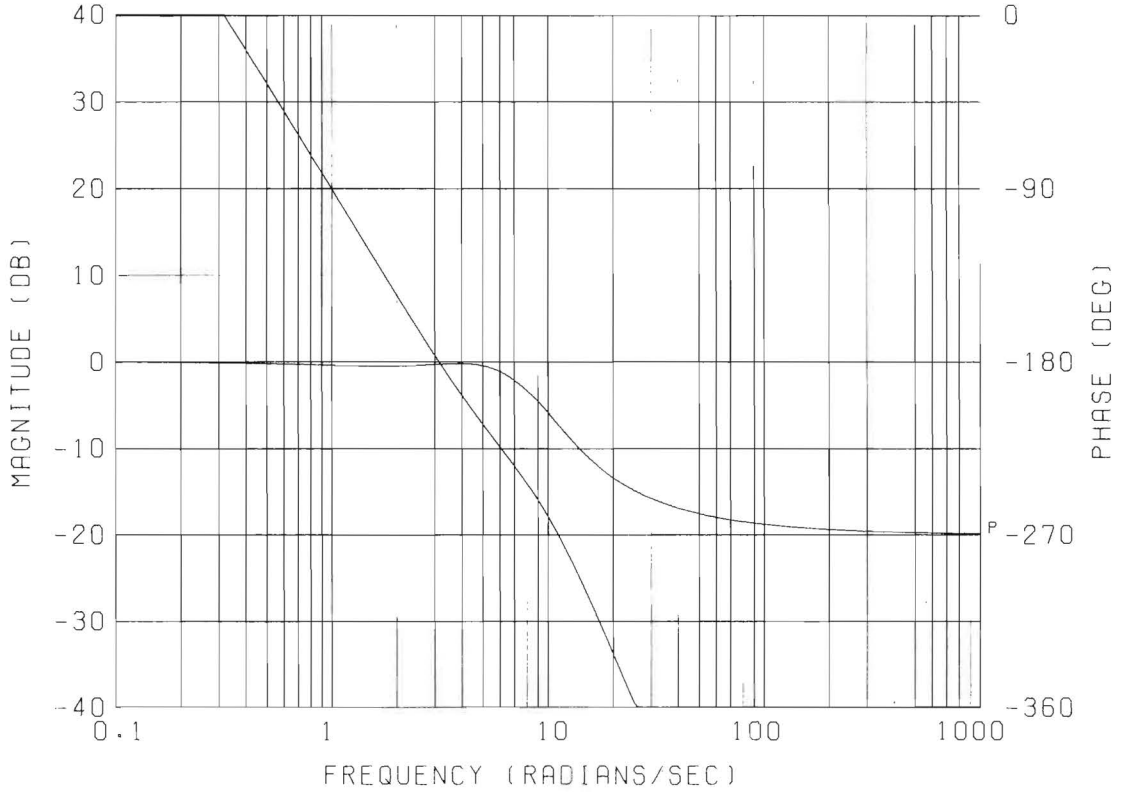

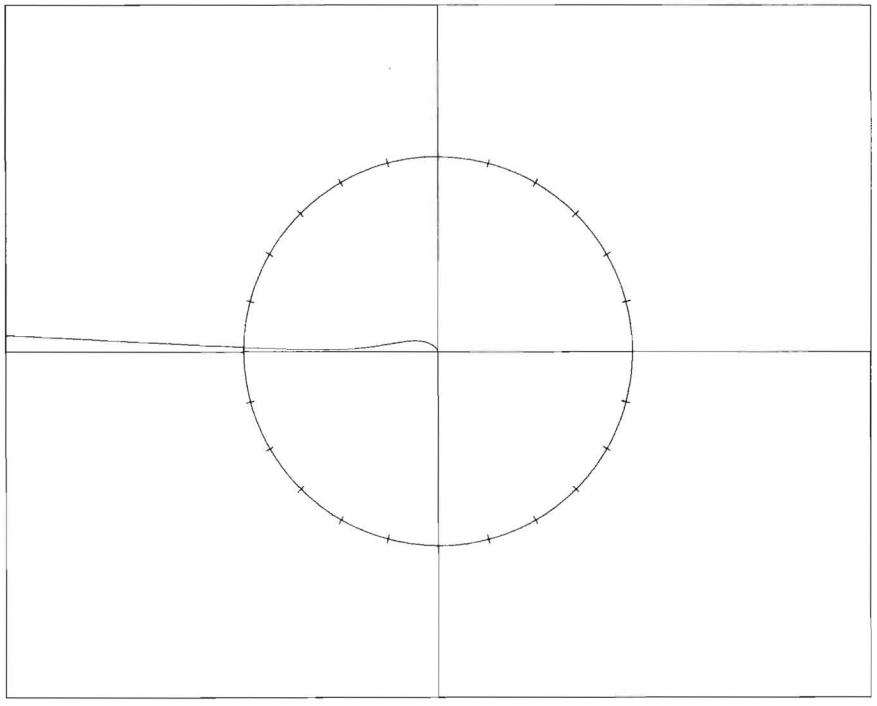

NYQUIST PLOT

Figure 9. Nyquist and Bode Plots for Linear, Continuous DLG Model with $\tau_L = 0.3$, $k_2 = 1.0$, and R = 100 feet.

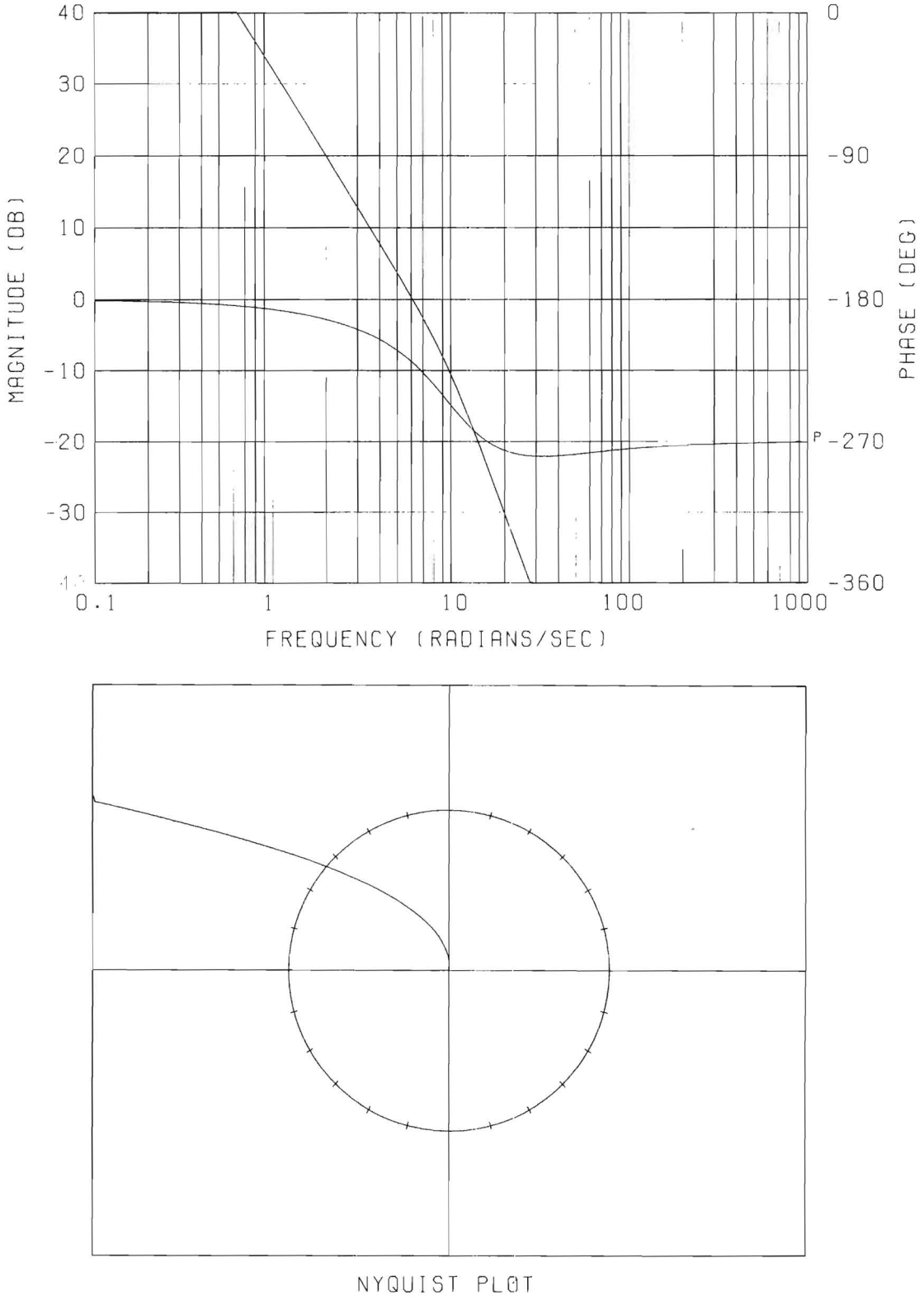

Figure 10. Nyquist and Bode Plots for Linear, Continuous DLG Model with $\tau_L = 0.3$, $k_2 = 1.0$, and R = 25 feet.

Alternately, the Bode plot may be used; stability requires that the magnitude be below zero dB at the frequency at which the phase passes through 180° as well as all higher frequencies.

For interpretation of the Nyquist plots in Figures 6 through 10, Figure 11 shows the complete locus obtained by adding the negative frequency segment and the "infinite radius" closure portions to that obtained from the automated plot routine. Examination of the open loop transfer function shows that the limiting value of HG(s) as ω approaches zero increases without bound at an angle of 180°. Similarly, for large ω the locus of HG(s) approaches 90°. It can be seen from Figure 11-d that the DLG system for $\tau_L = 0.3$ will be stable without lead network compensation for those values of gain k and range R such that the Nyquist critical point is to the left of the point where the locus crosses the negative real axis (as point B in Figure 11-d), but unstable otherwise.

Inspection of the Nyquist or Bode plots for $\tau_L = 0.3$ and various range values (Figures 6-10) shows that the system is stable without compensation for the higher values of R, but it becomes unstable as the missile approaches the target. A tabulation of the gain margin (the amount by which the gain can be increased without causing instability) as a function of range is given in Table II. For unity gain ($k_1 = 1$), the system is stable for $R \geq 200$ ft., and unstable for $R \leq 100$ ft. Furthermore, the Nyquist shape is such that the open loop gain could be increased by a factor of about six without appreciably changing the range at which the system becomes unstable.

Since the system for $\tau_L = 0.3$ is stable except near flight termination (a common phenomenon in closed-loop guidance systems) even for gain k_1 as high as six, DLG simulation runs were made for $\tau_L = 0.3$. The DLG system was stable throughout the flight in the simulation; it was in fact rather sluggish in its response. In order to increase the amount of lead or anticipation in the DLG system, the time constant τ_L was increased by an order of magnitude to $\tau_L = 3.0$.

The Bode and Nyquist plots were repeated for this new value of τ_L. Figures 12 through 15 show the fixed-point Bode and Nyquist plots for $\tau_L = 3.0$ and the loop gain increased by a factor of $k_2 = 9.0$. The parameters for these plots are as given in Table III, and the resulting gain margin as a function of range is tabulated in Table IV.

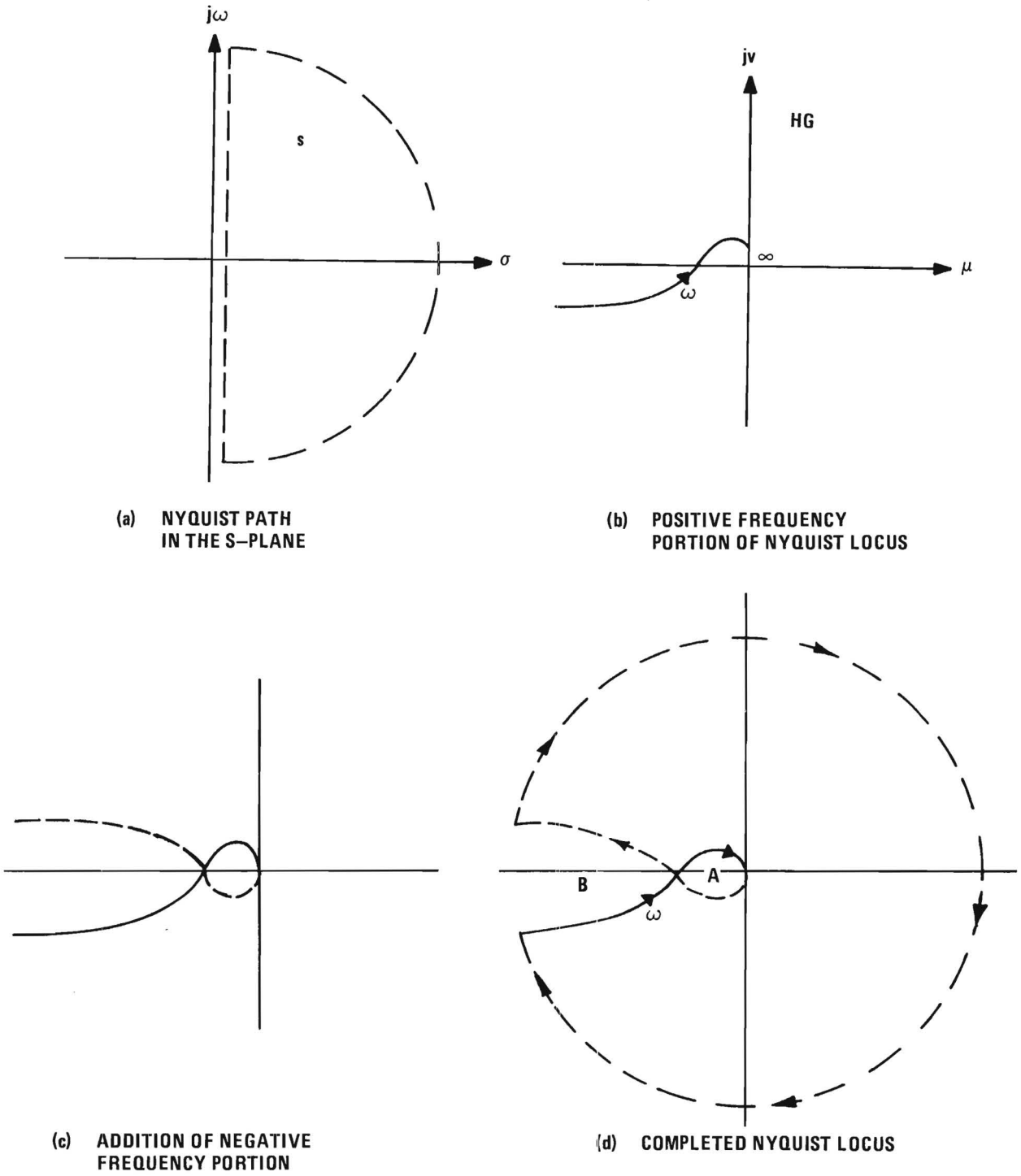

(a) NYQUIST PATH IN THE S–PLANE

(b) POSITIVE FREQUENCY PORTION OF NYQUIST LOCUS

(c) ADDITION OF NEGATIVE FREQUENCY PORTION

(d) COMPLETED NYQUIST LOCUS

Figure 11. Nyquist Path Closure for Linear, Continuous DLG Model.

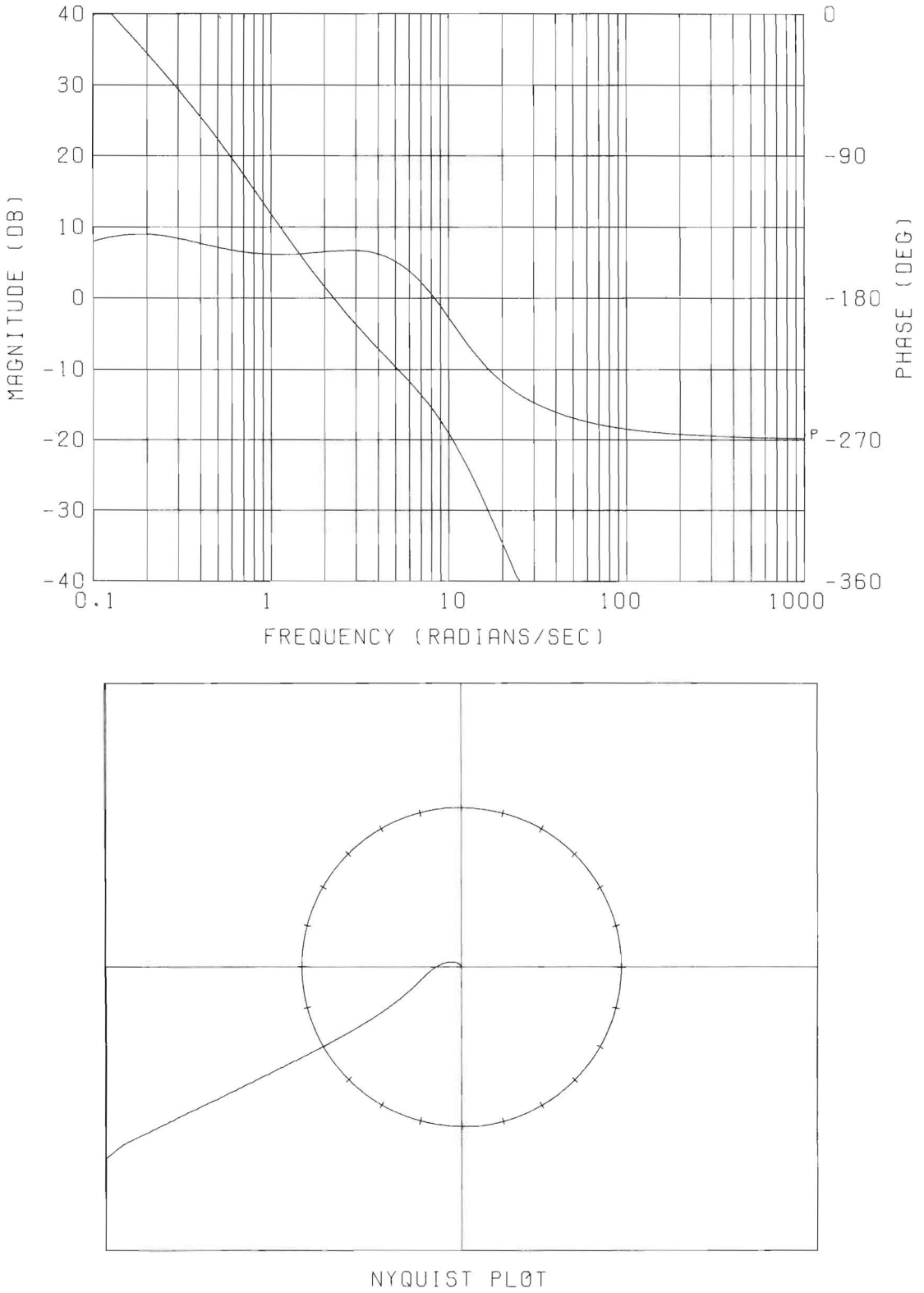

Figure 12. Nyquist and Bode Plots for Linear, Continuous DLG Model with τ_L = 3.0, k_2 = 9.0, and R = 10,000 feet.

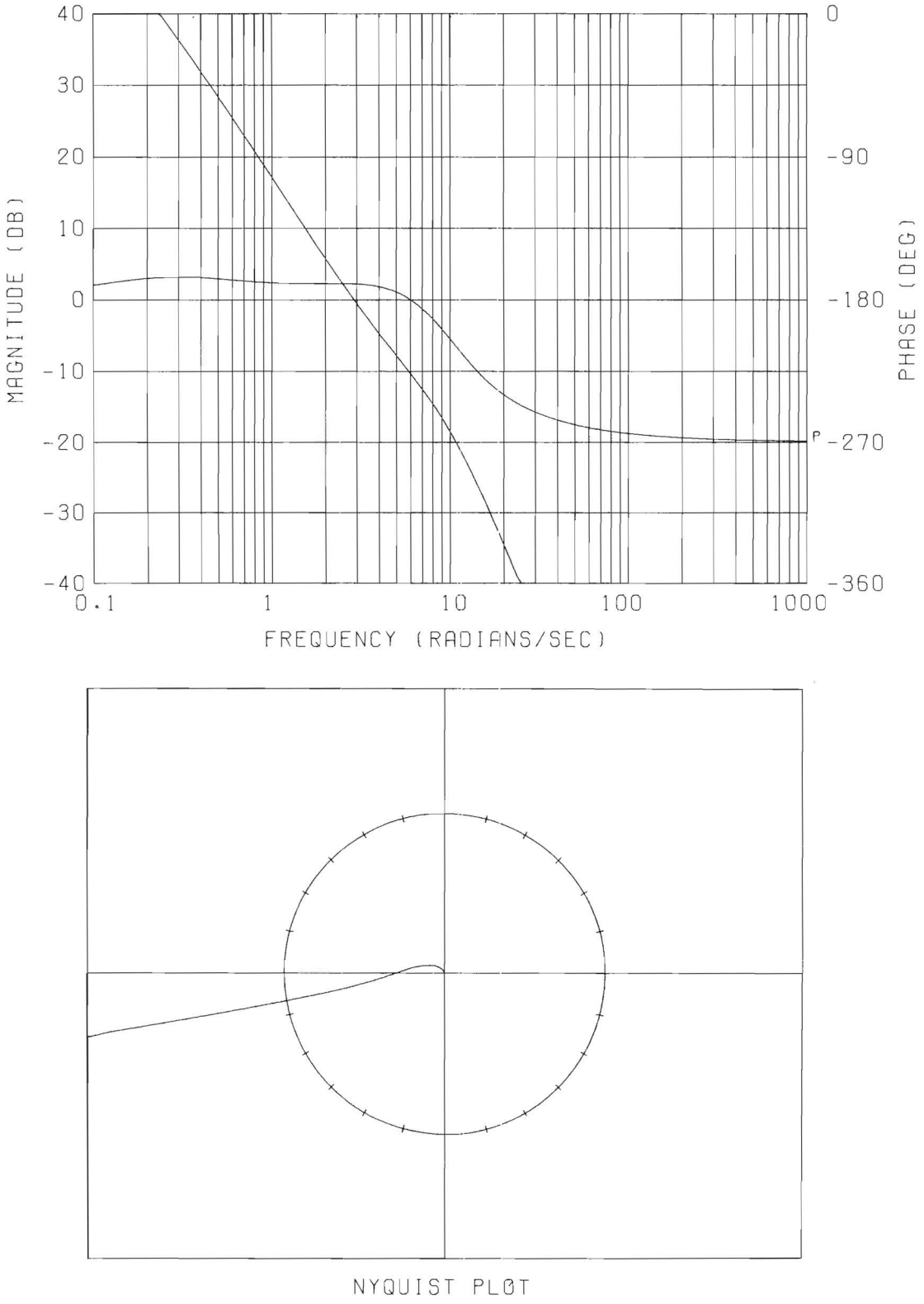

Figure 13. Nyquist and Bode Plots for Linear, Continuous DLG Model with $\tau_L = 3.0$, $k_2 = 0.0$, and R = 2,000 feet.

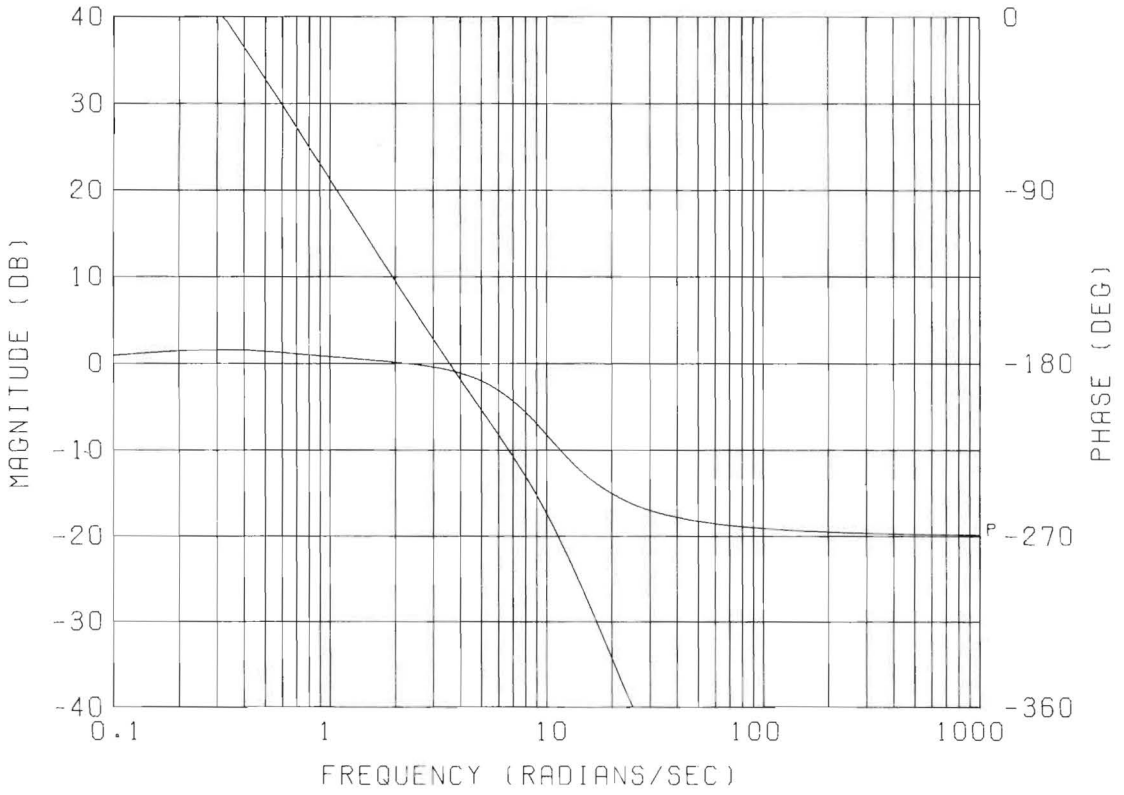

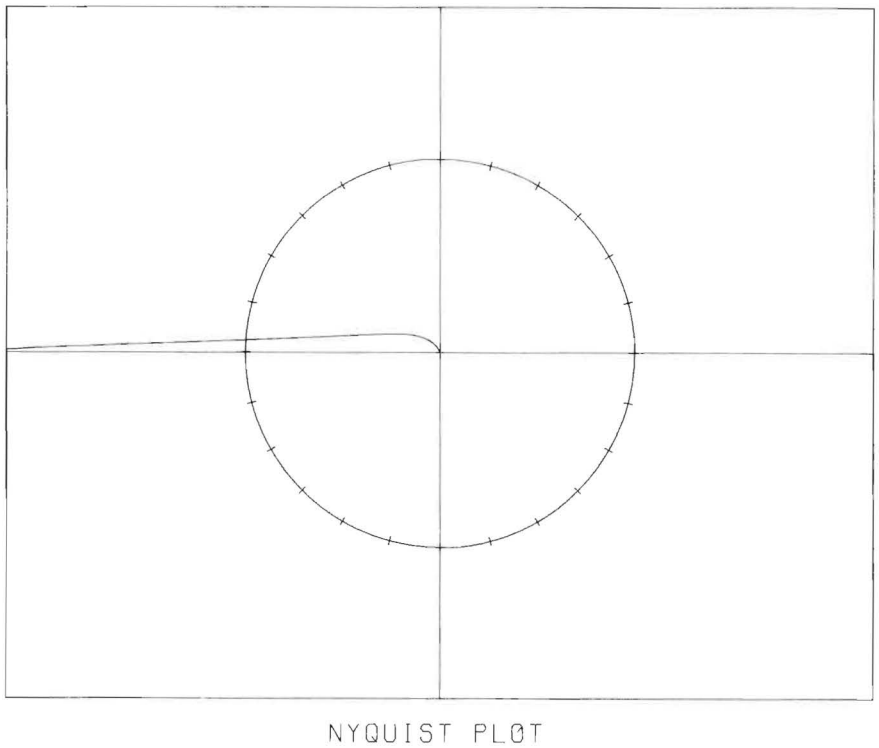

Figure 14. Nyquist and Bode Plots for Linear, Continuous DLG Model with τ_L = 3.0, k_2 = 9.0, and R = 1,000 feet.

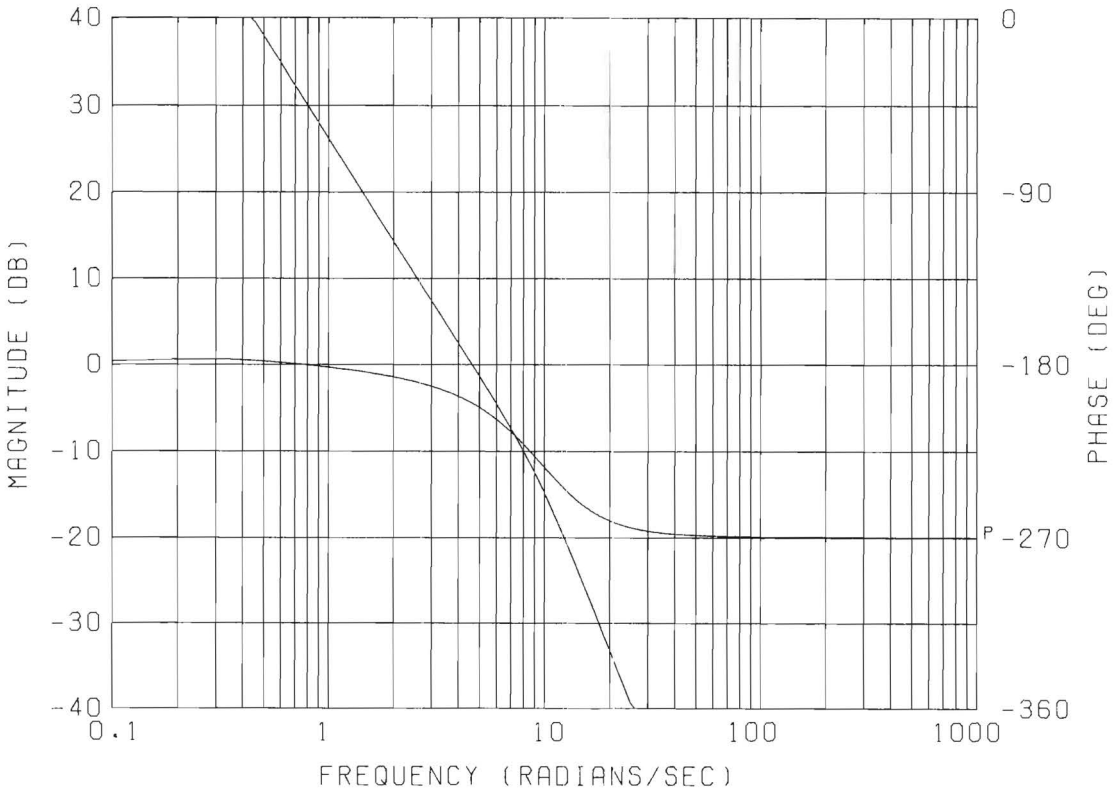

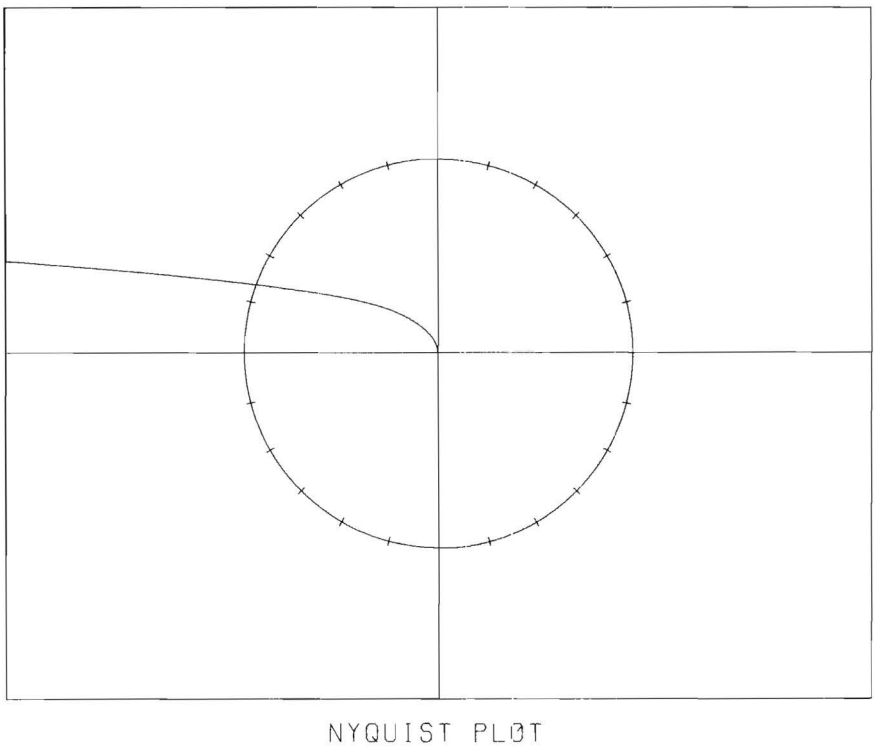

NYQUIST PLOT

Figure 15. Nyquist and Bode Plots for Linear, Continuous DLG Model with $\tau_L = 3.0$, $k_2 = 9.0$, and R = 500 feet.

TABLE II

GAIN MARGIN AS A FUNCTION OF RANGE FOR
THE DLG PARAMETER VALUES OF TABLE I

R (feet)	Gain Margin
10,000	10.4
8,000	9.5
6,000	10.4
4,000	10.4
2,000	9.5
1,000	9.5
500	8.0
200	6.5
100	Unstable
25	Unstable

TABLE III

DLG PARAMETERS FOR BODE AND NYQUIST PLOTS
IN FIGURES 12 THROUGH 15

$\tau_L = 3.0$	$k_1 = 1$	$k_3 = 1$
$k_2 = 9.0$	$k_\alpha = .5$	
$\omega_A = 10$	$\zeta_A = .7$	

TABLE IV

GAIN MARGIN OF DLG FOR PARAMETERS IN TABLE III

R (feet)	Gain Margin
10,000	6.1
8,000	6.1
6,000	5.8
4,000	5.2
2,000	3.2
1,000	Unstable
500	Unstable
200	Unstable
100	Unstable
25	Unstable

Similar to the case for $\tau_L = 0.3$, the Bode and Nyquist plots for $\tau_L = 3.0$ in the fixed-point-analysis show the system to be stable at long ranges and unstable at short ranges. Examination of the Nyquist plots or the tabulation of gain margins shows that the resulting DLG system is (fixed-point) stable for ranges of 2000 feet or above and unstable at 1000 feet or below.

It is seen from the basic shape of the Nyquist plots that a phase lead at the higher frequencies is needed in order to stabilize the system for the shorter range values. To simplify the design of lead network compensation, the automated Bode plot routine was used to generate a set of normalized lead network Bode plots on semi-transparent paper scaled the same as the DLG Bode plots. Design by the classical techniques is simplified by the overlay of these design charts. A sample of the lead network Bode plots (for $\omega_2 = 5\omega_1$)is shown in Figure 16.

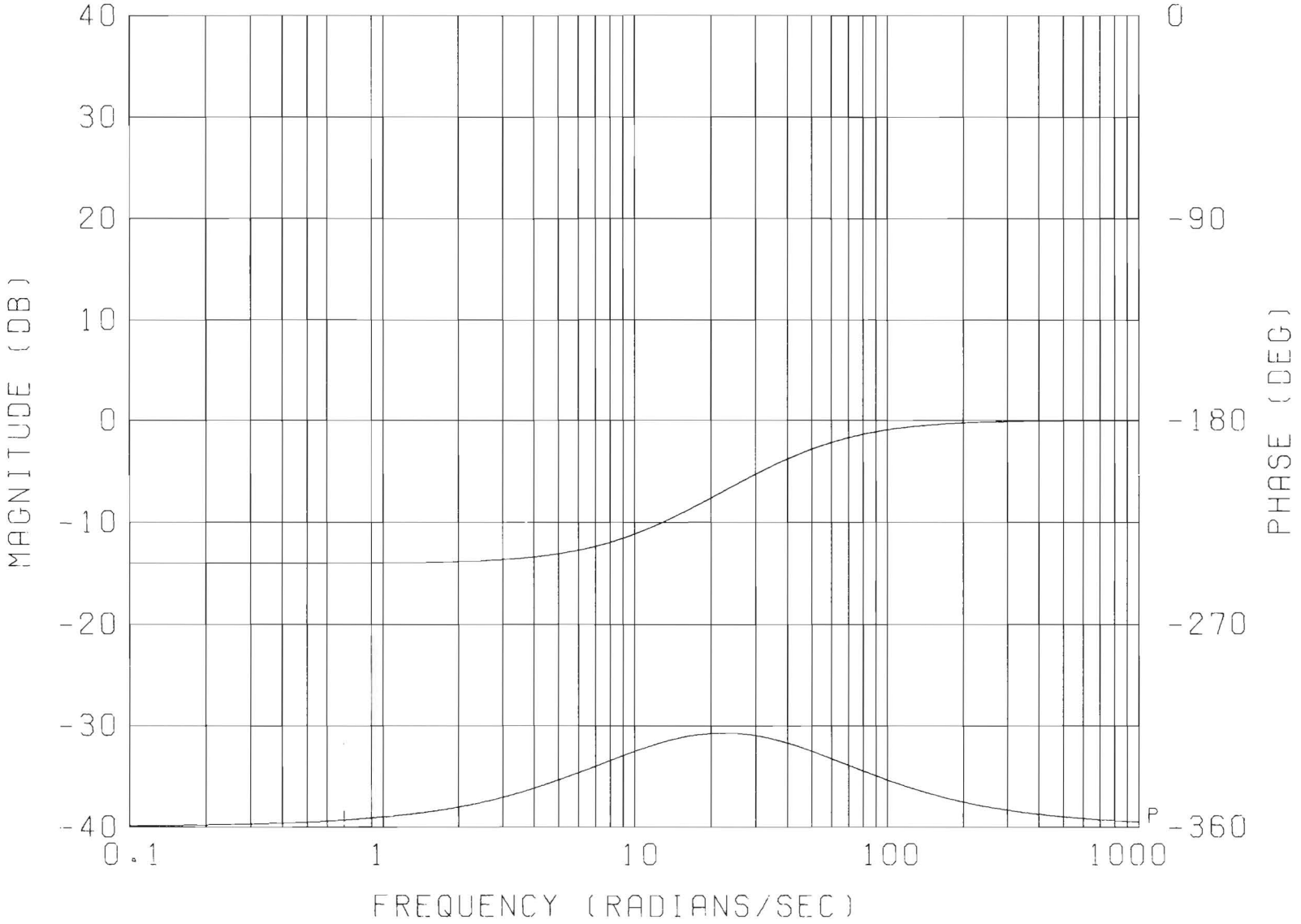

Figure 16. Bode Plot for Lead Network with a Break-Frequency Ratio of 5.

The uncompensated Bode and Nyquist plots for $\tau_L = 3.0$ and R = 1000 ft. given in Figure 14 indicate that the DLG system could be stabilized (at that fixed range) by compensation with a lead network centered around five or ten radians per sec; this would bend the Nyquist plot around the critical point. By trial and error with the lead template overlays, a lead network with $\omega_1 = 3$ and $\omega_2 = 15$ rad/sec has been selected. Note that the lead network must be selected in such a way that it does not de-stabilize the system at other values of range.

Simulation runs were made with $\tau_L = 3.0$ for various values of gain, k, first <u>without</u> the lead network. Interestingly enough, the runs were <u>stable</u> in spite of the fact that the fixed point analysis indicated an instability at the closer ranges. It is well known among control engineers that time-varying linear system stability cannot be rigorously established by fixed point analysis, but these techniques are still useful in designing compensation. In the DLG example, one suspects since the fixed point analysis indicates instability only within the last fraction of a second for a ten second flight and since the period of the predicted resulting oscillation is on the order of five seconds, that the instability simply has no time to build up before intercept occurs.

It is interesting to note here that simulation runs indicate that not only is the lead network not required for stability but furthermore that its presence actually reduces missile accuracy. The parameter choice was refined by "tuning" using the DLG simulation program and the results are included in the simulation section of this report. The fixed-point analysis described here has been useful in initially choosing stable DLG parameters and in investigating compensation networks. It also has provided the control design engineers with a better insight and feel for the system. The investigation of sensor nonlinearities and the effects of sampled-data operation in the following sections also depends heavily upon the fixed point analysis techniques. Of course, the results of any linear, fixed-point analysis of a time-varying nonlinear system must be verified by simulation or otherwise.

Page intentionally left blank

III. SIMULATION RUNS

During Phase I of the program, a two-dimensional digital simulation of a missile control system and the associated intercept geometry was developed and programmed for a UNIVAC-1108 computer. A description of the program along with a listing is given in the report covering that work [1].

Two simulation programs were used in Phase II, both being modifications of the original Phase I program. In the early part of the period, a three-dimensional (five degree of freedom) version of the model was created. This program was used to simulate missile flights in three dimensions, primarily to investigate the effect of cross-feed between the two control channels. The effect of other parameters could be evaluated with a two dimensional simulation and since the latter was more efficient and easier to work with, it was used in most of the simulation runs. The second simulation program was this two-dimensional simulation modified to include DLG. A listing of this program is given in the Appendix.

The simulation makes available a variety of data on each run, including miss distance, lateral acceleration profile, pitch angle profile, and lateral displacement profile. Various other quantities were calculated in the program, such as the angular difference between the instantaneous velocity and the collision path, the line-of-sight angle relative to the missile axis, and the estimated miss distance and time of nearest approach (based on maintaining the current velocity).

Most of the runs made with the two-dimensional simulation were oriented around the common set of geometry illustrated in Figure 17; also many of the parameters were common to most runs. These "nominal" values will be described here, and any deviations from them pointed out in the detailed discussion.

For most runs the target was assumed to be initially on the X axis at a range of 10,000 feet and moving vertically at 100 feet/second. The missile was launched horizontally (directly at the target) with a velocity of 1000 feet/second. When gravity was simulated, it was assumed to be acting downward. Thus the gravitational acceleration was approximately at right angles to the trajectory, producing a "worst case" effect.

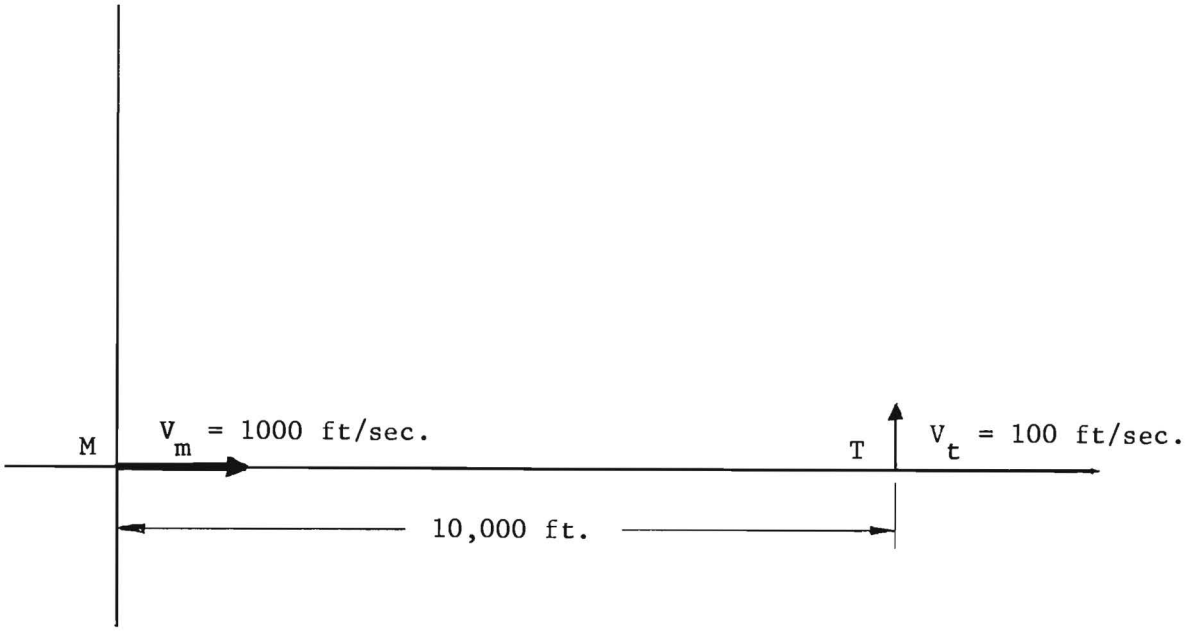

Figure 17. Geometry for Simulation Runs.

The missile airframe was assumed to have a natural frequency (ω_A) of 10 radians/second. In many of the early runs the damping ratio (ζ_A) was assumed to be 0.7, but a more lightly damped missile with $\zeta_A = 0.2$ was used in later simulation runs. The missile was assumed to have a lateral acceleration limit of 10 g. Variations in some of these values were introduced to study different effects. Different launch angles were used, target maneuvers were tried, and different airframe damping ratios were used. Sampling rates of 10, 20, and 30 per second were simulated for sampled data systems, and some runs were made for continuous data input.

The simulation runs were used to study a number of effects, including sampler location, sampling data rate, the sensor space-transfer function requirements, required field of view, variation of system parameters, and the effect of randomly missed pulses. Most of the runs were made for simulation of Dynamic Lead Guidance (DLG). A few runs were made simulating pursuit guidance for comparison. The results of these studies are discussed below.

A. DLG Parameter Choices

Among the earliest of the simulation runs on the DLG model were several made to examine the effect of varying τ_L and system gain. These runs were made to determine a suitable set of values for these parameters and were made concurrently with theoretical efforts discussed in Section II. All of these initial runs were made for a missile moving 1000 feet/second seeking a crossing target moving 50 feet/second. An airframe damping ratio of 0.7 was used, and the sensor characteristic was assumed to be linear with no restriction on the field of view. Calculated miss distances for various parameter choices are summarized in Table V.

Based on the above runs, $\tau_L = 3.0$ and a system gain (k_2) of 9 were initially selected as reasonable parameters. In later simulation runs, higher values were tried for both parameters and satisfactory performance was achieved with values of τ_L up to 5.0 and gains up to 12. The performance of the system with the latter parameters is shown in some of the Figures in Section IIIC.

TABLE V

COMPUTED MISS DISTANCES FOR VARIOUS VALUES OF τ_L AND SYSTEM GAIN

System Gain k_2	τ_L Seconds	Miss Distance Feet	Remarks
1	0.3	73	Sluggish
2	0.3	44	
6	0.3	23	
6	0.03	38	
6	3.0	1.3	
12	0.3	14	Oscillated
18	0.3	24	Oscillated
6	1.0	8.3	Sluggish
6	6.0	3.7	Oscillated
6	12.0	10.5	Oscillated
9	3.0	0.5	

B. Sensor Requirements

Using the system parameters determined in the above runs, the next simulation runs were devoted to examining the sensor requirements. A theoretical analysis of the sensor requirements was undertaken at the same time, and the results of this effort are presented in Section IV.

The sensor transfer function, modeled as three regions, consisted of a linear central region whose slope could be specified, a hard limited (saturation) region in which the output was independent of angle, and a third region beyond the field-of-view in which no signal could be sensed.

Runs made with the linear region having a slope of 1.0 and with the region being wide enough so that the line-of-sight (LOS) never left the linear region duplicated runs made before the sensor was modeled. When the linear region was narrowed, the missile became unstable and went into a maximum-rate turn when the LOS reached the limit region.

Other runs were tried in which a smooth transition between the linear and limit regions was modeled ("soft" saturation). This sensor model did not improve the performance; the missile still went into a maximum-rate turn when the LOS left the linear region. Details of this model and the simulation results are discussed more fully in Section IV.

Other sensor effects studied included variations in the slope of the linear region, small deviations from linearity, and boresight error. In general, it was found that the system will perform with sensor slopes slightly below 1.0, but that there is a definite lower limit to the sensor slope (for specific system parameters) that will yield a stable system. Small variations from linearity can be tolerated provided they do not reduce the slope beyond this critical value at any point. Reasonable boresight errors were found to have a negligible effect; as the range closes, heading errors due to boresight misalignment tend to vanish.

C. Sampling

The requirement for sampling originates in the expected data input to the sensor. Sampling schemes were investigated because the input data itself

might be pulsed. Such cases arise for pulsed radar sensors and for optical sensors which track pulsed laser marks.

The first sampling method which was investigated assumed that sampling of σ_m, the target LOS angle, occurred only in the sensor. The sampling action was simulated as sample-and-hold so that the sensor output remained constant between samples. Simulation runs showed this system to be unstable for low airframe damping although it could provide a stable system for high damping ratios. Figure 18 shows the acceleration profiles for two airframe damping constants for a 1000 ft/sec missile flying against a crossing target moving at 100 ft/sec. For $\zeta = 0.7$, the flight was satisfactory, but the missile oscillated between acceleration limits when ζ was reduced to 0.5 or less.

The system simulation that provided the data in Figure 18 did not include a shaping network. Similar runs were made for systems containing a lead network to determine if the system could be stablized. The results showed the opposite, however. When a network with $\omega_1 = 3$, and $\omega_2 = 15$ was used, the missile oscillated between acceleration limits for all values of ζ tried, including 0.7. The acceleration profile for these latter flights was similar to that shown for $\zeta = 0.5$ in Figure 18.

Analysis of the results of these simulation runs led to the conclusion that for a lightly damped airframe, a system with satisfactory stability is not likely to be achieved with sampling at the sensor. The major difficulty appeared to come from the continuous positive feedback of missile attitude (θ) while the relative line-of-sight angle (σ_m) was sampled. Consideration was then given to sampling schemes that would permit sampling of θ as well as σ_m. Several possible positions for locating samplers in the system were recognized, but in principle they reduced to the two shown as sampler 2 and sampler 3 in Figure 19. (Of course the sensor signal is still in sampled form.) Sampler 2 samples the complete error signal before input to the missile control system. Sampler 3 samples the output of the summing junction that combines θ with σ_m, but permits the function $f(\theta)$ to operate on a continuous basis.

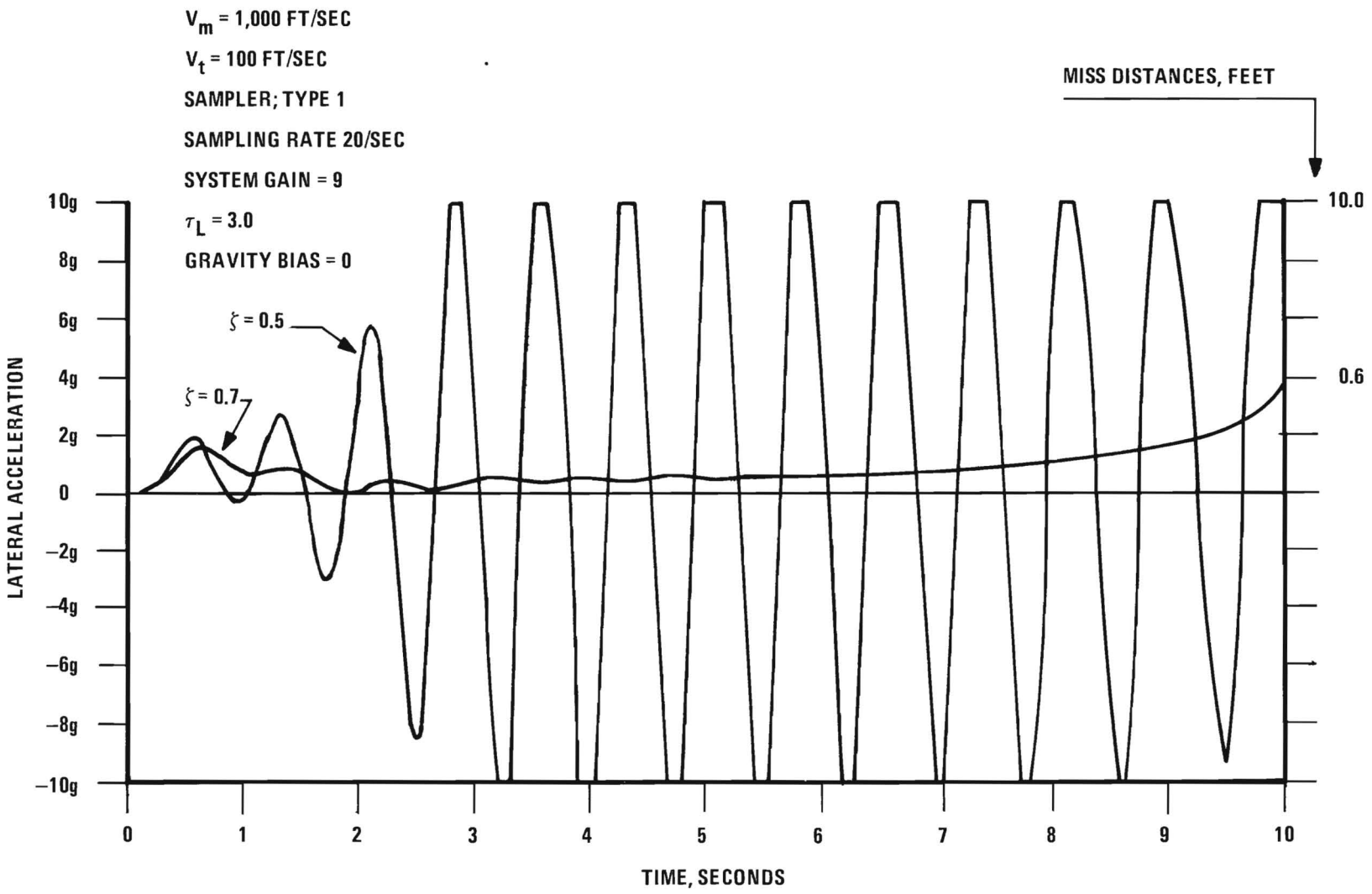

Figure 18. Acceleration Profiles for System with Type 1 Sampler.

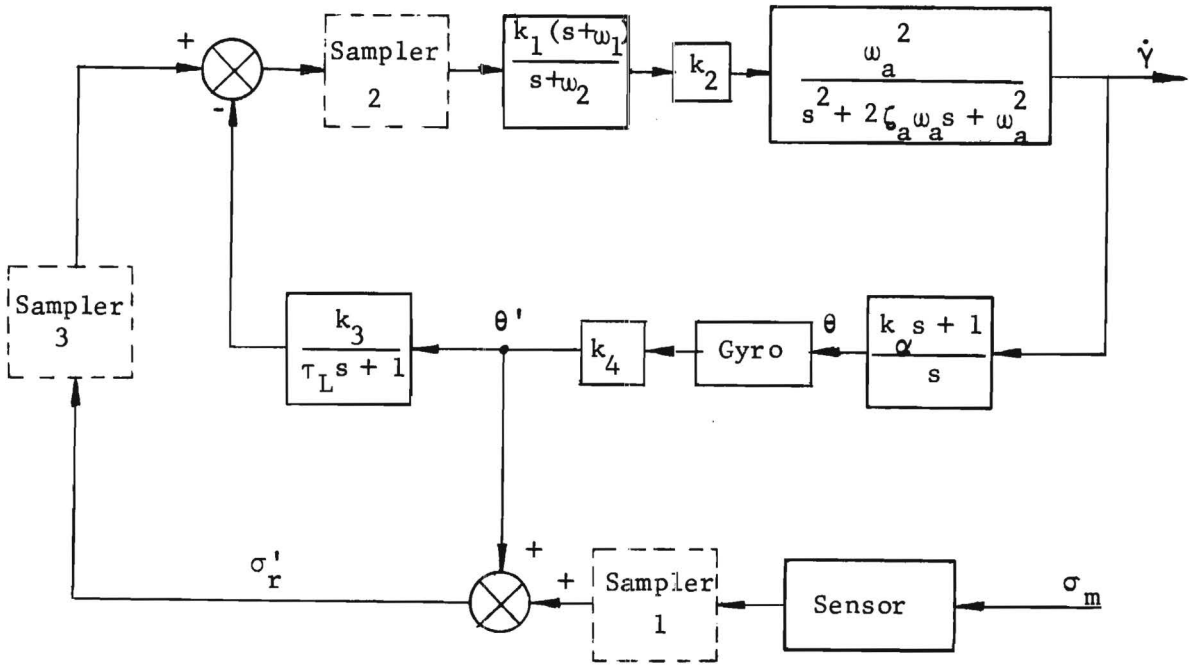

Figure 19. Three Sampler Locations in DLG System.

Both of these schemes were tested with simulation runs, and both were found to provide satisfactory stability and good intercept for sampling rates ranging from 10 to 30 samples per second. A number of runs were made for various values of overall system gain and lag constant τ_L in order to compare the two methods of sampling. The results of these runs showed the two to be essentially equal. When the two were run under identical conditions, their displacement profiles and acceleration profiles did not differ significantly.

Although theoretical analysis indicates that these systems become unstable during the last fraction of a second unless a shaping network is

used, the simulation runs indicated that good intercepts are achieved without the shaping network. Runs in which the compensation network was used showed the missile to be sluggish; also, the computed miss distances were larger.

It appears that the final "instability" might actually be a desirable part of the system. When flying against a crossing target, a dynamic lead guidance system attempts to fly a course somewhere between a pursuit course and a collision course, hence it is lagging with respect to a true collision course. Under these conditions, as intercept is approached, an increase in the turning rate of the vehicle is required, similar to that required by pursuit guidance. However, a properly designed dynamic lead guidance system can keep the required angular acceleration low enough so that intercept occurs. As the missile approaches intercept, it goes unstable with the angular acceleration toward the target increasing at its maximum rate. This high angular acceleration near intercept tends to reduce the miss distance. Use of a lead network to stabilize the missile during this phase of the flight reduces the system gain at the time when maximum response of the system is needed.

To illustrate the general flight characteristics of a sampled data DLG system, the time dependence of several parameters are shown in Figures 20-23. All of these data are for flights in which the missile velocity was 1000 ft/sec and the target was flying a crossing path at 100 ft/sec at an initial range of 1000 ft. The missile was launched horizontally pointed directly at the target which was moving upward. Normal gravity acting on the missile was assumed.

Figure 20 shows the displacement profiles of the missile trajectory for three different values of system gain and τ_L. Figure 21 shows the acceleration profiles for the same three flights, and Figure 22 shows the difference between γ_m, the angle of the missile velocity vector, and γ_{col}, the angle of the collision path as seen from the missile. Figure 23 shows the angle of the line-of-sight to the target relative to the missile axis for the same flights. Note that the maximum LOS angle was less than 10° on all three flights. These maximum angles are typical for flights against 100

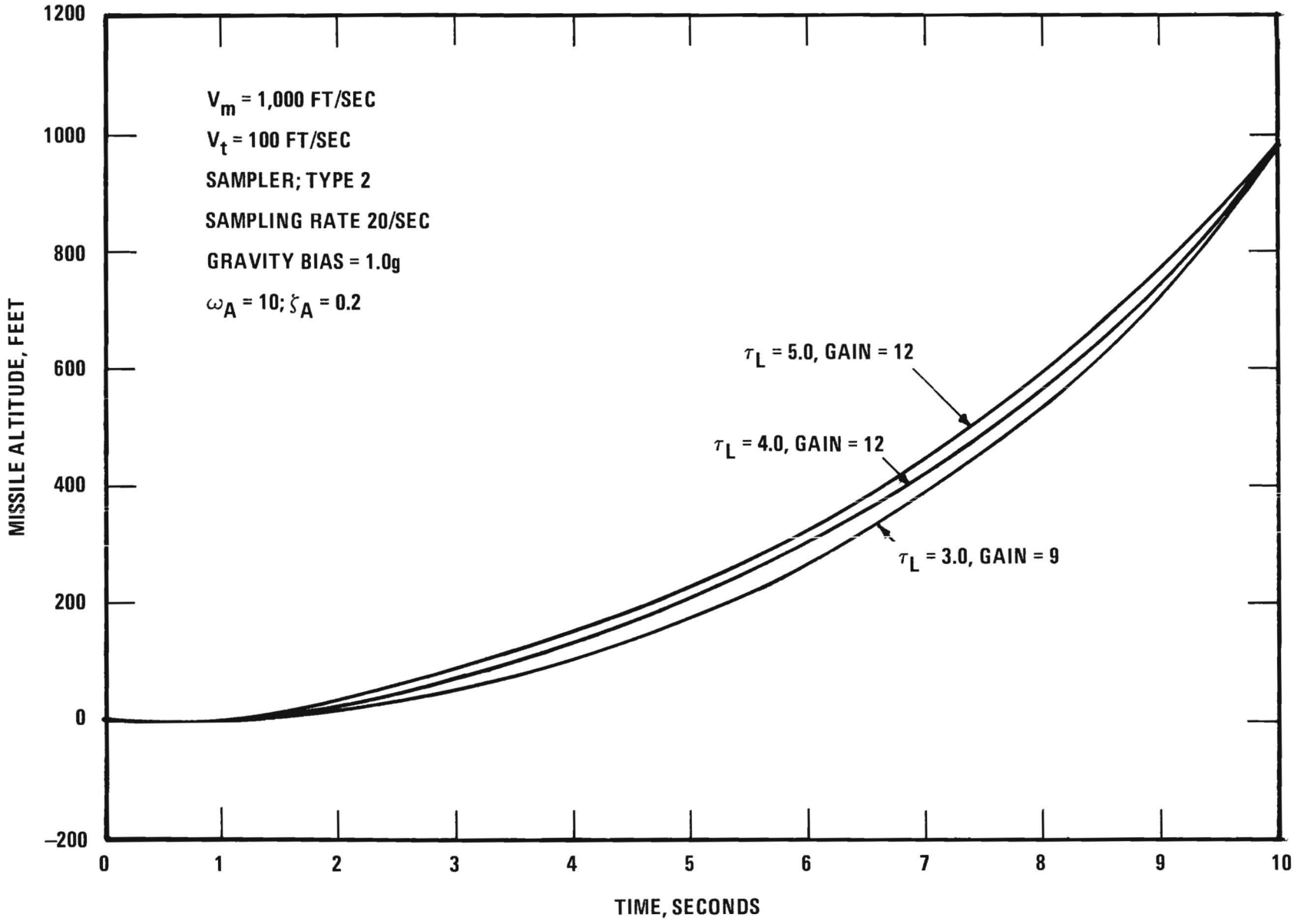

Figure 20. Missile Displacement Profile. Target Moving Vertically in a Straight Line.

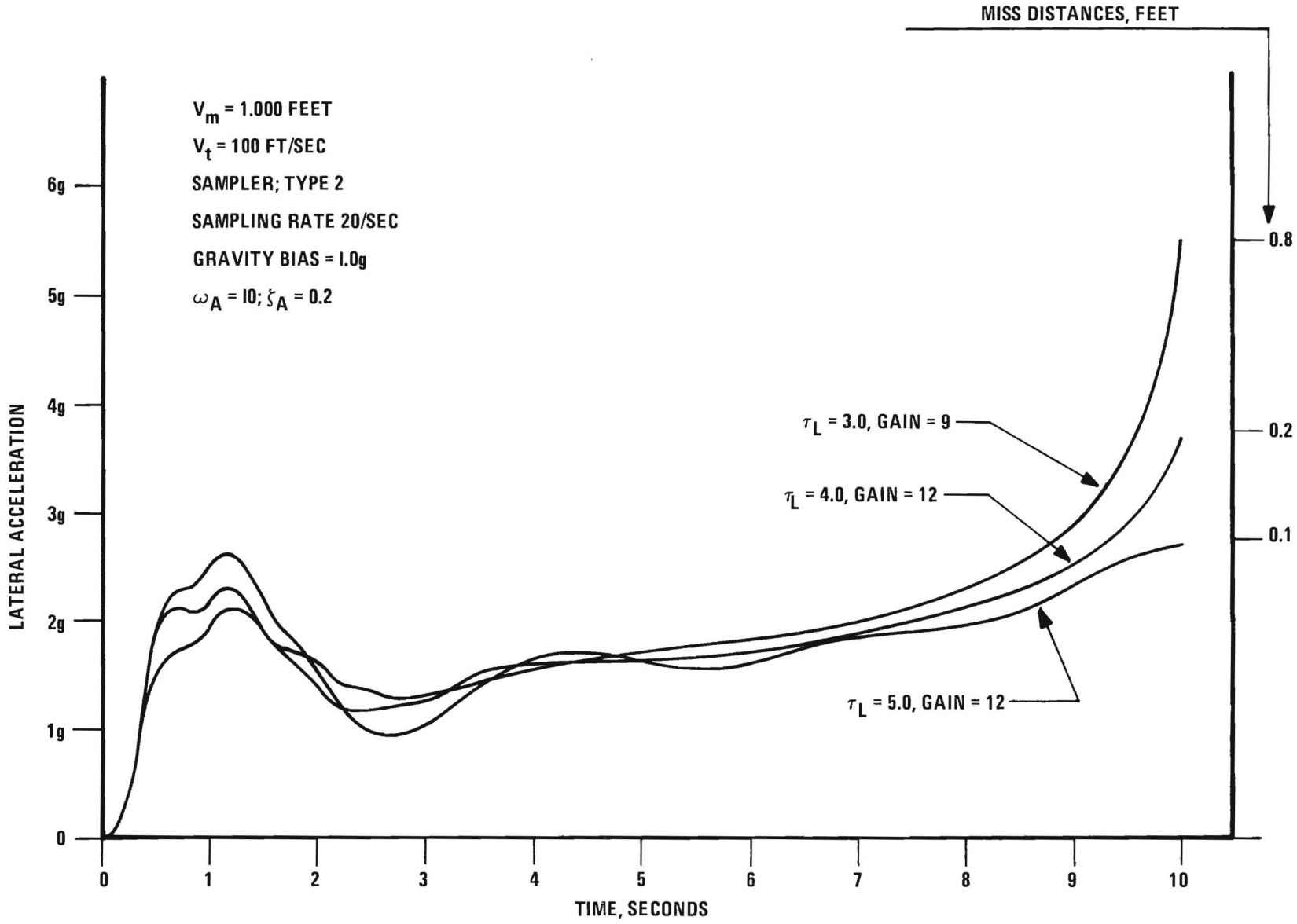

Figure 21. Missile Acceleration Profile. Target Moving Vertically in a Straight Line.

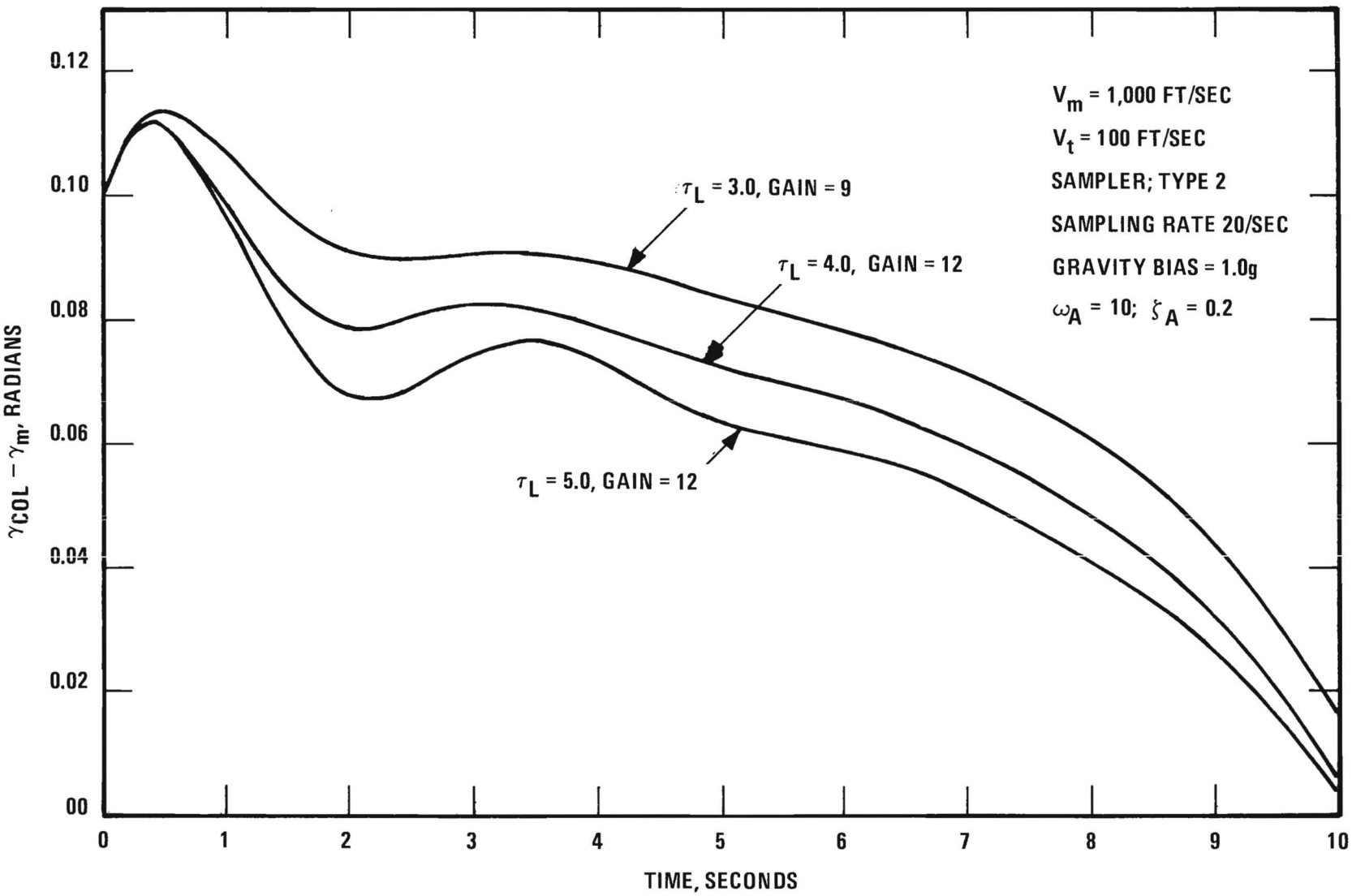

Figure 22. Angular Difference Between Collision Path and Missile Velocity Vector. Target Moving Vertically in a Straight Line.

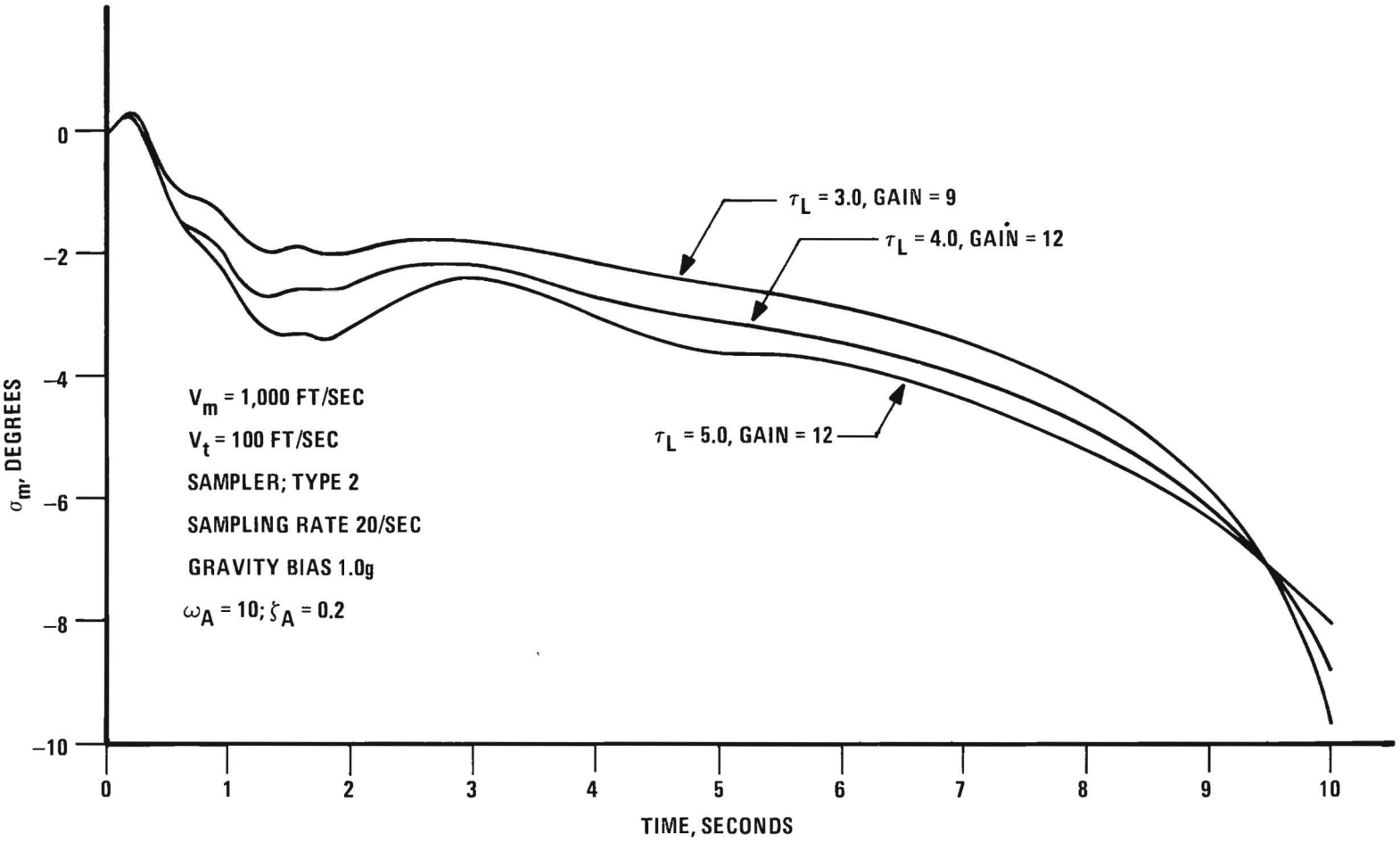

Figure 23. Missile Line-of-Sight Angle. Target Moving Vertically in a Straight Line.

ft/sec crossing targets. Targets flying paths other than 90° crossing paths had smaller maximum LOS angles. For the missile and target velocities simulated, a field-of-view of ±10° is ample for all target paths.

D. Missed Pulses

Using a computer routine to generate pseudo-random numbers, the occurrence of missed pulses on a random basis was simulated. The simulation was used to test the performance of sampled data systems with up to 10% of the pulses missed. The effect on the missile of a single missed pulse was modeled as a continued "hold" in the sample-and-hold network; the network output was held constant until the next valid pulse was received.

Runs were made for sampling rates of 10, 20, and 30 samples per second. The flight profiles differed slightly from those on similar runs with no missed pulses, but the differences were too small to portray graphically. Good intercepts were achieved in each case, with the most noticable effect being a slight increase in miss distance. The miss distances for the three flights are compared with those for flights with no missed pulses in Table VI.

TABLE VI

MISS DISTANCES COMPUTED ON SIMULATED FLIGHTS

Sampling Rate Samples/second	Miss Distance, Feet	
	All pulses present	10% missed pulses
30	-0.047	0.181
20	-0.036	-0.526
10	0.045	0.540

Missile launched horizontally directly at target, V_m = 1000 ft/sec.
Target moving vertically, V_t = 500 ft/sec.

E. Effects of Gravity

A gravitational effect was included in the model; a parameter (G_{bias}) specified the gravitational pull so that runs could be made with or without gravity simulated. Runs in which the missile flight path were approximately horizontal so that gravity was acting perpendicular to the missile axis showed that the effect of gravity did not degrade the performance of the system significantly. With gravity present, the flight trajectory dropped somewhat below that for no gravity, but the control system compensated for the effect and good intercepts were indicated. Figure 24 compares the displacement profiles for two flights that were identical except for the presence of gravity in one and not in the other. A comparison of the acceleration profiles for the same two flights is shown in Figure 25.

F. Target Maneuvers

Although most of the simulation runs were made for crossing targets traveling in a straight line, some runs were made for maneuvering targets. Basically, two types of realistic maneuvers were examined: (1) placing the target in a circular turn, and (2) letting the target decelerate while traveling a straight line. Both maneuvers were examined for values that subjected the target to accelerations well above 1.0 g.

For the turning maneuver, the missile (V_m = 1000 ft/sec) was launched directly at the target which was located at a range of 10,000 feet. The target (V_T = 100 ft/sec) was initially moving at right angles to the LOS, but went into a turn toward the missile at the instant of launch. Target turning rates of 4.5, 9, 18, and 24 degrees/second were simulated; these produced total turns during the flight of approximately 1/8, 1/4, 1/2, and 3/4 of a full circle. Excellent intercepts were achieved with miss distances less than one foot in each case. The 18 degrees/second turn produced the largest miss distance (0.6 feet), with the target moving almost perpendicular to the missile path at intercept. The missile displacement and acceleration profiles for this flight are shown in Figure 26.

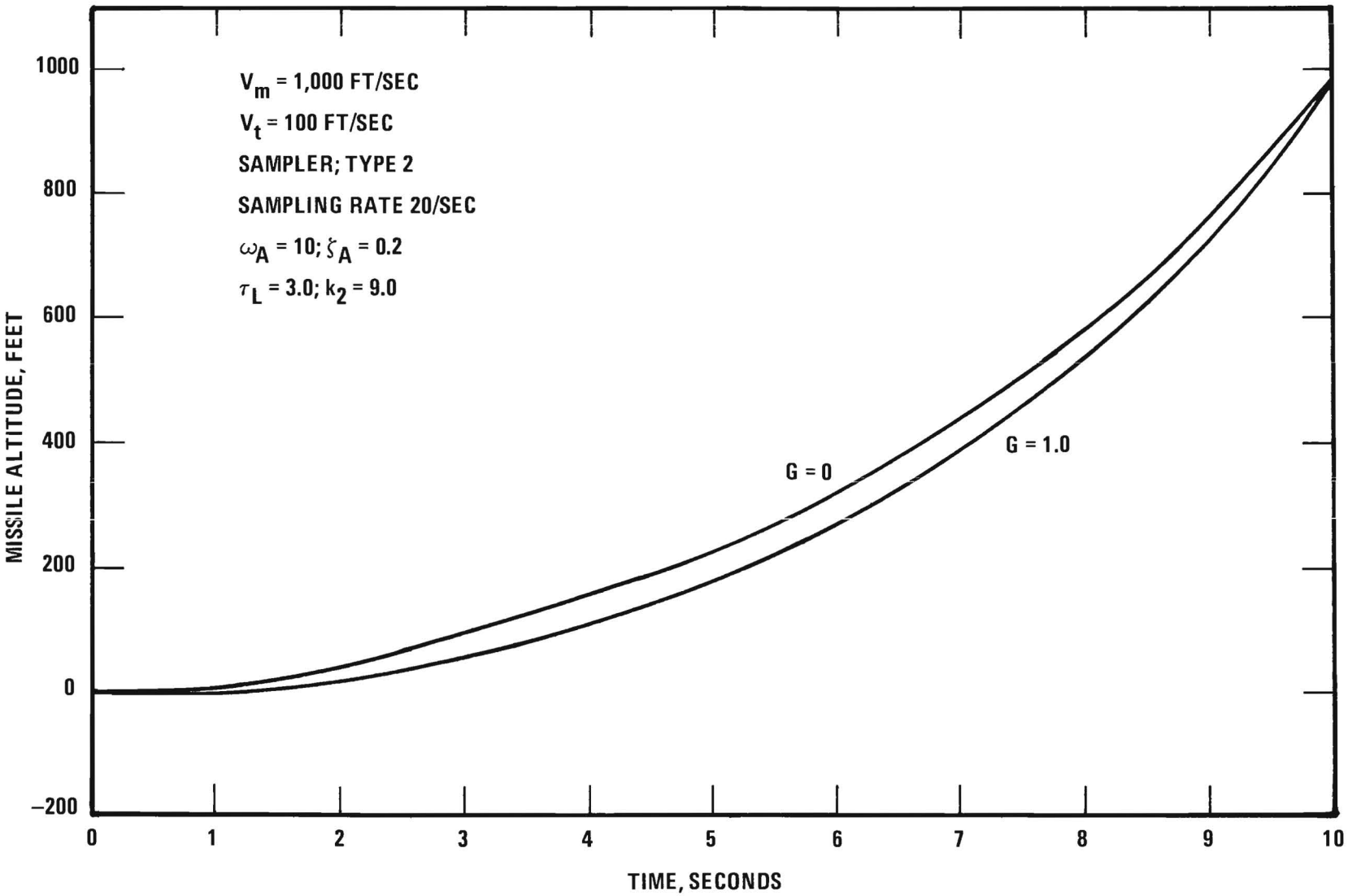

Figure 24. Missile Displacement Profiles With and Without Gravity Bias. Target Moving Vertically in a Straight Line.

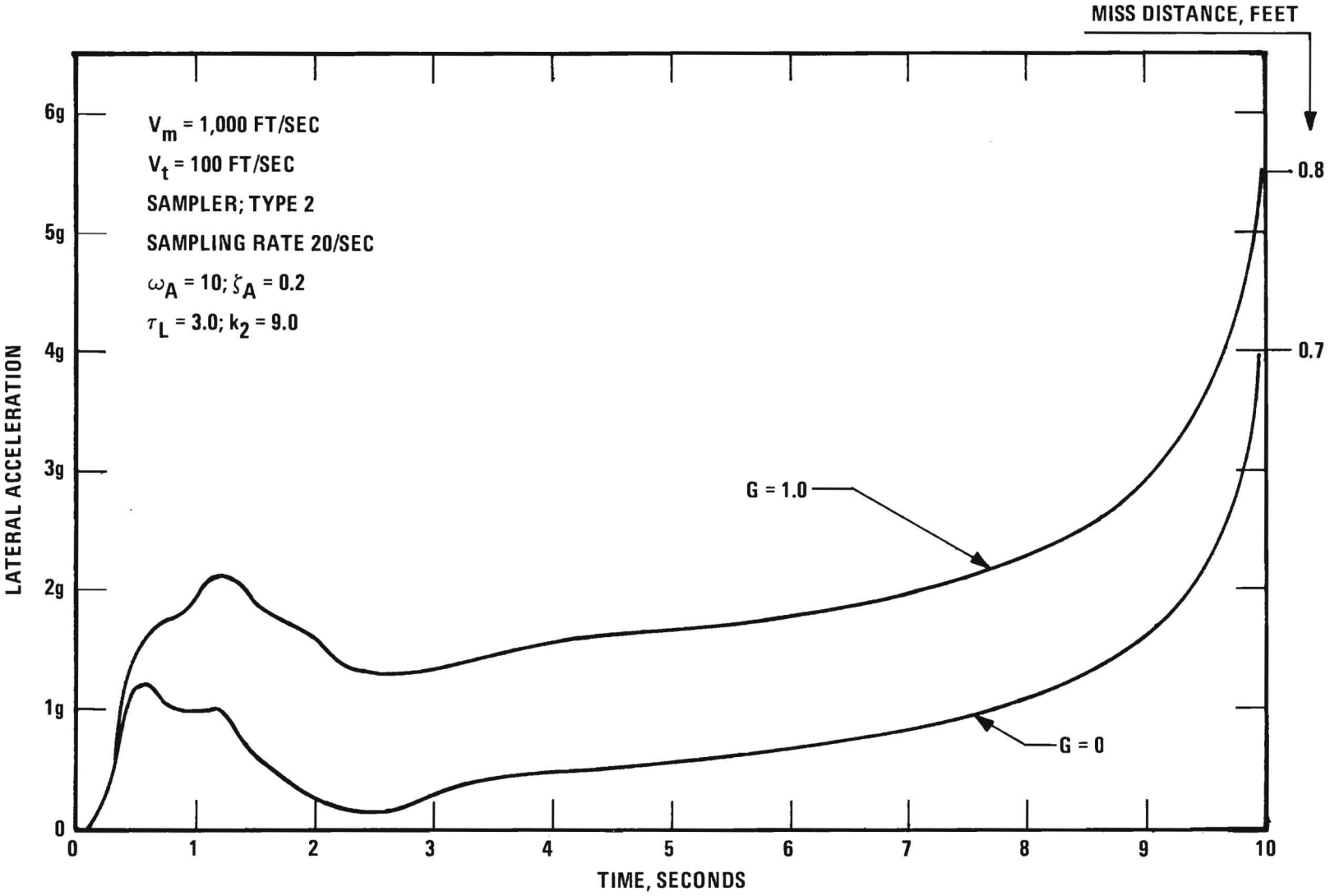

Figure 25. Missile Acceleration Profiles With and Without Gravity Bias. Target Moving Vertically in a Straight Line.

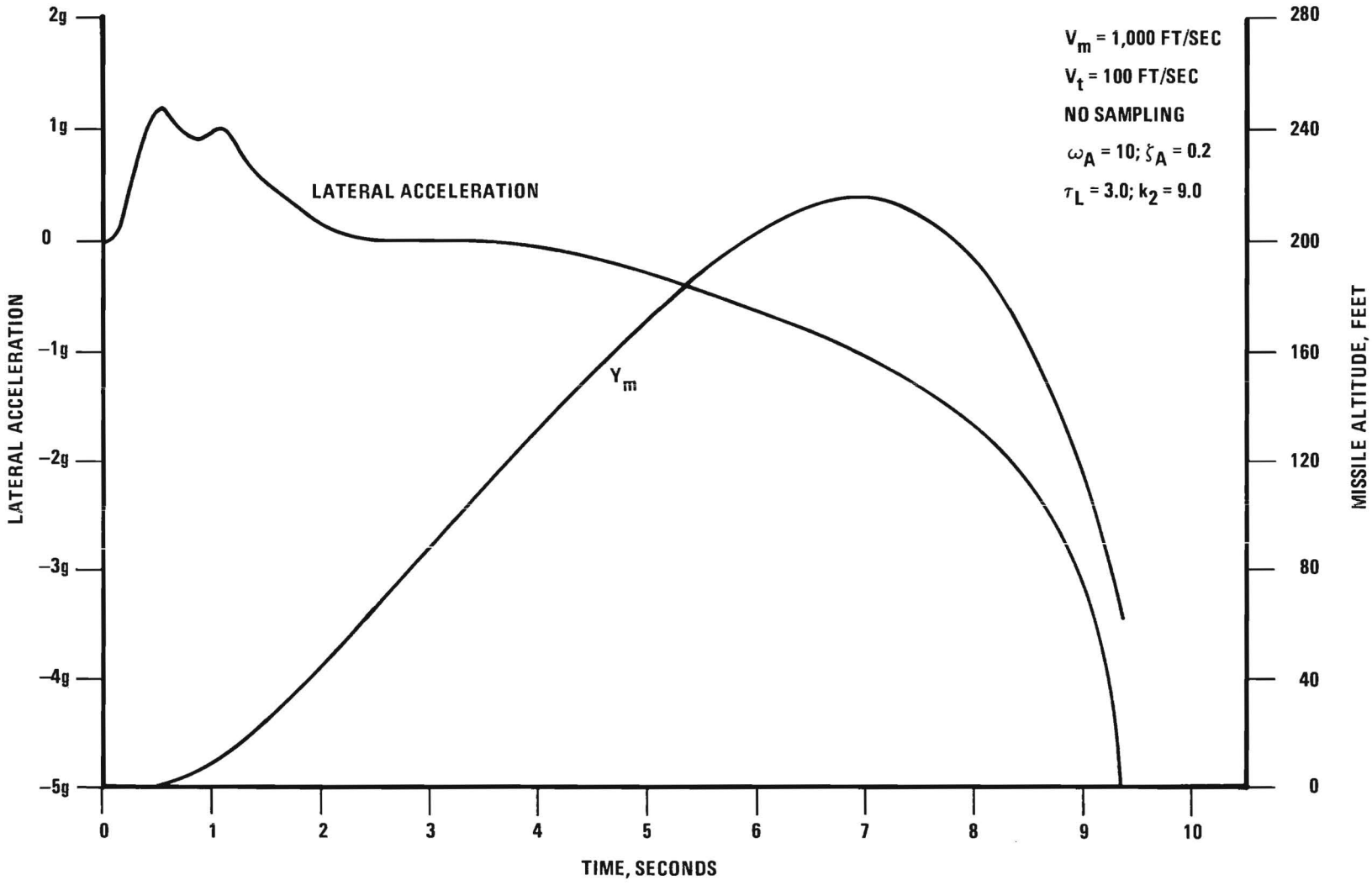

Figure 26. Missile Acceleration and Displacement Profiles for Maneuvering Target. Target Launched Vertically and Turning 18 degrees/sec Towards Missile. Miss Distance 0.6 feet.

For the simulations of deceleration, the target moving on a crossing path at 100 feet/second was subjected to a uniform deceleration beginning at 8.0, 9.0, and 9.5 seconds. These times correspond approximately to 2.0, 1.0, and 0.5 seconds before intercept. For the first two cases the missile responded well and gave good intercepts (miss distances < 0.5 feet) for decelerations of 50 feet/sec^2 (1.5 g). When the deceleration was begun at 9.5 seconds, the missile did not have time to respond completely. The miss distance for a deceleration of 50 feet/sec^2 was 3.7 feet.

G. Cross-Feed

A limited investigation of cross-feed effects was made early in the program using the three-dimensional simulation of a proportional lead guidance system, rather than DLG, with a strapdown seeker. These studies showed that a moderate rate of cross-feed between the two channels of a homing missile does not pose any serious problem. Any error introduced in one channel due to cross-feed from another is largely overcome by the tracking response of the victim channel.

Figure 27 shows the lateral acceleration profiles for the horizontal and vertical planes for the first second of a simulated flight with 10% cross-feed between channels. For this flight, the target was simulated as traveling a crossing path in the horizontal plane at 500 feet/second. The missile was launched in the horizontal plane so that initially there was no error signal present in the vertical channel. The horizontal acceleration immediately rose to the limit imposed on the missile (10.6 g in each plane, giving 15.0 g total). Cross-feed to the vertical channel produced acceleration in the vertical plane, but the vertical channel immediately responded to try to null the error (note that the ordinates for the two curves are scaled differently). The initial oscillations in the vertical channel are largely attributed to the high seeker response frequency (300 radians/second) used in the simulation. At the end of one second the error in the vertical channel had been reduced to a negligible value and remained low during the rest of the flight. The simulation indicated intercept with a calculated miss distance of 0.3 feet.

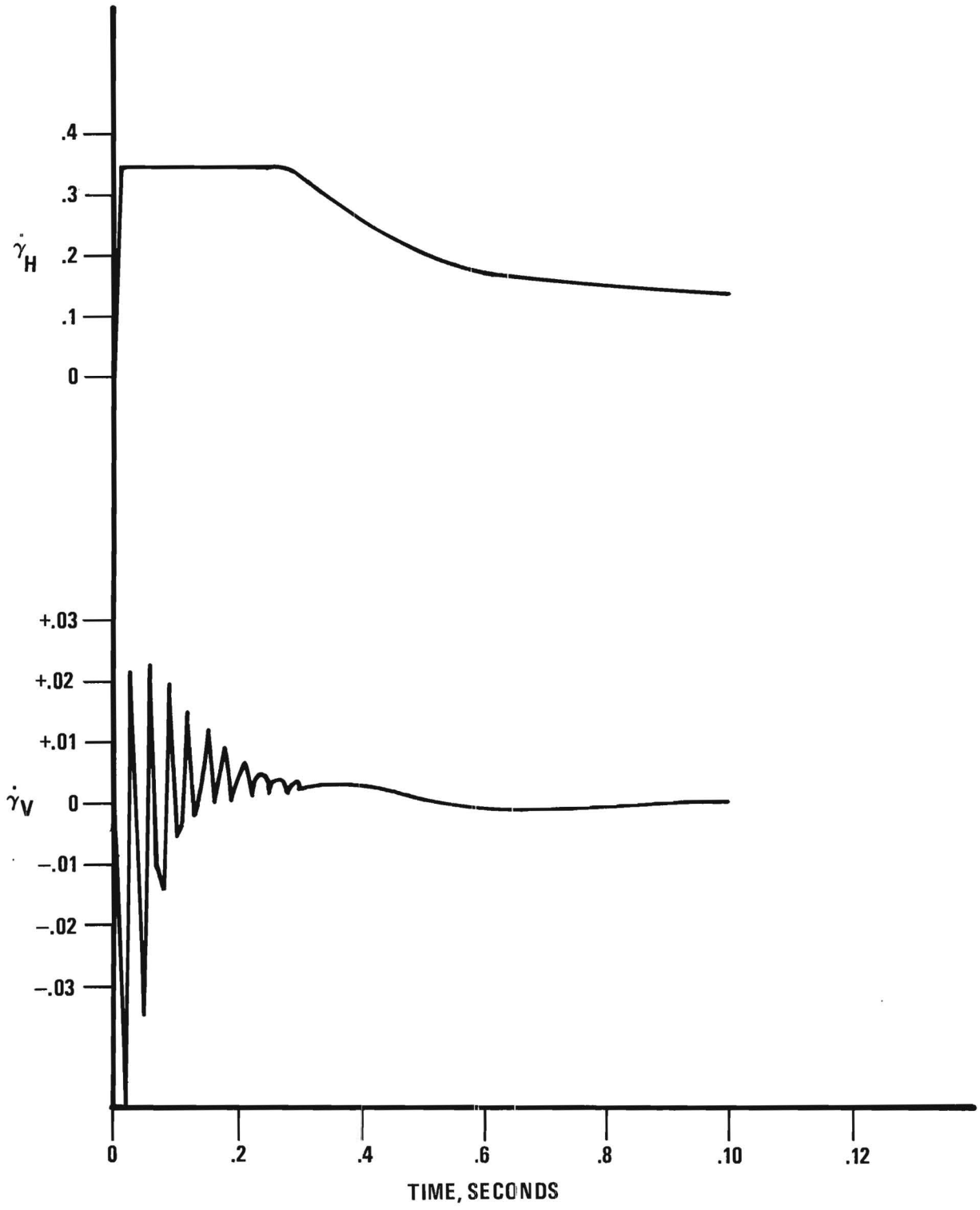

Figure 27. Angular Velocity in Horizontal and Vertical Planes for Target Positioned in Horizontal Plane, Crossfeed 0.1.

H. Gyroscope Feedback

Implementing DLG requires feedback of the missile attitude angle θ. Theory decrees that ideally the feedback rate should be unity. The precision with which this feedback rate must be accomplished in a real system is important, so an investigation of the feedback accuracy requirements was made. A constant, k_4, was introduced as a multiplier of the gyro output in the simulation, and runs were made for values ranging from 0.9 to 1.1. Computed outputs show that varying k_4 produces an effect almost analogous to varying overall system gain. Lowering k_4 from 1.0 tends to make the system sluggish and increase the miss distance. Raising k_4 above 1.0 tends to make the system more oscillatory but reduces miss distance. Table VII lists the computed miss distances for five values of k_4. These values show that the feedback rate is not so critical that a high degree of precision is required in designing gyroscope feedback loop gain.

TABLE VII

MISS DISTANCES FOR VARIOUS GYROSCOPE FEEDBACK RATES

Gyro Output Multiplier k_4	Computed Miss Distance feet
0.9	2.0
0.95	1.2
1.0	0.6
1.05	0.3
1.1	0.2

IV. SENSOR REQUIREMENTS

A. Nonlinear Sensor Characteristics Problem

The linearity requirements for sensors used in a tactical missile employing Dynamic Lead Guidance (DLG) are investigated in this section of the report. Earlier sections have shown by both theoretical analysis and digital computer simulation that DLG parameters can be chosen so that the guidance system performs well in comparison with the "Proportional Navigation" guidance concept when all components are ideal. Typical strapped-down sensors available for use with DLG have input-output characteristics as shown in Figure 28. In addition to local variations, the sensor characteristic is seen to have a pronounced saturation effect for larger magnitude inputs. As will be shown, this saturation has a significant effect upon the stability of a missile using Dynamic Lead Guidance. The effects of saturation upon the performance of DLG have been investigated and are presented in this section.

In order to investigate the effect upon DLG of sensor saturation, the digital simulation described earlier was modified so that the sensor was modeled as being ideal except for the existence of (hard) saturation or limiting. This model is as given in Figure 29. Simulation runs were made with various values for the linearity limit, L, between one and twenty degrees. In each case where the sensor input reached the linearity limit, the guidance system went hard-over in an unstable turn away from the target. Further runs were made with the hard saturation sensor model replaced with a "soft" saturation as in Figure 30; i.e., with a model in which a smooth curve is used to model the saturation in the sensor. As was the case for hard saturation, the soft saturation model for the sensor resulted in an unstable guidance system with the missile going into a hard turn away from the target.

Since either sensor saturation model leads to instability, one might suspect that the equivalent "gain reduction" associated with saturation might be the destabilized factor. To test this idea, the sensor was modeled with another nonlinear characteristic, the anti-saturation curve as shown in Figure 31. This characteristic is a reflection about the $\sigma_{out} = \sigma_{in}$

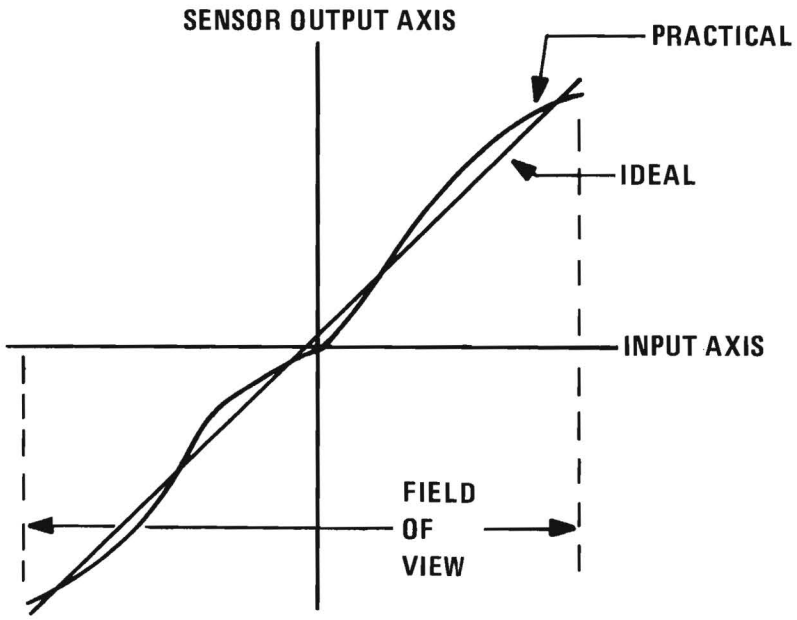

Figure 28. Typical Sensor Characteristics.

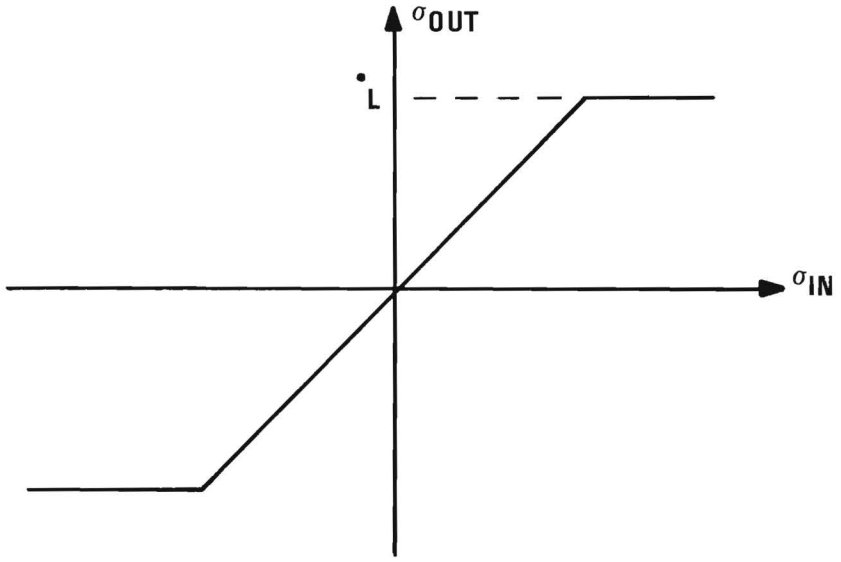

Figure 29. Sensor Characteristics Model with Hard Limiting.

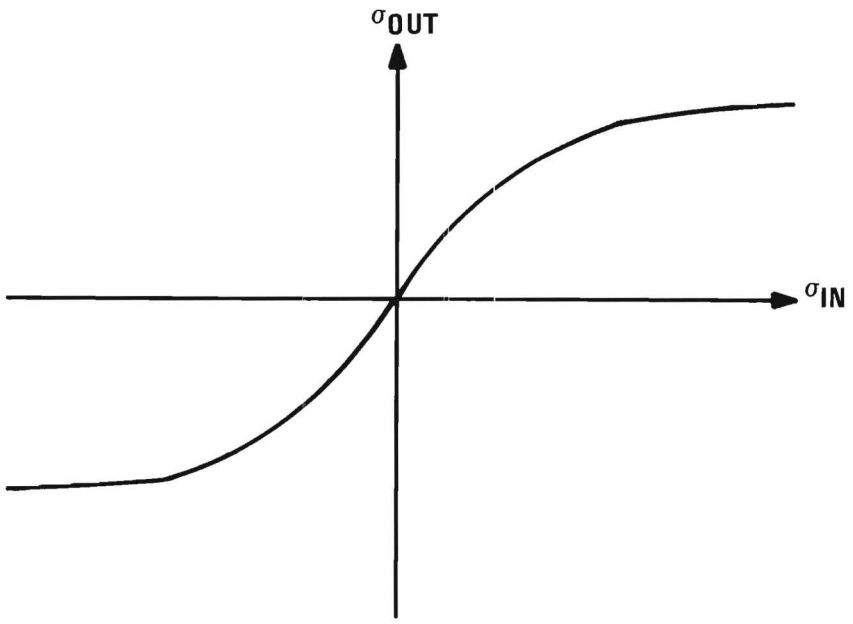

Figure 30. Sensor Characteristics Model with Soft Saturation.

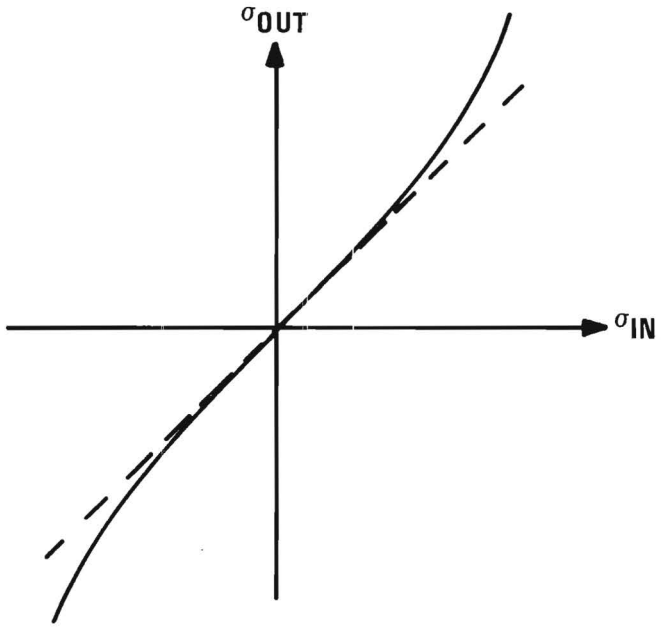

Figure 31. Sensor Characteristics Model with Soft Anti-Saturation.

line of the soft saturation characteristic. The simulation run which used this anti-saturation sensor model was stable although the resulting miss distance was greater than for a linear sensor model.

B. Elementary Stability Analysis

A practical "feel" for the DLG stability problem resulting from saturation in the sensor characteristic curve can be gained from a steady state analysis of the block diagram of the system which is repeated here as Figure 32. Consider the missile-target situation described in Figure 33. Assume that at launch the missile was pointed at a target which is moving cross-range with velocity V_T. The built-in lead in the DLG system will result in the missile turning so that its center-line is pointing ahead of the current target position. Observe from the block diagram in Figure 32 that the driving signal for DLG is based upon σ_R' , (the missile's approximated value of σ_R, the line-of-sight angle relative to the reference direction). The missile-referenced line-of-sight angle, σ_m, and the missile attitude, θ, are combined in the guidance calculations to estimate σ_R according to

$$\sigma_R' = \theta + \sigma_m \ . \tag{8}$$

Consider now the effect of saturation in the sensor; suppose the sensor output magnitude is σ_L rather than the actual value of σ_m. Then, for Figure 33 geometry, the estimated value of reference line-of-sight angle, σ_R' and the guidance system will react as if it had a smaller lead angle built up than desired. In its attempt to further increase the lead angle, the guidance system is seen to turn the missile further and further away from the target.

The basic problem to be treated, now that the simulation and intuition have shown that some nonlinear sensor characteristics are unsatisfactory for use with DLG, is that of establishing sensor characteristic requirements for a stable DLG system. The methods or tools available for the stability analysis of a nonlinear control system include Phase Plane analysis, Lyapunov theory, Describing Function theory [2], and the Popov Criteria [3]. The phase

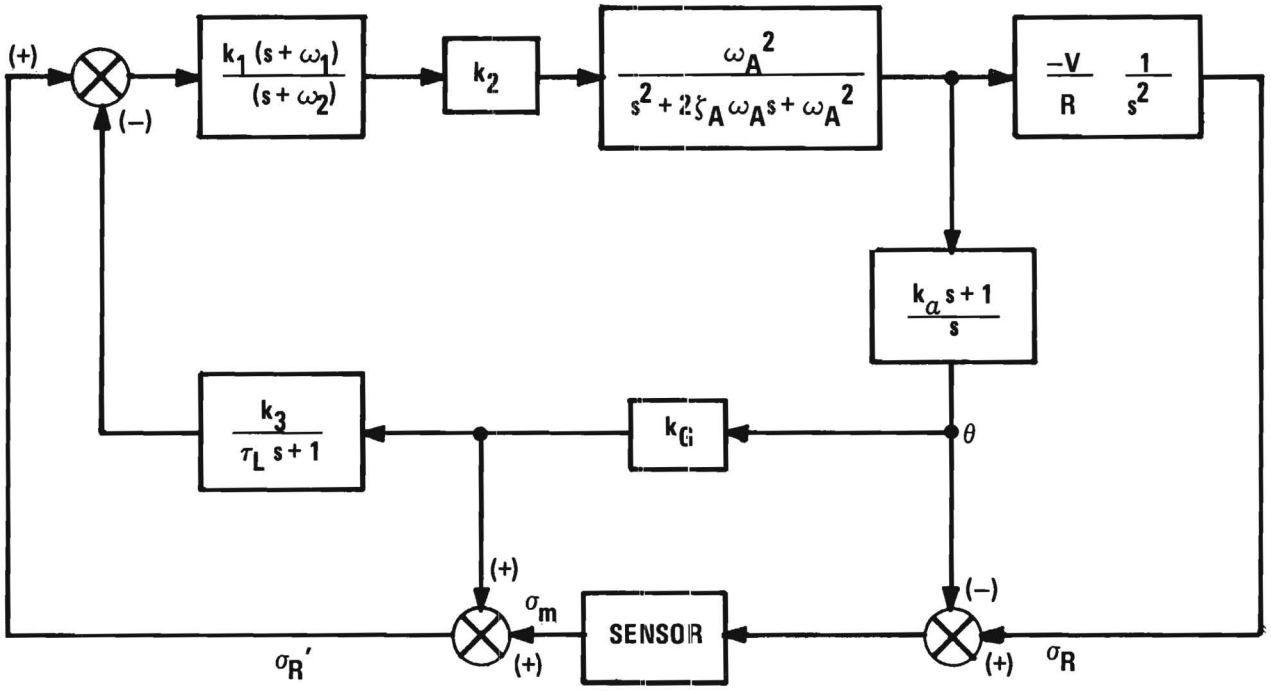

Figure 32. DLG Block Diagram.

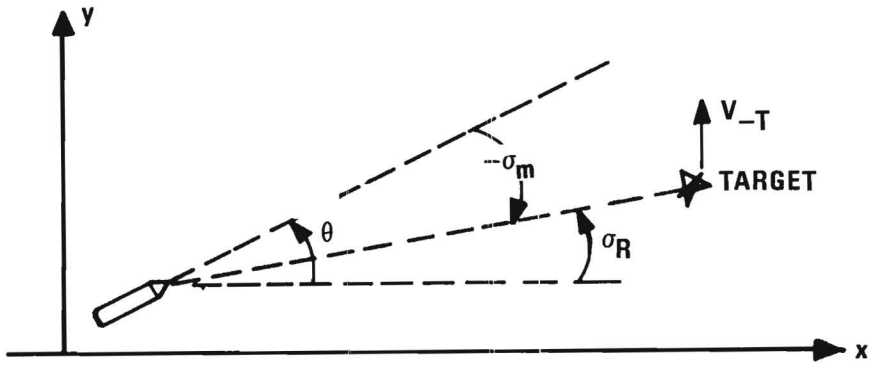

Figure 33. Flight Geometry.

plane method is useful for lower order systems and not of value here; Lyapunov's second method is powerful but difficult to apply. Popov's criteria would seem ideal at first glance since it establishes a region in the characteristic plane for which the system is stable; unfortunately, however, the system to be analyzed here is open-loop-unstable so that Popov's criteria is not applicable.* In the next section, the Describing Function method is applied to the nonlinear sensor problem.

C. Stability Analysis by the Describing Function Method

The Describing Function method is based upon the low-pass (frequency) nature of control systems. The nonlinearity in the control system model is replaced by an "equivalent" transfer function which is dependent upon the magnitude of the signal into the nonlinearity. The transfer function used is based upon the fundamental component of the Fourier series of the nonlinearity output for a sinusoidal input signal.

The describing function, or "equivalent transfer function," for the hard saturation nonlinearity given by Figure 29 is shown by Thaler and Pastel [2] to be an equivalent gain given by

$$K_D = \frac{2}{\pi}\left[\sin^{-1}(Q) + Q\sqrt{1 - Q^2}\right];\ 0 < Q < 1, \tag{9}$$

where Q is the ratio of the magnitude of the input signal to the saturation level. Figure 34 is a plot of the equivalent gain vs. magnitude of the saturation nonlinearity input. It can be seen from Figure 34 that an input twenty percent greater than the saturation knee gives an equivalent gain of 0.925 as compared to unity gain for no saturation.

The Describing Function stability analysis of the DLG system with a nonlinear sensor will be accomplished by considering the sensor to be an unknown gain. Conventional linear system analysis tools such as Bode and Nyquist plots, root locus plots, and the Routh-Hurwitz criteria may then be used to establish the range of equivalent sensor gains for which the guidance system is stable. This information in turn establishes the degree

---

*Page 367 of Hsu and Meyer [3].

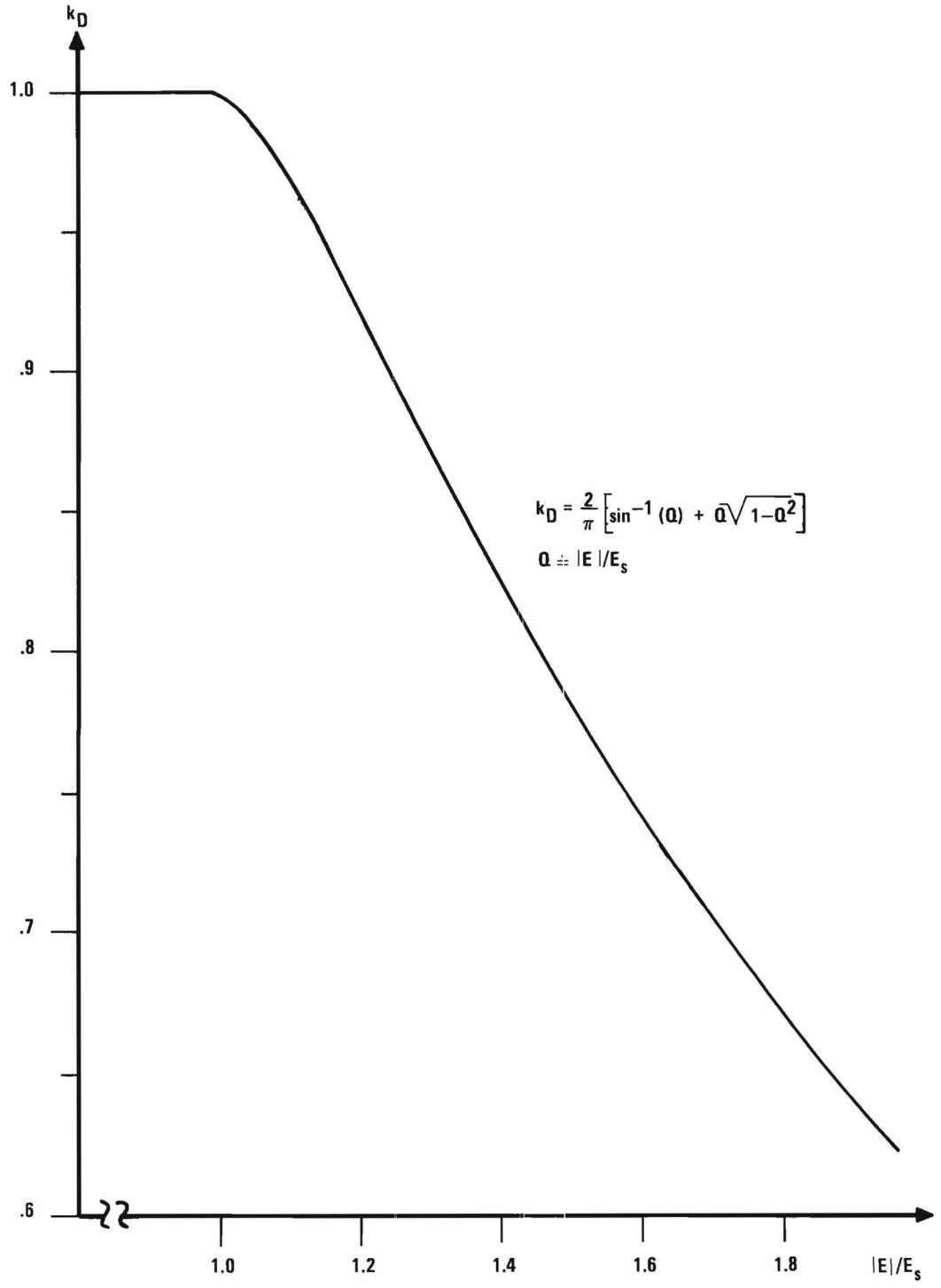

Figure 34. Describing Function for a Saturation Nonlinearity.

of saturation allowable in the sensor characteristic. Although the linear system is time-varying in that the range, R, is varying with time, the analysis will be made for various fixed values of range. The results will then be verified by comparison of the critical gain value with simulation results.

The Bode and Nyquist plots required for the Describing Function analysis must be for the loop opened at the sensor position; i.e., the loop gain to be varied in the analysis is to be the sensor "equivalent gain." The system block diagram shown in Figure 32 can be rearranged using normal block diagram algebra* to appear as in Figure 35. The inner feedback loop is then further reduced by block diagram algebra so that the diagram can be drawn as in Figure 36. The function $G_1(s)$ found by block diagram reduction is given by

$$G_1(s) = \left\{\left[K_1K_2\ \omega_A^2\ (s + \omega_1)\ s\ (\tau_L s + 1)\right]\ \left[(s^2 + 2\zeta_A\omega_A s + \omega_A^2)\right.\right.$$

$$\cdot(s + \omega_2)s(\tau_L s + 1) + K_1K_2\omega_A^2\ (s + \omega_1)\ K_G(K_\alpha s + 1)$$

$$\left.\left.\cdot(K_3 - \tau_L\ s - 1)\right]\right\}\ . \qquad (10)$$

The open loop transfer function (as seen from the sensor location) required for the describing function analysis then is given by

$$HG = K_p \cdot G_1(s) \cdot H(s) \qquad (11)$$

where

K_p = "equivalent sensor gain,"

$H(s) = (K_\alpha s^2 + s + \frac{V}{R})/s^2$, and

$G_1(s)$ is as defined above.

Before Bode and Nyquist plots of this open-loop transfer function may be interpreted as to system stability, the number of poles of the open-loop transfer function in the right half plane, if any, must be determined. The Nyquist criteria, for example, determines the difference in the number of

*Page 367 of Del Toro and Parker [4].

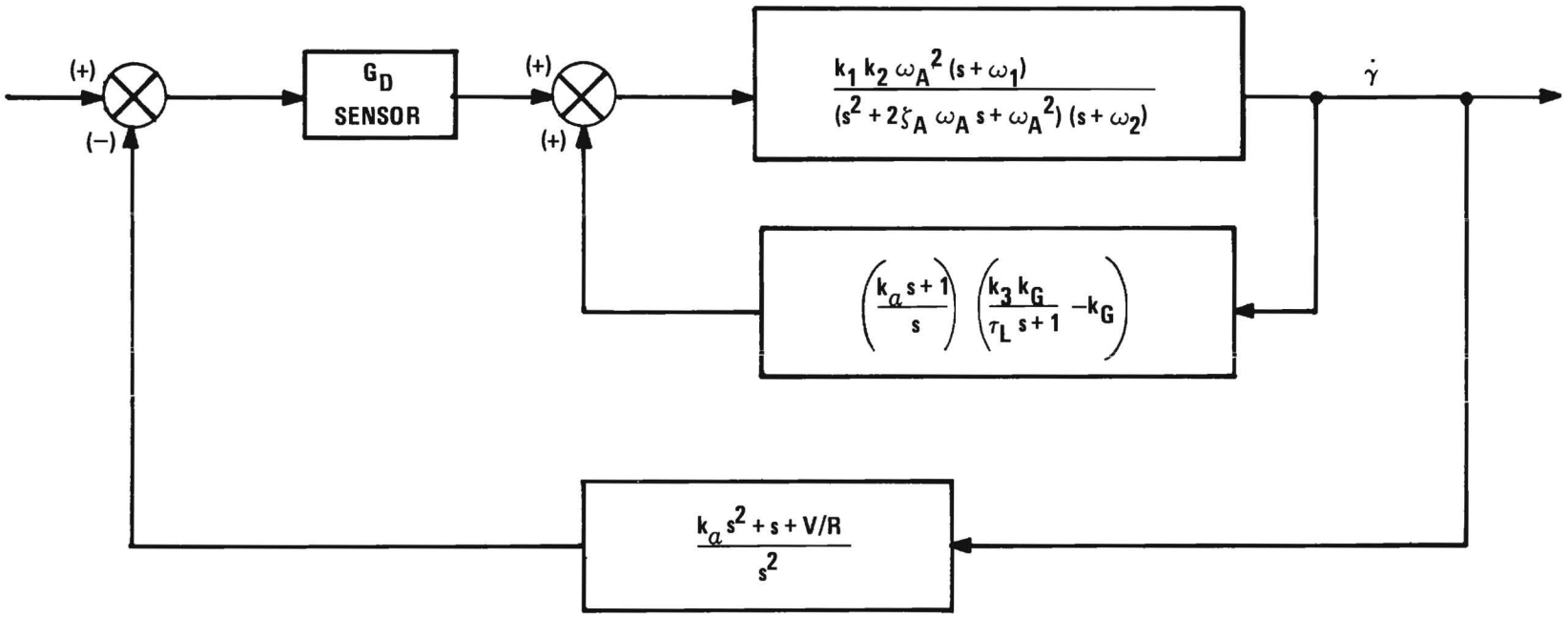

Figure 35. DLG Block Diagram for Describing Function Analysis.

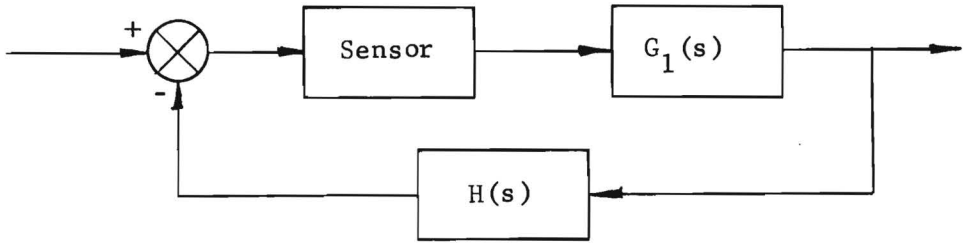

Figure 36. Generalized Block Diagram of Describing Function Analysis.

poles and zeros of the closed loop transfer function in the right-half-plane. Since the open loop poles are the closed loop zeros, the Nyquist criteria determines the difference between the number of closed loop poles and open loop poles (in the right-half-plane).

Since H(s) is seen to contain no right-half-plane poles, any unstable poles of the open loop transfer function must be poles of $G_1(s)$. The form of $G_1(s)$ is such that one cannot tell by inspection whether or not it contains any unstable roots; the Routh-Hurwitz criteria will be applied to establish the number of unstable roots of $G_1(s)$. For this test, typical parameter values given in Table VIII will be used. For this set of parameters the transfer function reduces to

$$G_1(s) = \left\{ \frac{900(3s + 1)}{(3)s^3 + (43)s^2 - (1036)s - 2600)} \right\} , \qquad (12)$$

which is seen to contain at least one unstable pole since there is a variation of coefficient signs in the denominator polynomial.

Application of the Routh-Hurwitz test [4] to the denominator polynomial of $G_1(s)$ results in the following array given in Table IX. Since there is one change in sign among the first column in the array, there is known to be exactly one unstable pole contained in $G_1(s)$, at least for the typical

TABLE VIII

TYPICAL DLG PARAMETERS

$\tau_L = 3$	$\omega_1 = 1$	$\omega_2 = 1$	$k_3 = 1$
$K_s = 1$	$K_2 = 9$	$K_1 = 1$	$K_\alpha = 0.5$
$\omega_A = 10$	$\zeta_Z = 0.7$		

TABLE IX

ROUTH-HURWITZ ARRAY

3	-1036	0
43	-2600	0
-12,249	0	0
-2,600	0	0
0	0	

parameters used. Actual solution for the poles of $G_1(s)$ verified the Routh-Hurwitz result. For the aforementioned parameters, one has

$$G_1(s) = \left\{ \frac{300(3s + 1)}{(s - 14.23)(s - 26.25)(s - 2.33)} \right\} . \qquad (13)$$

It is concluded that for these typical parameters the open loop transfer function has one pole in the right-half-plane: unless the characteristics of the total system Nyquist plot change suddenly for a small change in these parameters, it will be assumed for this study that the open loop transfer function contains one unstable pole for all parameter values of interest. Thus the Nyquist criteria at the sensor location will require one encirclement of the critical point for stability of the missile using DLG.

For the actual preparation of the Bode and Nyquist plots, a digital computer program was developed which calculates the complex function $HG(j\omega)$ for a range of frequencies and plots $HG(j\omega)$ as both a Bode plot and a Nyquist plot. The plotting is performed with Georgia Tech's CAL-COMP plotter and the digital program is presented and described in the Appendix.

Figures 37 through 40 are the Bode and Nyquist plots of the guidance system (as seen from the sensor location) for values of range, R, from 10,000 ft. down to 100 ft. The parameters used for this group of runs are given in Table X.

The interpretation of these Nyquist plots (from the sensor) requires construction of the complete Nyquist locus for one example; the closure can be mentally visualized for the other range values. The Nyquist plots come from the computer/CALCOMP showing HG(s) for a finite range of positive frequencies as shown in Figure 41b. The next step in the development of the complete HG(s) locus for the Nyquist path shown in Figure 41a is the drawing of the negative frequency portion (mirror image of real frequency portion) as shown in Figure 41c. Evaluation (analytically) of the limit of $HG(j\omega)$ as ω approaches zero shows that the locus approaches infinity along a path parallel to the positive real axis; this same information is available from the Bode plots. The Nyquist locus is completed (Figure 41d) by adding the complete circle at infinity which corresponds to the small semicircle near the origin in the s-plane as shown in Figure 14a.

Encirclements will be counted as positive when clockwise [4]. The encirclements of the critical point (-1 + j0 in the HG plane) are related to stability in that

$$N = Z_r - P_r \tag{14}$$

where N is the number of encirclements, Z_r is the number of zeros of (1 + HG) in the right-half-plane (Z_r must be zero for stability), and P_r is the number of poles of 1 + GH(s), or of HG(s), in the right-half-plane. Since there is known to be one unstable root in the open loop

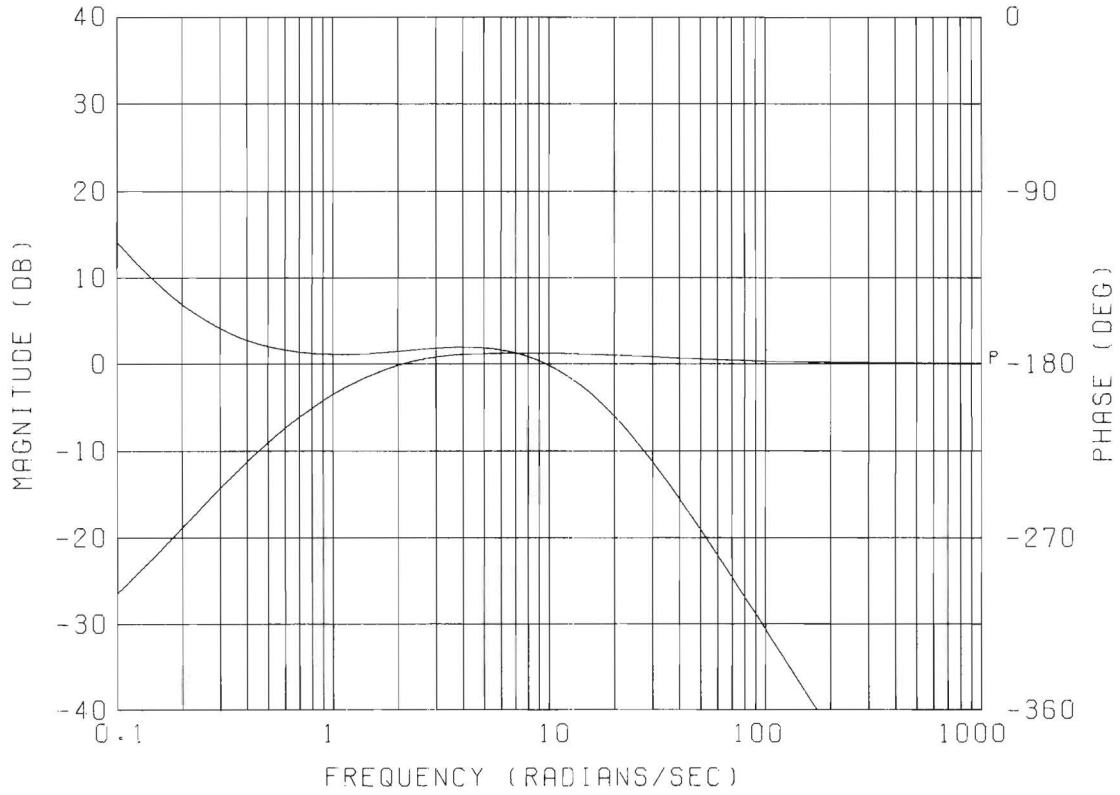

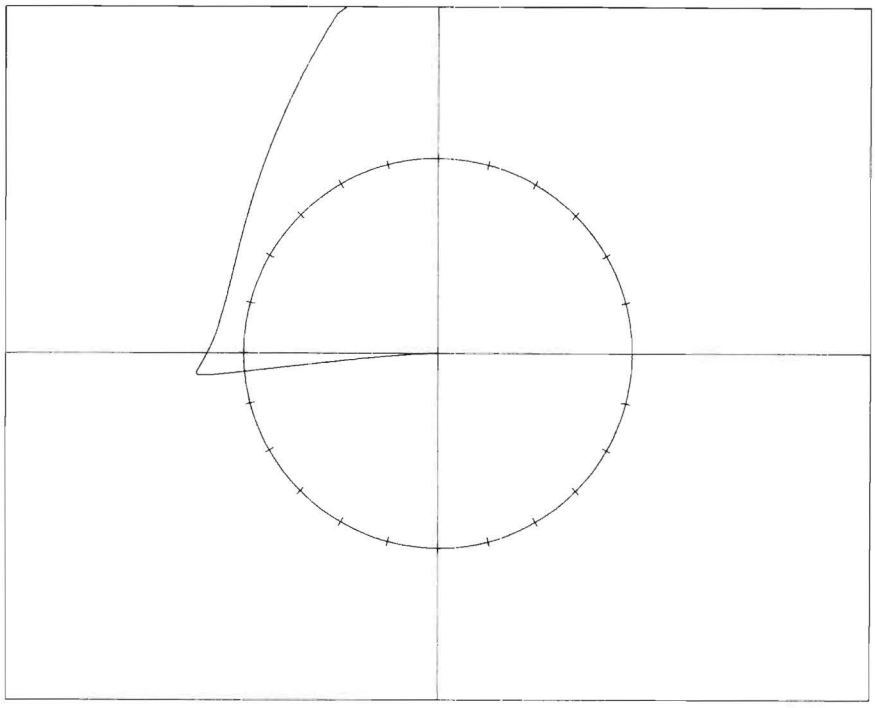

NYQUIST PLOT

Figure 37. Nyquist and Bode Plots for Describing Function Analysis of DLG System with τ_L = 3.0, k_2 = 6.0, and R = 10,000 feet.

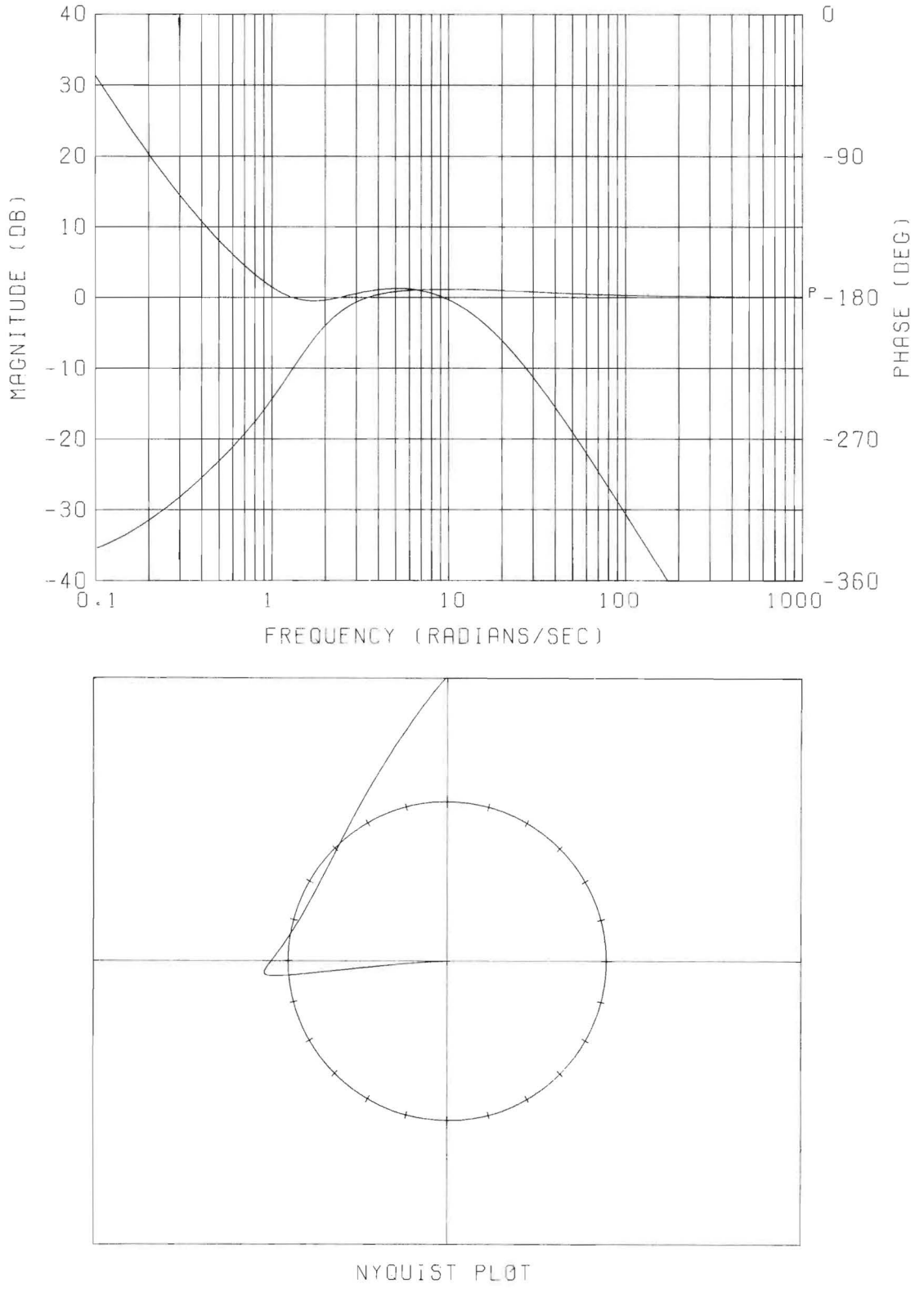

Figure 38. Nyquist and Bode Plots for Describing Function Analysis of DLG System with τ_L = 3.0, k_2 = 6.0, and R = 1,000 feet.

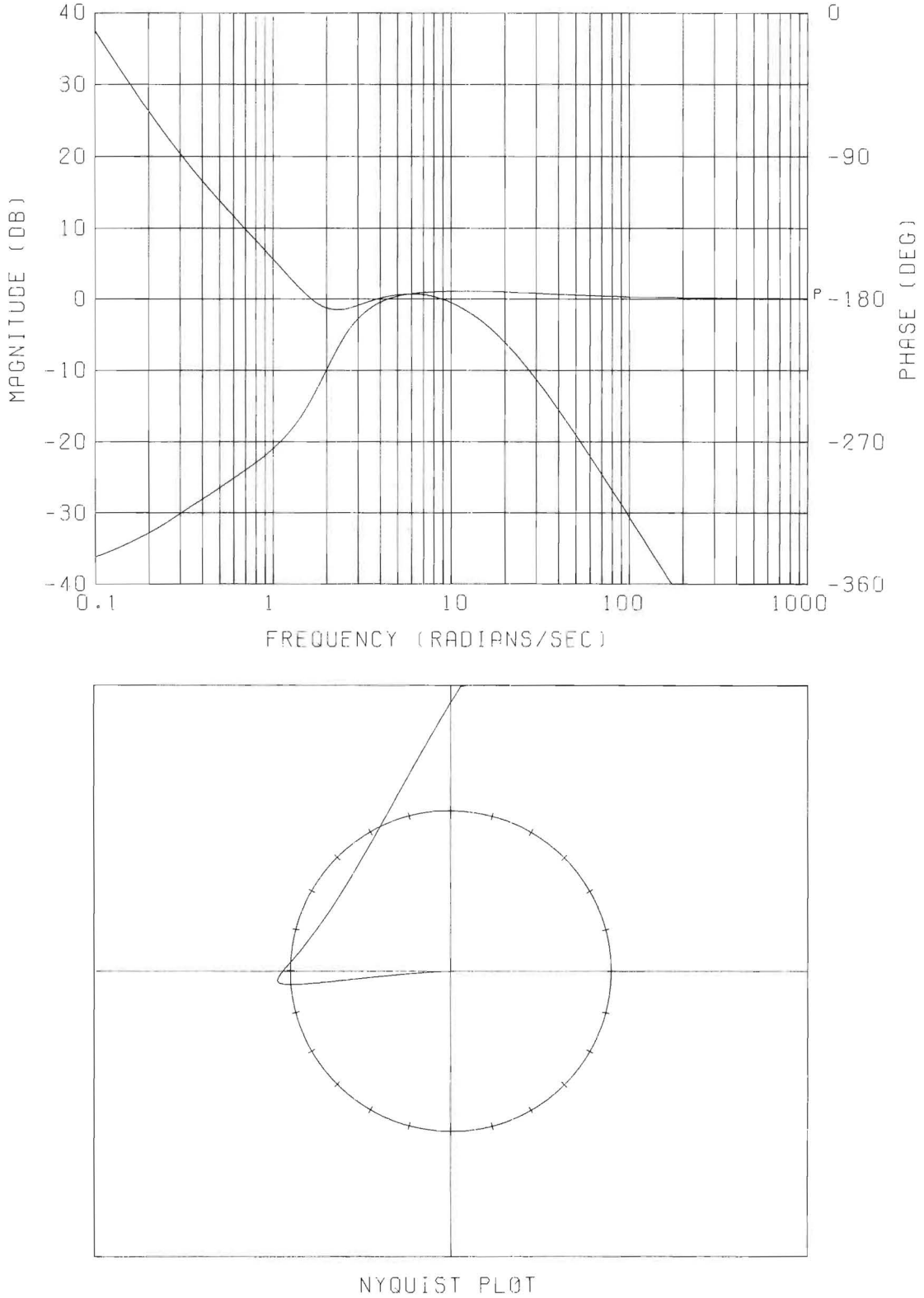

Figure 39. Nyquist and Bode Plots for Describing Function Analysis of DLG System with $\tau_L = 3.0$, $k_2 = 6.0$, and R = 500 feet.

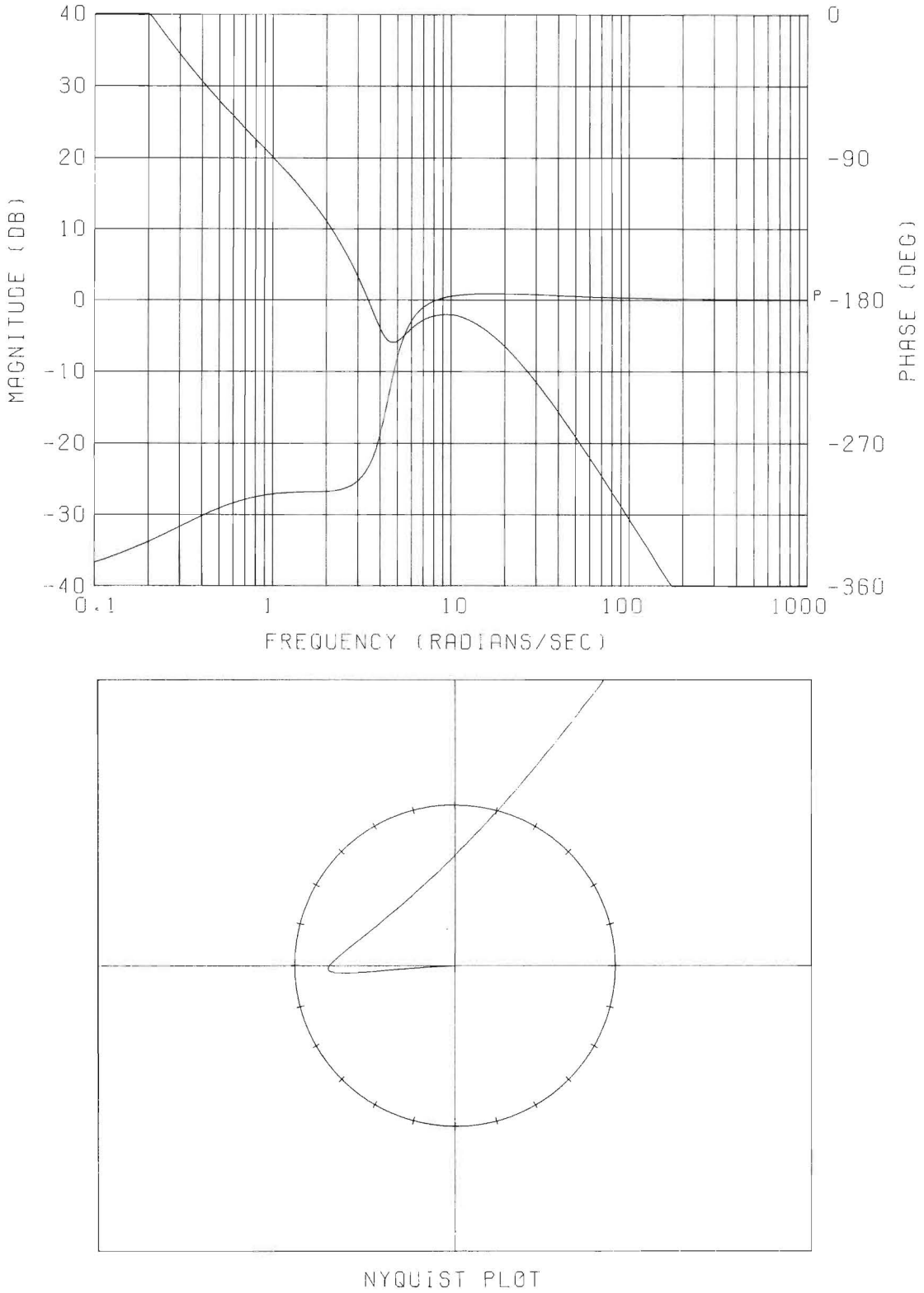

Figure 40. Nyquist and Bode Plots for Describing Function Analysis of DLG System with τ_L = 3.0, k_2 = 6.0, and R = 100 feet.

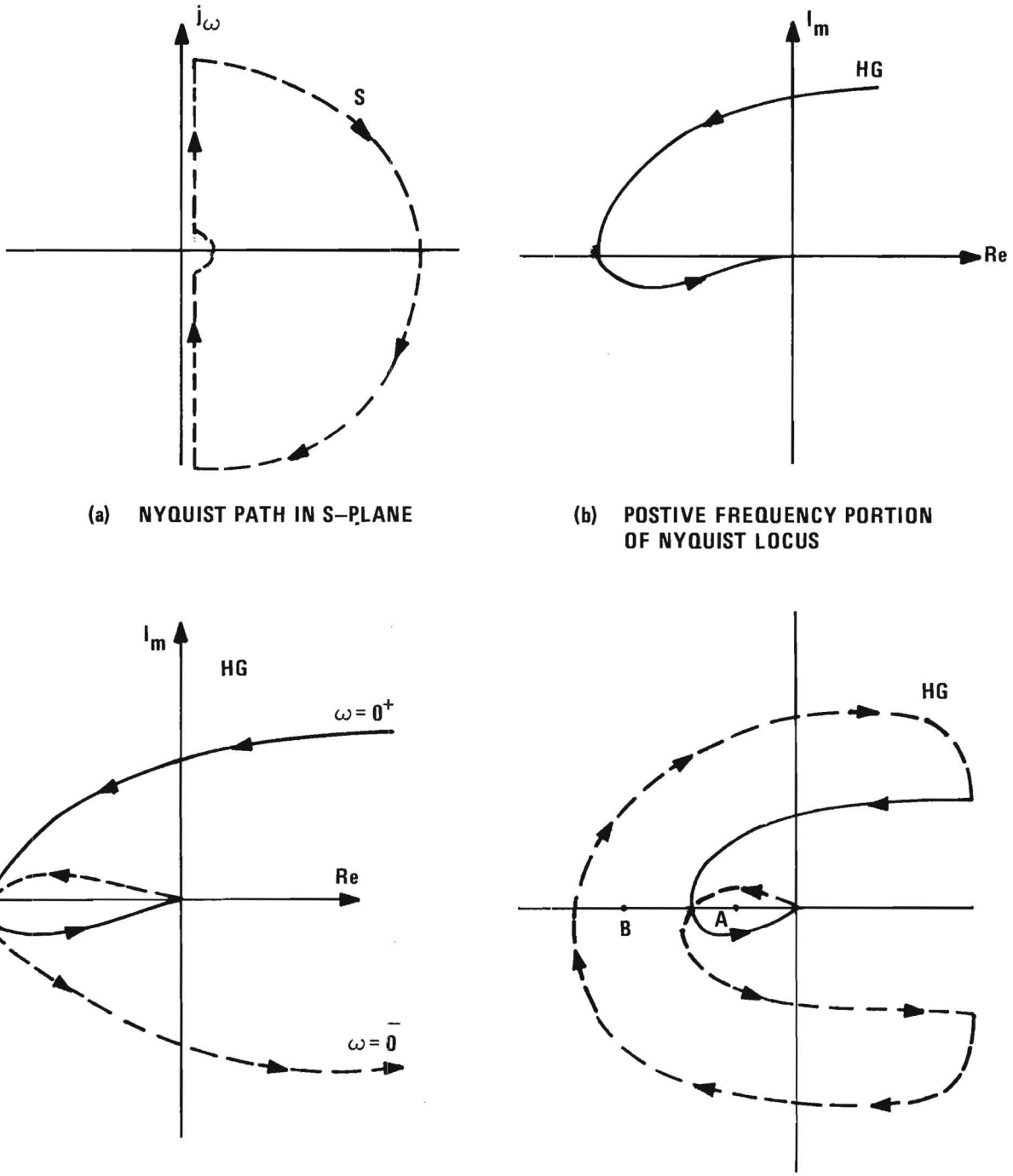

(a) NYQUIST PATH IN S–PLANE

(b) POSTIVE FREQUENCY PORTION OF NYQUIST LOCUS

(c) ADDITION OF NEGATIVE FREQUENCY PORTION

(d) COMPLETED NYQUIST LOCUS

Figure 41. Nyquist Path Closure for Describing Function Analysis.

TABLE X

PARAMETERS USED IN FIXED-POINT ANALYSIS
DESCRIBED BY FIGURES 37-40

$\omega_A = 10$	$\zeta_A = .2$
$K_\alpha = .5$	$K_G = 1$
$K_1 = 1$	$K_3 = 1$
$K_2 = 6$	$\tau_L = 3$
$\omega_1 = 1$	$V = 1000$
$\omega_2 = 1$	

transfer function, one has $P_r = 1$. For the stability analysis, first assume that the critical point is at point A in Figure 41d. Then the number of clockwise encirclements, N, would be -1 so that $Z_r = N + P_r = -1 + 1 = 0$, and the DLG system would be closed-loop stable. If, on the other hand, the critical point is at point B, there would be +1 encirclements and $Z_r = 1 + 1 = 2$, and there would be two unstable roots in the closed loop system. One concludes that if the Nyquist plot crosses the negative real axis to the left of the critical point, the system is stable; otherwise it is unstable.

Recall that the open loop transfer function as seen from the sensor is given by $K_D \cdot H(s) \cdot G_1(s)$ and that the Nyquist plots are of $H(s) \cdot G_1(s)$ only. Thus the total system will be stable if and only if the "equivalent gain" of the nonlinear sensor characteristic is sufficiently large; more specifically, if the locus of $H(s)\ G_1(s)$ crosses the negative real axis at $H(s)\ G_1(s) = -h$, then the system is stable if the equivalent gain, K_D, satisfies

$$K_D\, h > 1 \ . \qquad (15)$$

Furthermore, since the describing function equivalent gain for a saturating function is always less than unity, the system can only be stable when $h > 1$ and the signal at the sensor is not large enough to reduce the equivalent gain below 1/h. Table XI shows how h, $(K_D)_{min}$, and $\left(\frac{\sigma_m}{\sigma_{sat}}\right)_{max}$ vary with missile-target range for the parameters of Table X. Figure 42 is a plot of the minimum equivalent gain vs. range for the above Nyquist plots. Figure 43 shows a portion of the root locus (for a somewhat more lightly damped vehicle) showing roots in the right-half-plane for low sensor gains.

TABLE XI

RANGE DEPENDENCE OF
h, (K_D) min, AND (σ_m/σ_{sat}) max

R	h	$\left(K_D\right)_{min}$	$\left(\frac{\sigma_m}{\sigma_{sat}}\right)_{max}$
10000	1.19	.84	1.37
8000	1.19	.84	1.37
6000	1.18	.85	1.35
4000	1.17	.86	1.33
2000	1.16	.87	1.31
1000	1.11	.90	1.25
500	1.10	.91	1.23
200	Unstable		
100	Unstable		
25	Unstable		

h = Nyquist cross over.

$\left(K_D\right)_{min}$ = minimum sensor equivalent gain for stability.

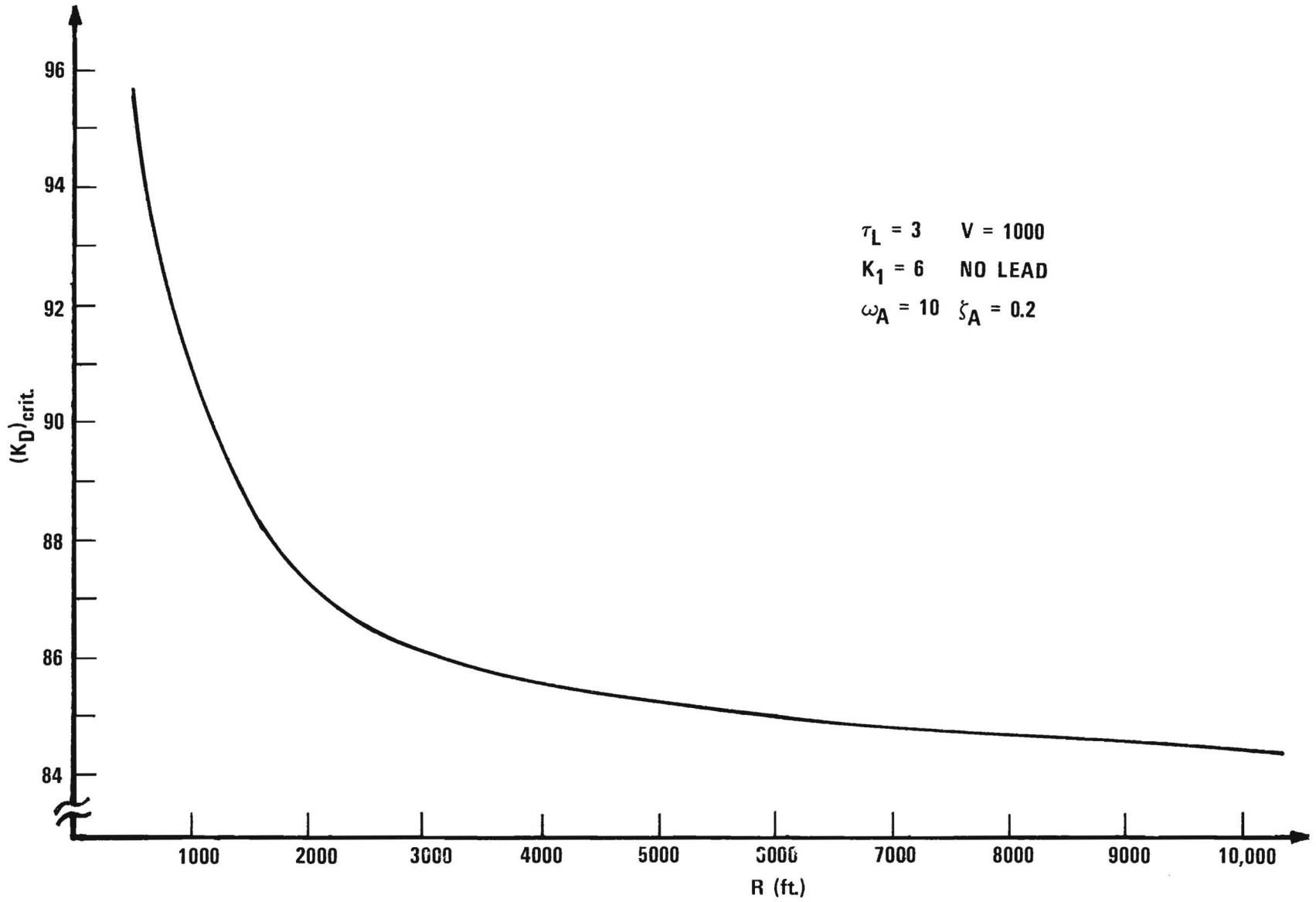

Figure 42. Minimum Sensor "Gain" for Stable System Based upon Fixed-Point Analysis.

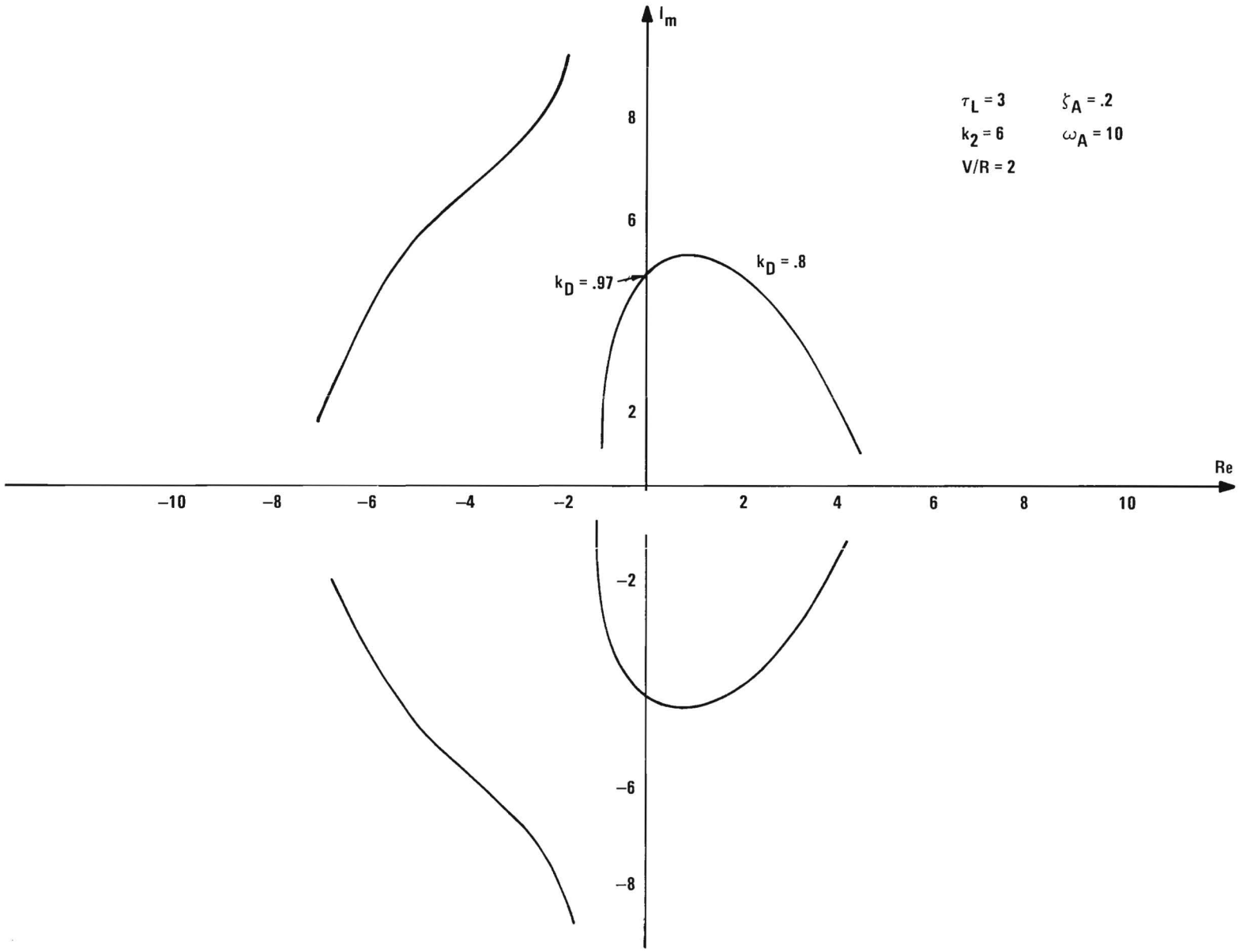

Figure 43. DLG Root Locus as Seen from Sensor Position.

In order to verify the fixed-point analysis just described, the digital simulation of the DLG system was modified so that the X-axis separation of the missile and the target remains constant while Y-axis motion is allowed; this condition should approximate the constant-range assumption made for the fixed-point analysis. The simulator was run for ranges of 500, 1000, 4000, and 8000 feet and for sensor gains just above, at, and just below the critical values obtained from the Bode-Nyquist analysis or from Figure 42. In each case the stability or instability was as predicted, verifying the linear, fixed-point analysis.

As a check on the applicability of the fixed-point analysis to the time-varying DLG system, a simulation run with the normal DLG system was made with a linear sensor characteristic for sensor gains of K_s = .95, .90, .85, .80, and .75. The missile-to-target line-of-sight angle as a function of time is plotted for each gain value in Figure 44. It can be seen from the figure that the DLG system is stable for K_s = .95 and 0.90, unstable for K_s = .75 and .80, and is marginal for K_s = 0.85.

Recall from Figure 42 that the minimum equivalent sensor gain for stability in the fixed-point analysis was between .84 and .87 for values of range between 10,000 and 2,000 feet and became larger for smaller ranges. The reasonableness of the time-varying system being stable for a lower sensor equivalent gain than that predicted by the fixed-point analysis for the smaller values of range, R, is argued on the basis that instabilities originating late in flight have insufficient time to develop. It is quite encouraging that the fixed point analysis predicts a stability limit, or critical gain, so well for a time-varying system. From Figure 34 the magnitude of the signal into the nonlinear sensor must be below 1.35 times the saturation level if the DLG system is to be stable.

The Nyquist analysis was repeated for the forward gain k_2 increased from 6 to 12 and for the time constant τ_L increased from 3 to 5 sec for further analysis. The associated Bode and Nyquist plots are given in Figures 45 through 47 and a tabulation of the critical value of "equivalent sensor gain" vs. range is given in Table XIII. Basically, the system responds a little faster for these larger parameters, and is more sensitive to saturation.

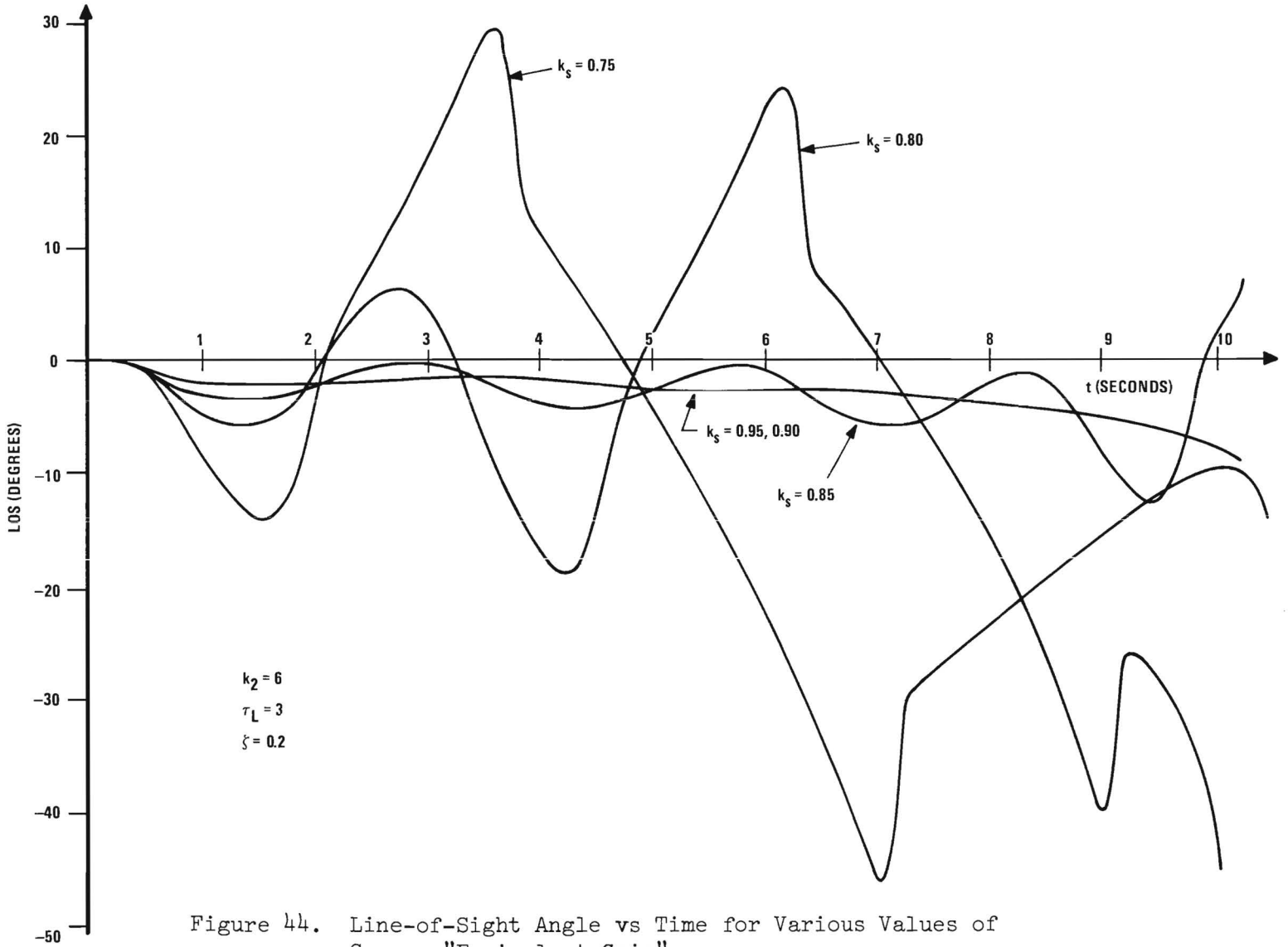

Figure 44. Line-of-Sight Angle vs Time for Various Values of Sensor "Equivalent Gain".

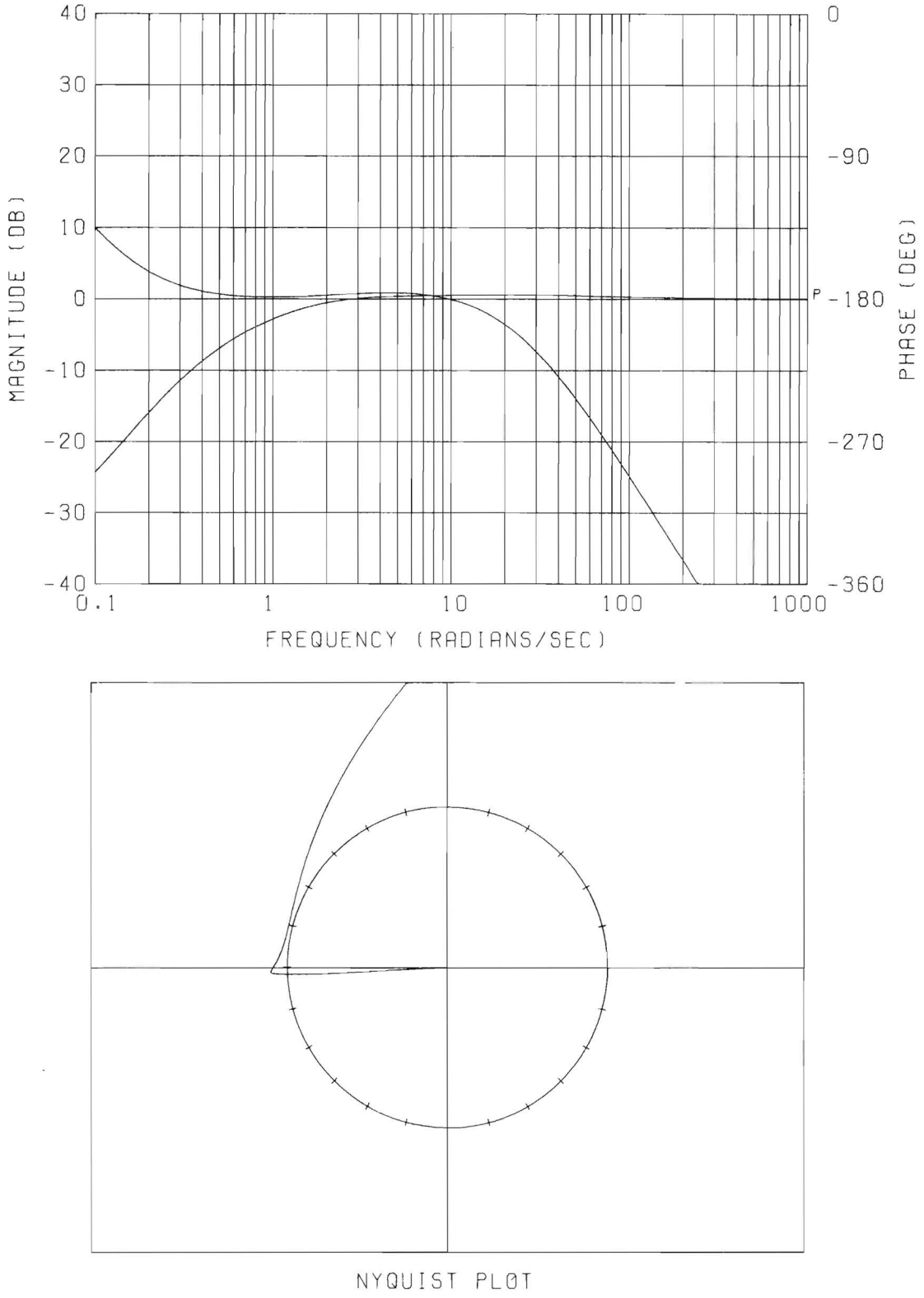

Figure 45. Nyquist and Bode Plots for Describing Function Analysis of DLG System for $\tau_L = 5.0$, $k_2 = 12.0$, and R = 10,000 feet.

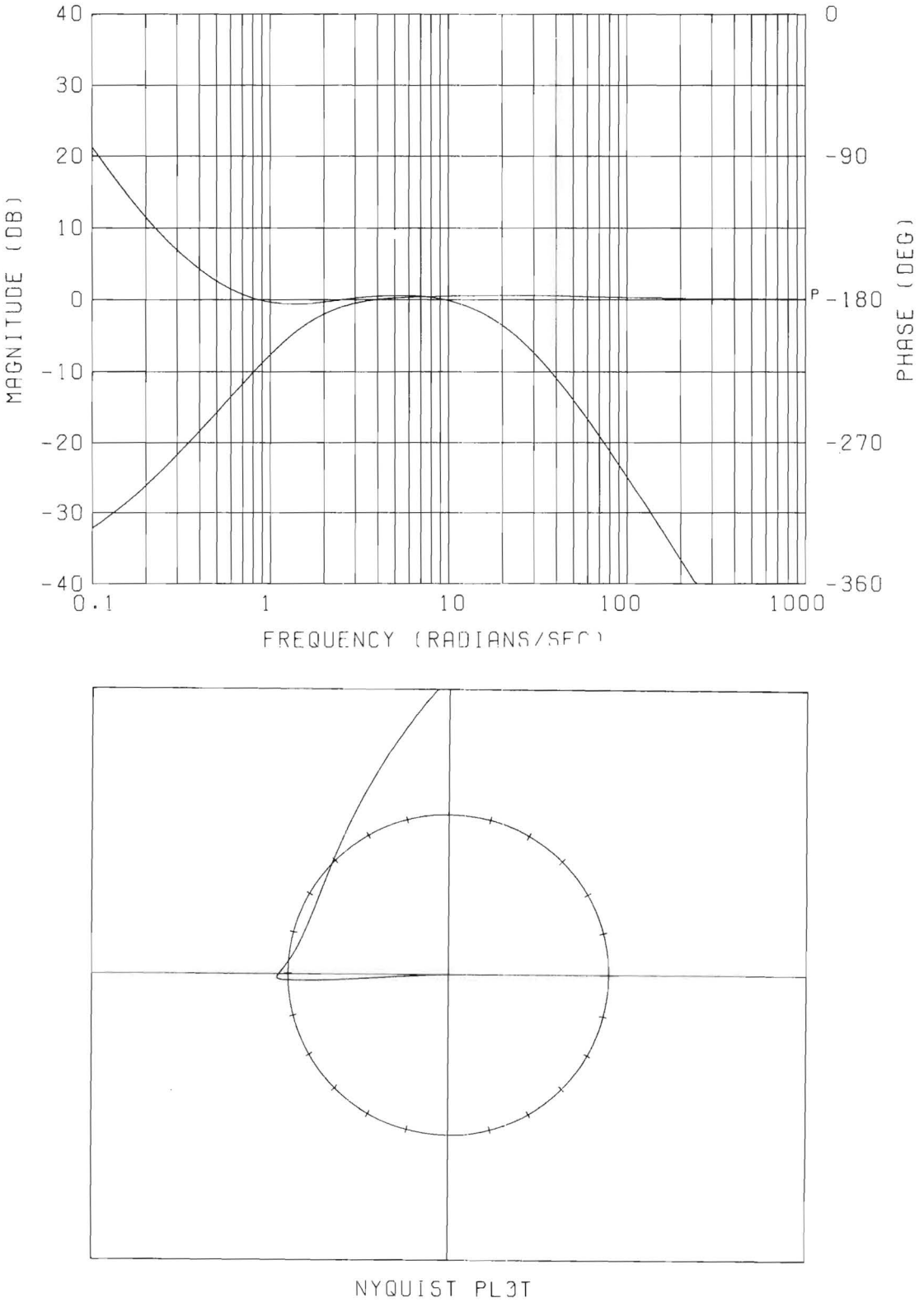

Figure 46. Nyquist and Bode Plots for Describing Function Analysis of DLG System for $\tau_L = 5.0$, $k_2 = 12.0$, and R = 2,000 feet.

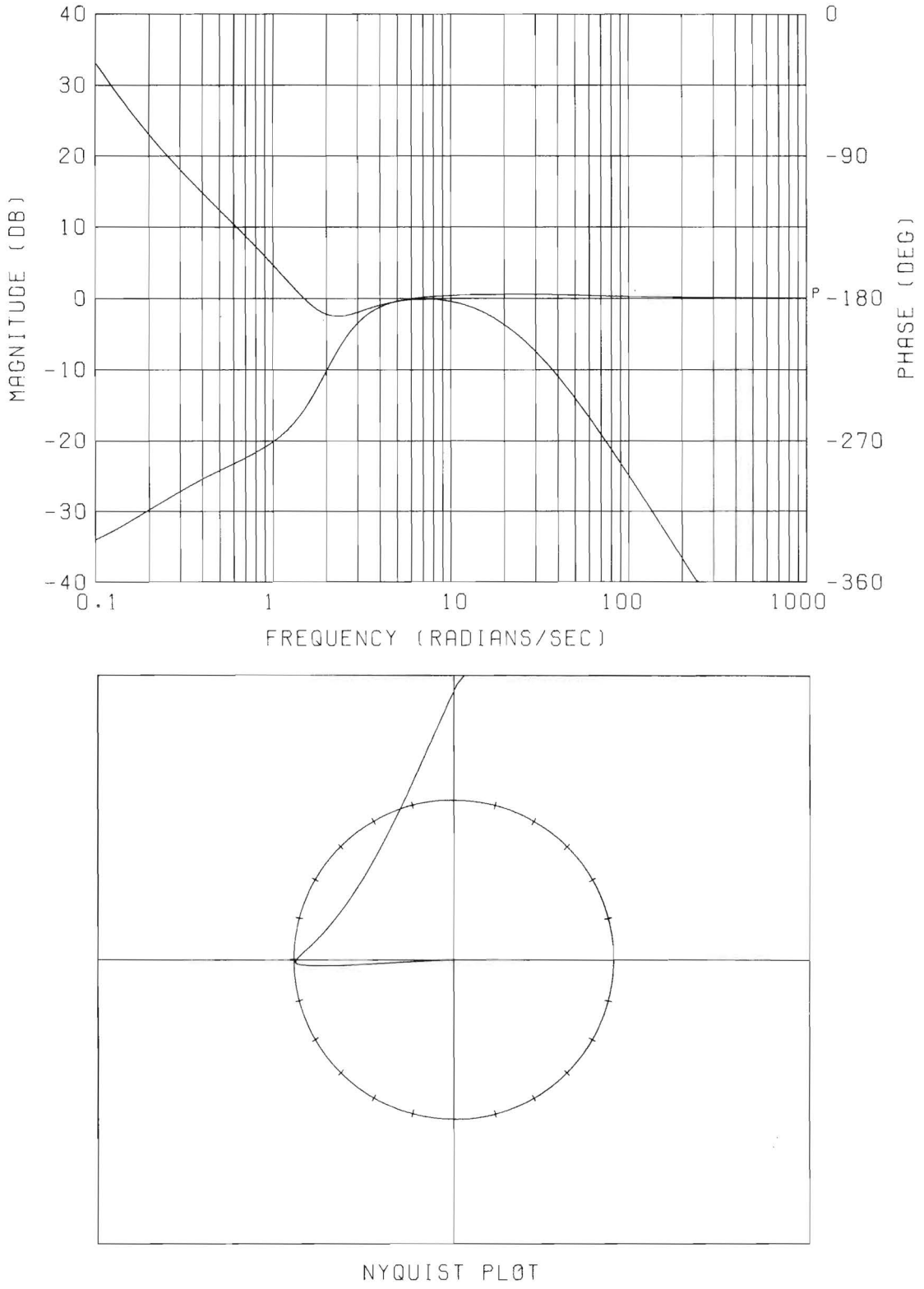

Figure 47. Nyquist and Bode Plots for Describing Function Analysis of DLG System for τ_L = 5.0, k_2 = 12.0, and R = 500 feet.

TABLE XII

PARAMETERS USED IN FIXED-POINT ANALYSIS
DESCRIBED BY FIGURES 45-47

$\omega_A = 10$	$\zeta_A = .2$
$K_\alpha = .5$	$K_G = 1$
$K_1 = 1$	$K_3 = 1$
$K_2 = 12$	$\tau_L = 5$
$\omega_1 = 1$	$V = 1000$
$\omega_2 = 1$	

TABLE XIII

SENSOR LOCATION

R	h	$\left(K_D\right)_{min}$	$\left(\frac{\sigma_m}{\sigma_{sat\ max}}\right)$
10000	1.1	.91	1.23
8000	1.1	.91	1.23
6000	1.09	.92	1.21
4000	1.08	.93	1.19
2000	1.07	.94	1.17
1000	1.04	.96	1.12
500	U n s t a b l e		
200	U n s t a b l e		
100	U n s t a b l e		
25	U n s t a b l e		

D. Summary of Analysis and Results

The Describing Function Analysis of the sensor nonlinearity can be summarized as follows. Two approximations were made in the DLG system so that the influence of the sensor nonlinearity upon system stability could be studied analytically. First, the nonlinearity was represented by its describing function, a "gain" dependent upon signal amplitude, so that linear stability analysis techniques could be used to establish the level of saturation allowable in the sensor. Second, since the resulting linear system has a time-varying coefficient, V/R(t), the analysis is approximated by performing fixed-point analyses at representative values of range, R.

The fixed-point analysis allows visualization (through the Bode and Nyquist plots) of the basis of instability and offers the possibility of the design of passive compensation networks to reduce the critical value of sensor "equivalent gain" so that more sensor saturation can be tolerated without the system becoming unstable.

The Describing Function analysis has shown that the DLG system does indeed become unstable as the sensor enters a region of saturation and reduces the sensor "equivalent gain" below a threshold which increases with time-of-flight. The sensitivity of the system stability to sensor saturation is seen to be a basic feature or characteristic of Dynamic Lead Guidance which results from the sensor being located at a point in the system which is open-loop unstable. From the Nyquist plots, it appears that a simple phase-shift compensation at the sensor would not improve the sensor sensitivity problem. Note that a similar study can be made for a sampled-data model by using the Z-transforms for the linear portion of the system.

V. DYNAMIC LEAD GUIDANCE USING A DISCRETE SENSOR

Of the strapdown sensors available for use with a Dynamic Lead Guidance (DLG) system, some of the most promising ones operate on a pulsed rather than continuous wave basis. For such systems the line of sight (LOS) angle information is updated periodically rather than being continuously variable. This means that the sensor output, σ_m, will be a piecewise-constant function of time and that the discrete sensor can be modeled as a continuous sampler followed by a sample-and-hold circuit [5] as shown in Figure 48. Such closed loop systems containing sample-and-hold devices are referred to as Sampled-Data Control Systems and the analysis and design of such systems composed of linear, time-invariant components is straight forward with the use of the Z-transform [6,7] method.

In this section, three configurations of DLG with different sampler locations will be analyzed on a linearized, fixed-point basis to gain a better understanding of stability problems which have been encountered with the sampled-data version of the simulation program. In configuration I, the only sample-and-hold circuit will be at the sensor output (see Figure 48). While this configuration seems the natural one to use, simulation results show that for a lightly damped vehicle, the DLG system is unstable for this sampler configuration. For configuration II, the sample-and-hold device is positioned in front of the lead network location and in configuration III, the sampler is located after the summing of the gyro and sensor outputs. The sampler location for each configuration is indicated by circled Roman numerals in Figure 48.

A. Sampled-Data Stability Analysis Via the Z-Transform

In order to perform a sampled-data stability analysis using the Nyquist criteria, it is desired to determine the Z-transform of the open-loop transfer function. Due to the absence of samplers between the three dynamic boxes shown in Figure 49, the Z-transform of the open-loop system cannot be found by multiplying together the Z-transforms of the individual boxes but rather must be found as the Z-transform of the product of the three s-domain transfer functions.

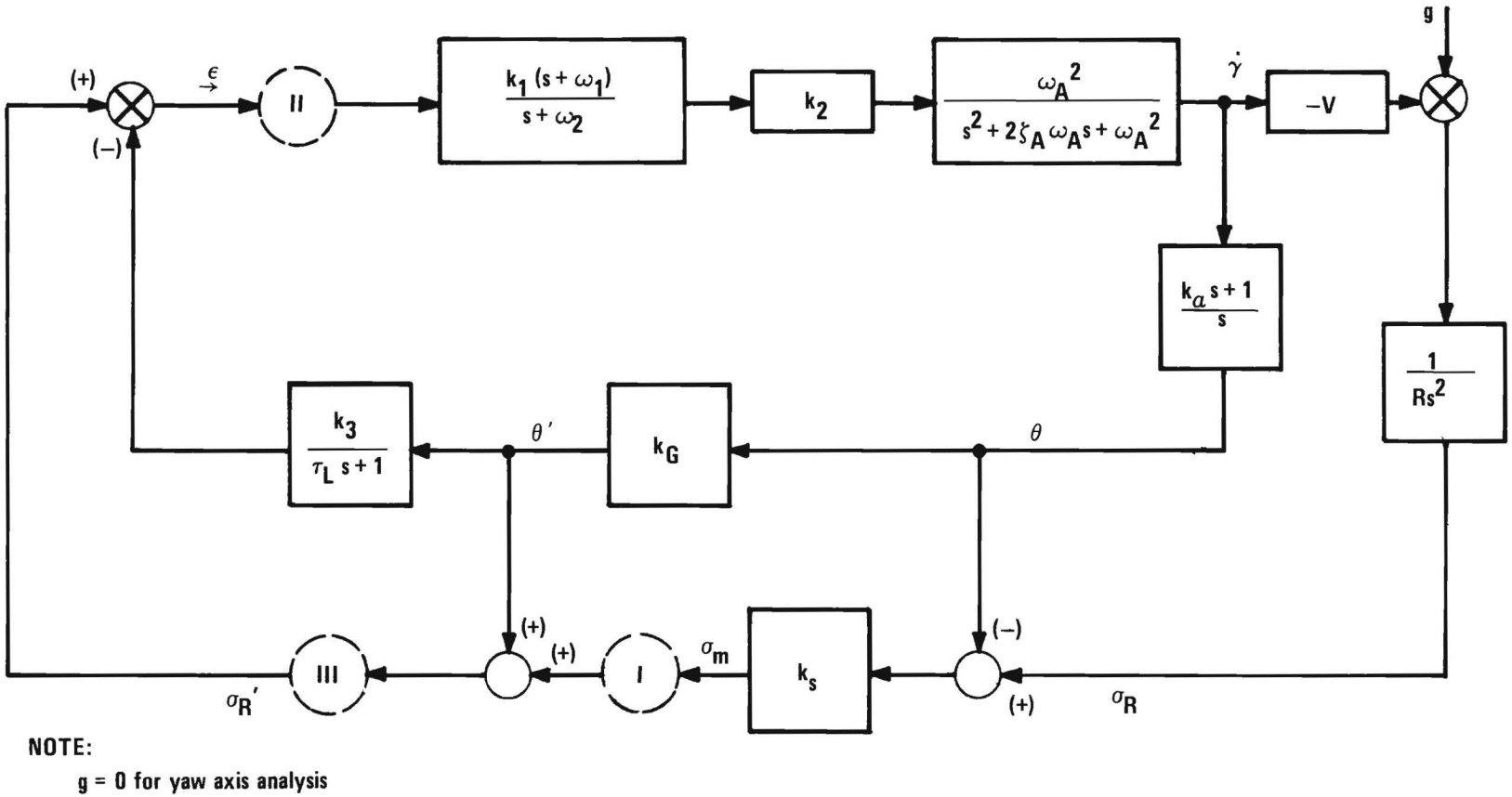

Figure 48. DLG Block Diagram Showing Three Possible Locations for Sampler.

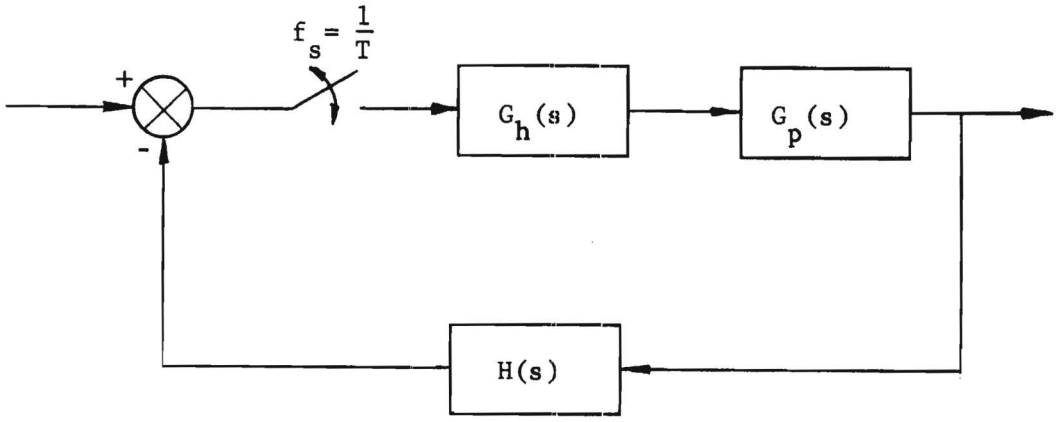

Figure 49. Sampled-Data Control System Block Diagram.

The boxcar, or zero-order, hold circuit has Laplace transform

$$G_h(s) = \frac{1 - e^{-Ts}}{s} \tag{16}$$

where "T" is the sampling period. The presence of the exponential e^{-Ts} in the hold circuit transfer function represents a pure time delay of length T. Unfortunately, the presence of anything other than ratios of polynominals in s complicates the normal method of finding the Z-transform. This problem can be solved in at least two ways.

One method of avoiding the exponential is to employ Pade's approximation [8] which is

$$e^{-Ts} \approx \left\{ \frac{1 - \frac{1}{2} Ts + \frac{1}{12} T^2 s^2}{1 + \frac{1}{2} Ts + \frac{1}{12} T^2 s^2} \right\} , \tag{17}$$

so that the Laplace transform of the zero order hold becomes

$$G_h(s) = \frac{1 - e^{-Ts}}{s} \approx \left\{ \frac{T}{1 + \frac{T}{2} s + \frac{T^2}{12} s^2} \right\} . \tag{18}$$

A better approach involves using the time delay interpretation of e^{-Ts} and performing block diagram manipulation of the system diagram as shown in Figure 50. (The equivalent effect of time delay upon the Z-transform is also used.)

For stability analysis, the term $\left\{ \frac{1}{H(s)} \right\}$ at the output in Figure 50-f can be ignored (assuming H(s) contains no right-half-plane zeros) and the <u>open-loop</u> transfer function is expressed as

$$OL(s) = \left\{ \left[\frac{1}{s} \cdot G_p(s) \cdot H(s) \right] - \left[\frac{1}{s} \cdot G_p(s) \cdot H(s) \right] e^{-Ts} \right\} \quad . \tag{19}$$

Before going to the Z-domain with OL(s), consider a similar case:

$$X(s) = G(s) \left[1 - e^{-Ts} \right] = G(s) - G(s) \cdot e^{-Ts} \quad . \tag{20}$$

Note that the real translation theorem in Laplace transform theory states that

$$\mathcal{L}\left\{ f(t - T)\, U_{-1}\,(t - T) \right\} = e^{-Ts}\, \mathcal{L}\left\{ f(t) \right\} \quad . \tag{21}$$

Thus,

$$\begin{aligned} X(s) &= G(s) - G(s) \cdot e^{-Ts} \\ &= \mathcal{L}\left\{ g(t) \right\} - G(s) \cdot e^{-Ts} \\ &= \mathcal{L}\left\{ g(t) \right\} - \mathcal{L}\left\{ g(t - T)\, U_{-1}\,(t - T) \right\} \quad , \end{aligned} \tag{22}$$

and the time function is

$$x(t) = g(t) - g(t - T)\, U_{-1}\,(t - T). \tag{23}$$

The <u>real translation</u> theorem in Z-transform theory is given by

$$\mathcal{Z}\left\{ f(t - T)\, U_{-1}\,(t - T) \right\} = z^{-1}\, \mathcal{Z}\left\{ f(t) \right\} \quad . \tag{24}$$

Thus,

$$X(z) = \mathcal{Z}\left\{g(t)\right\} - z^{-1} \cdot \mathcal{Z}\left\{g(t)\right\}$$

$$= G(z) - z^{-1} \cdot G(z) = \left\{\left(\frac{z-1}{z}\right) \cdot G(z)\right\} \quad . \tag{25}$$

Thus, returning to the problem at hand, the open-loop Z-transform is given by:

$$OL(z) = \left(\frac{z-1}{z}\right) \cdot \mathcal{Z}\left\{\frac{1}{s} \cdot G_p(s) \cdot H(s)\right\} \quad . \tag{26}$$

Once the Z-transform of the open loop transfer function is determined, the Nyquist criteria can be used to investigate the relative stability of the closed loop system. The Nyquist locus for a sampled data system is the unit circle in the Z-plane since all poles of the closed loop system must lie within this circle for the system to be stable.

B. Application of Sampled-Data Nyquist Criteria to the DLG System

For nominal values (unity) of the gains k_G, k_z, and k_s, the linearized DLG block diagram for configuration I sampling can be redrawn (as in the section on the analysis of nonlinear sensor characteristics) to appear as in Figure 49, where $G_p(s)$ and $H(s)$ were derived earlier and are repeated here.

$$G_p(s) = \left\{\left[k_1 k_2\, \omega_A^2 (s + \omega_1) s(\tau_L s + 1)\right] / \left[(s^2 + 2\zeta_A\, \omega_A s + \omega_A^2)\right.\right.$$

$$\cdot (s + \omega_2)\, s(\tau_L s + 1) + k_1 k_2\, \omega_A^2\, (s + \omega_1)\, k_G (k_\alpha s + 1)$$

$$\left.\left. \cdot (k_3 - \tau_L s - 1) \right]\right\} \tag{27}$$

$$H(s) = (k_\alpha s^2 + s + \frac{V}{R})/s^2 \quad . \tag{28}$$

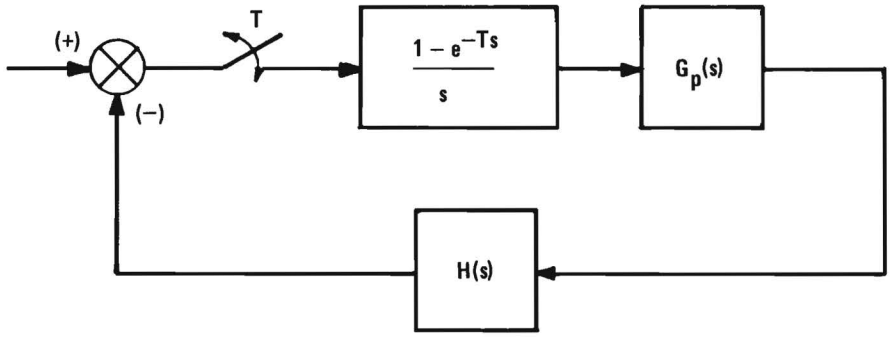

a.

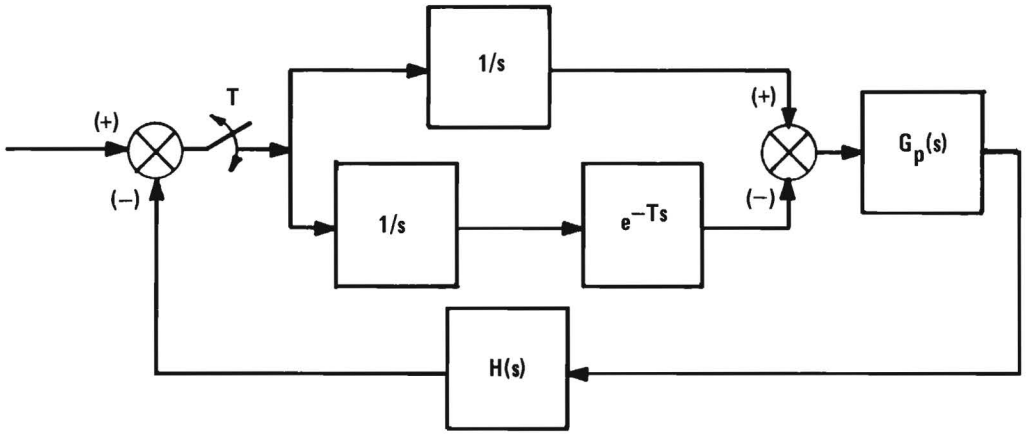

b.

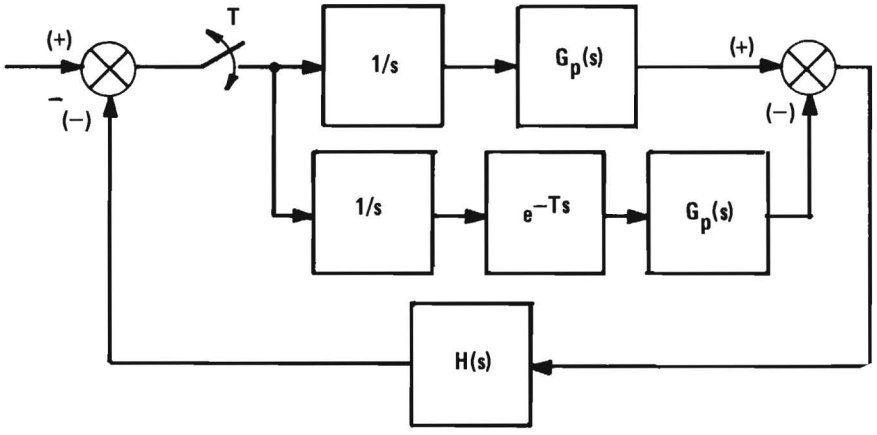

c.

Figure 50. Block Diagram Manipulation.

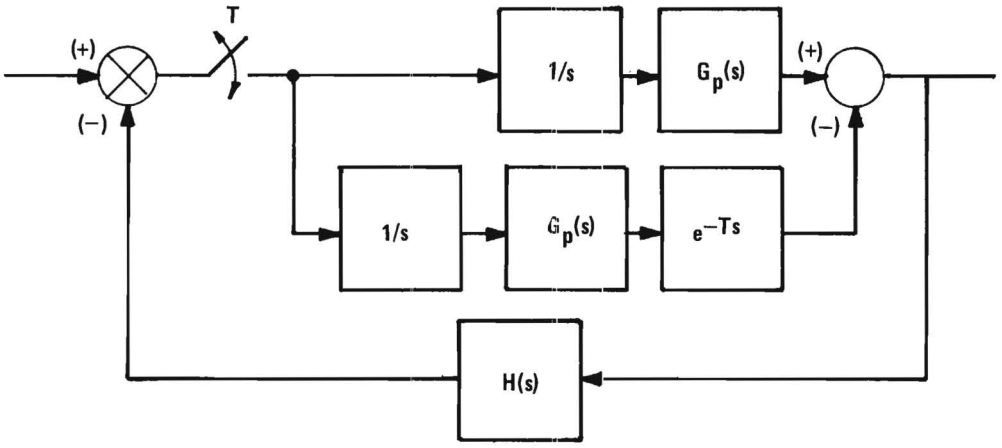

d.

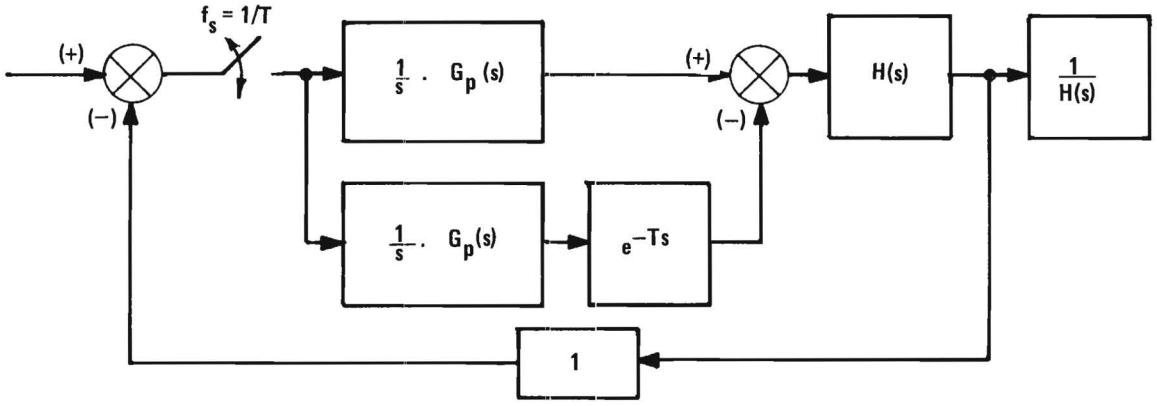

e.

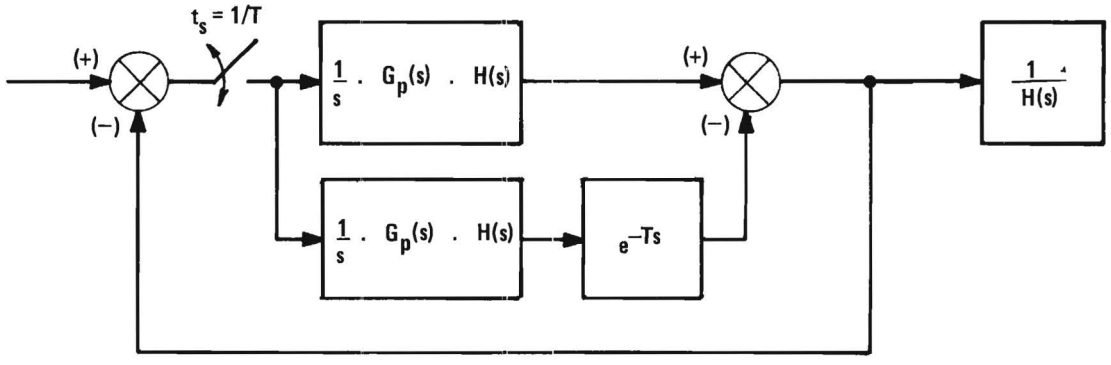

f.

Figure 50 (Continued). Block Diagram Manipulation.

TABLE XIV

NOMINAL DLG PARAMETERS

$k_1 = 1$	$\zeta_A = .2$
$k_2 = 12$	$k_3 = 1$
$\omega_A = 10$	$k_G = 1$
$\omega_1 = 1$	$k_\alpha = .5$
$\omega_2 = 1$	$V/R = .25$
$\tau_L = 5$	$(V = 1000, R = 4000)$

Using the nominal parameters in Table XIV, the transfer functions become

$$H(s)G_p(s) = \left\{ \frac{1200(5s + 1)(.5s^2 + s + .25)}{s^2(5s^3 + 21s^2 - 2496s - 5900)} \right\}. \tag{29}$$

Following the procedure described earlier for sampled data Nyquist analysis, the product $\frac{1}{s} \cdot G_p(s) \cdot H(s)$ is formed and its poles are found to be at the following values of s.

$$s_1 = -2.343 \qquad s_2 = +21.531 \qquad s_3 = -23.387$$

$$s_4 = s_5 = s_6 = 0.$$

A partial fraction expansion [5] of the term $\frac{1}{s} G_p(s) H(s)$ yielded:

$$\frac{1}{s} \cdot G_p(s) \cdot H(s) = \left\{ \frac{-.254232}{s^3} - \frac{2.18054}{s^2} - \frac{4.67155}{s} \right.$$

$$\left. - \frac{1.29671}{(s + 2.3434)} + \frac{3.08880}{(s - 21.5308)} + \frac{2.88037}{(s + 23.3875)} \right\}. \tag{30}$$

Taking the Z-transform term-by-term using standard tables [7] gives the following:

$$\mathcal{Z}\left\{\frac{1}{s}\cdot G_p(s)\cdot H(s)\right\} = \left\{(-.050846)\,\frac{z(z+1)T^2}{2(z-1)^3} - (.436108)\,\frac{Tz}{(z-1)^2}\right.$$

$$- (.934310)\frac{z}{(z-1)} - (.259522)\,\frac{z}{(z-e^{-2.3434T})}$$

$$\left. + (.617760)\,\frac{z}{(z-e^{21.5308T})} + (.576074)\,\frac{z}{(z-e^{-23.3875T})}\right\} \tag{31}$$

Finally, the Z-transform of the open loop transfer function for sampling configuration I is obtained by multiplication by $(\frac{z-1}{z})$.

$$OL(z) = \left\{(-.050846)\,\frac{T^2(z+1)}{2(z-1)^2} - (.436108)\,\frac{T}{(z-1)}\right.$$

$$- (.934310)(1) - \frac{(.259522)(z-1)}{(z-e^{-2.3434T})}$$

$$\left. + \frac{(.617760)(z-1)}{(z-e^{21.5308T})} + \frac{(.576074)(z-1)}{(z-e^{-23.3875T})}\right\}. \tag{32}$$

Using the aforementioned automated Nyquist plot routine (modified for sampled-data systems), the Nyquist plots for configuration I sampling with sampling rates of 30, 20, and 10 samples per second and V/R = .25 were found to be as given in Figures 51, 52, and 53. The closure of each of these Nyquist plots is as shown in Figure 54. The number of clockwise encirclements of a point on the negative-real-axis is zero for points to the right of point P and is plus-one for points to the left of point P. Since the open-loop system has one unstable pole, the Nyquist criteria for stability is -1 encirclement of the point -1 + j0; the system with configuration I sampling is seen to be unstable for all three sample rates considered at a range of 4000 feet (for V = 1000 ft/sec). Fixed-point analyses of the continuous DLG system have shown that V/R = .25 gives stability results representative of the actual time-varying system. The analysis results (instability) agree with DLG simulation results.

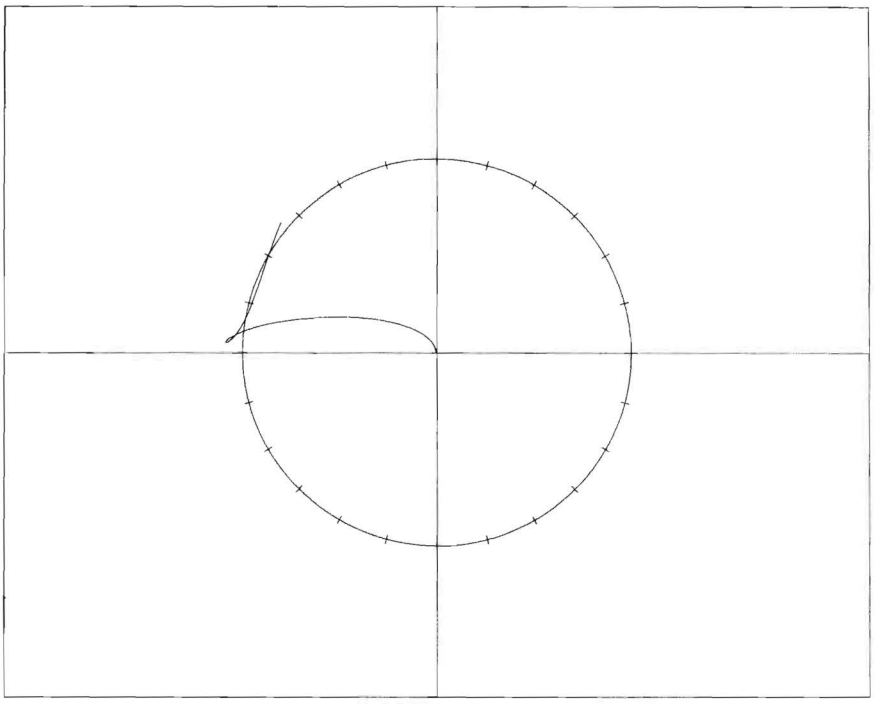

Figure 51. Nyquist Plot for DLG System with Configuration I Sampler Operating at 30 Samples/Second.

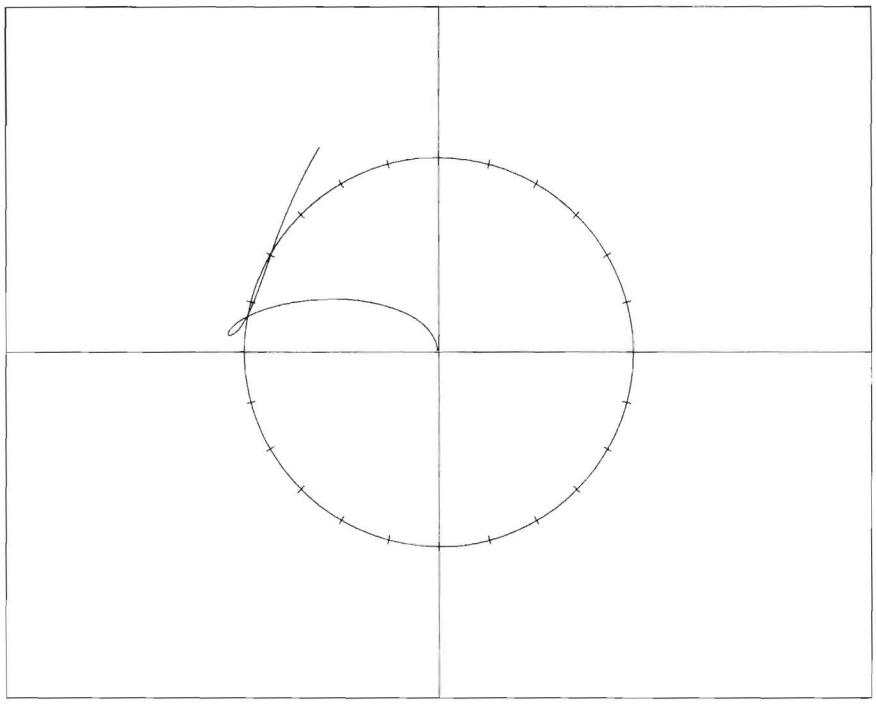

Figure 52. Nyquist Plot for DLG System with Configuration I Sampler Operating at 20 Samples/Second.

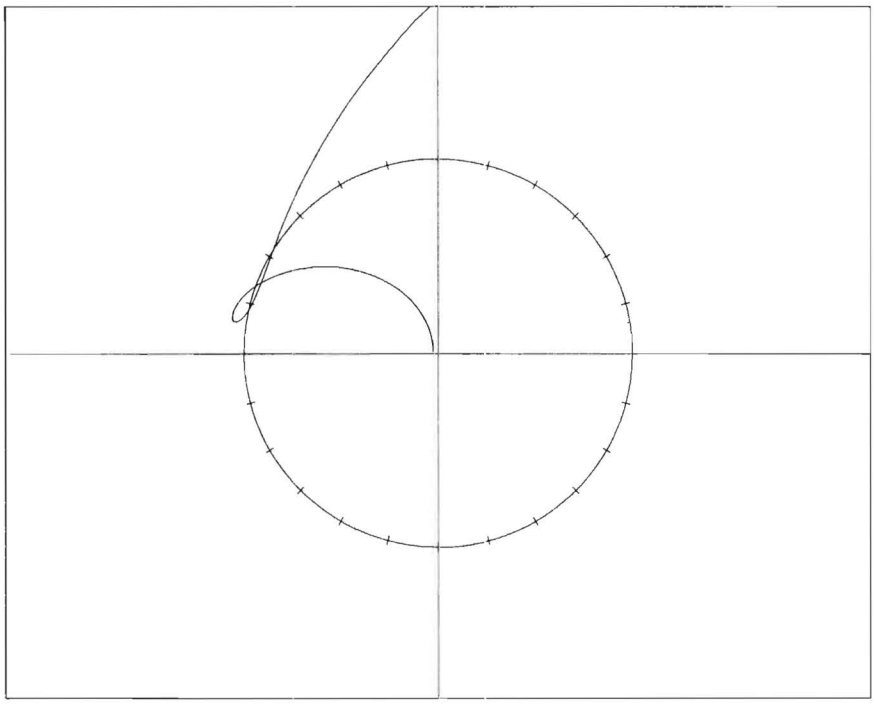

Figure 53. Nyquist Plot for DLG System with Configuration I Sampler Operating at 10 Samples/Second.

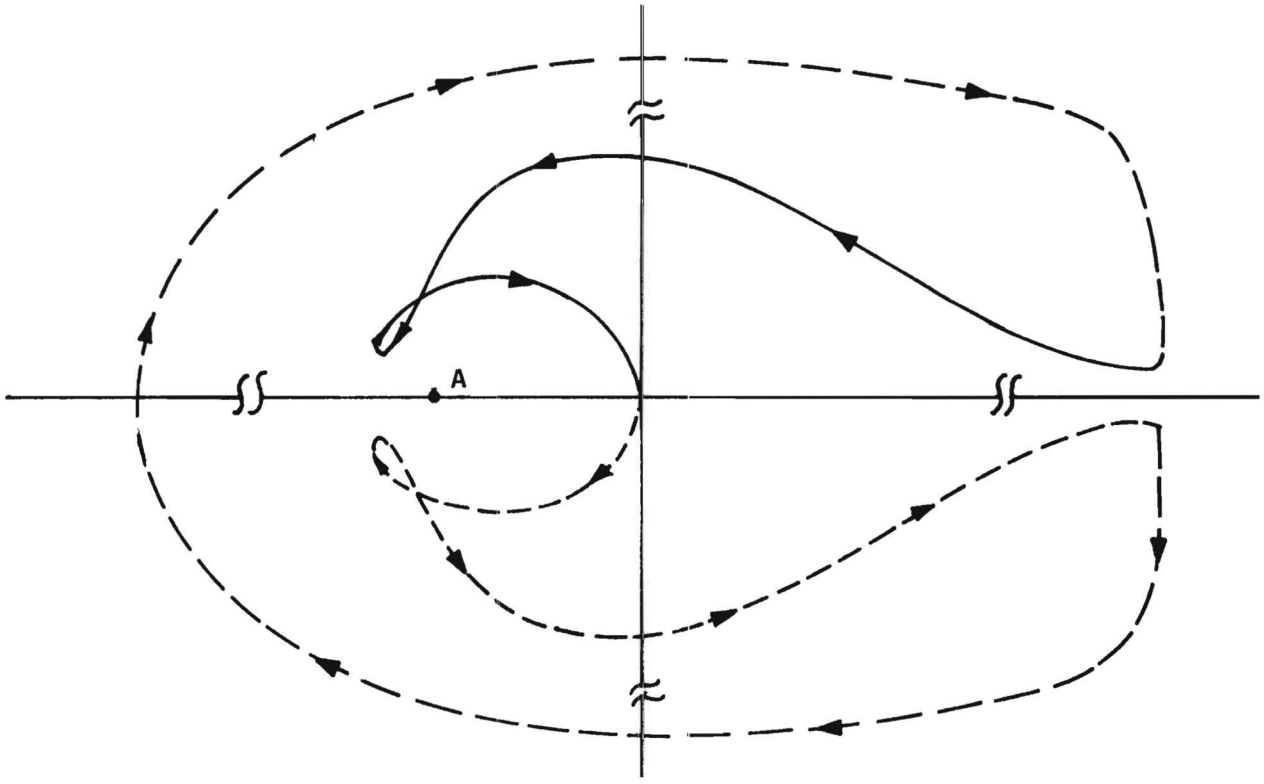

Figure 54. Nyquist Path Closure for Configuration I Sampling.

The analysis procedure is repeated for configuration II. For this configuration, Figure 48 can be recast into the form of Figure 49 with the following forward and feedback transfer functions:

$$G_p(s) = \left\{ \left[k_1 k_2 (s + \omega_1)\ \omega_A^2 \right] / \left[(s + \omega_2)(s^2 + 2\zeta_A \omega_A s + \omega_A^2 \right] \right\} \tag{33}$$

$$H(s) = \frac{k_G k_3 (k_\alpha s + 1)}{s(\tau_L s + 1)} + \frac{V k_s}{R s^2} \quad . \tag{34}$$

For the same nominal parameters (Table XVI),

$$H(s)G_p(s) = \left\{ \frac{240\left[s(.5s + 1) + (1/4)(5s + 1) \right]}{s^2(s^2 + 4s + 100)(s + .2)} \right\} \quad . \tag{35}$$

From this, the poles of $\left\{ \frac{1}{s} \cdot G_p(s)\ H(s) \right\}$ are found to be as follows:

$$s_1 = -2 - j\sqrt{96} \qquad s_2 = -2 + j\sqrt{96}$$

$$s_3 = -.02 \qquad s_4 = s_5 = s_6 = 0$$

The partial fraction expansion of $\left\{ \frac{1}{s} \cdot G_p(s) \cdot H(s) \right\}$ is as follows:

$$\left\{ \frac{1}{s} \cdot G_p(s) \cdot H(s) \right\} = \left\{ \frac{(3.0)}{s^3} + \frac{(11.88)}{s^2} - \frac{(54.51)}{s} \right.$$

$$\left. + \frac{(.04583 - j.04154)}{(s + 2 + j\sqrt{96})} + \frac{(.04583 + j.04154)}{(s + 2 - j\sqrt{96})} + \frac{(54.41)}{(s + 0.2)} \right\} \quad . \tag{36}$$

The Nyquist plots for configuration II sampling with sampling rates of 30,20, and 10 samples per second are given in Figures 55, 56, and 57; the closure of these Nyquist plots is as shown in Figure 58. Since this system is open-loop-stable, the criteria for stability is zero encirclements of the critical point, -1 + j0. Observe from Figure 58 that points on the negative real axis to the left of point P are not encircled while those to

the right are encircled twice. The system will be stable so long as the Nyquist plot crosses the negative-real-axis to the left of the critical point. Inspection of Figures 55, 56, and 57 shows that the DLG system with configuration II sampling is stable for nominal system parameters (see Table XV) and sampling frequencies of 30, 20, and 10 samples per second for V/R = .25. Table XV shows the gain and phase margins for the three sample rates. The gain margins were verified by simulation.

For configuration III sampling, the forward and feedback transfer functions corresponding to Figure 49 are as follows:

$$G_p(s) = \left\{ \frac{k_2 \omega_A^2 \, s(\tau_L s + 1)}{(s^2 + 2\zeta_A \omega_A s + \omega_A^2)\, s(\tau_L s + 1) + k_2 \omega_A^2 k_3 \, (k_\alpha s + 1)} \right\} \tag{37}$$

$$H(s) = \left\{ \frac{V/R}{s^2} \right\} . \tag{38}$$

Substitution of the nominal parameters from Table XIV results in

$$H(s) \cdot G_p(s) = \left\{ \frac{300(s + 0.2)}{s[s^4 + (4.2)s^3 + (100.8)s^2 + (140)s + (240)]} \right\} \tag{39}$$

TABLE XV

GAIN AND PHASE MARGINS FOR CONFIGURATION II SAMPLING AT VARIOUS SAMPLING RATES

f_s	Gain Margin	Phase Margin (deg)
10	2.9	22
20	2.8	22
30	2.8	19

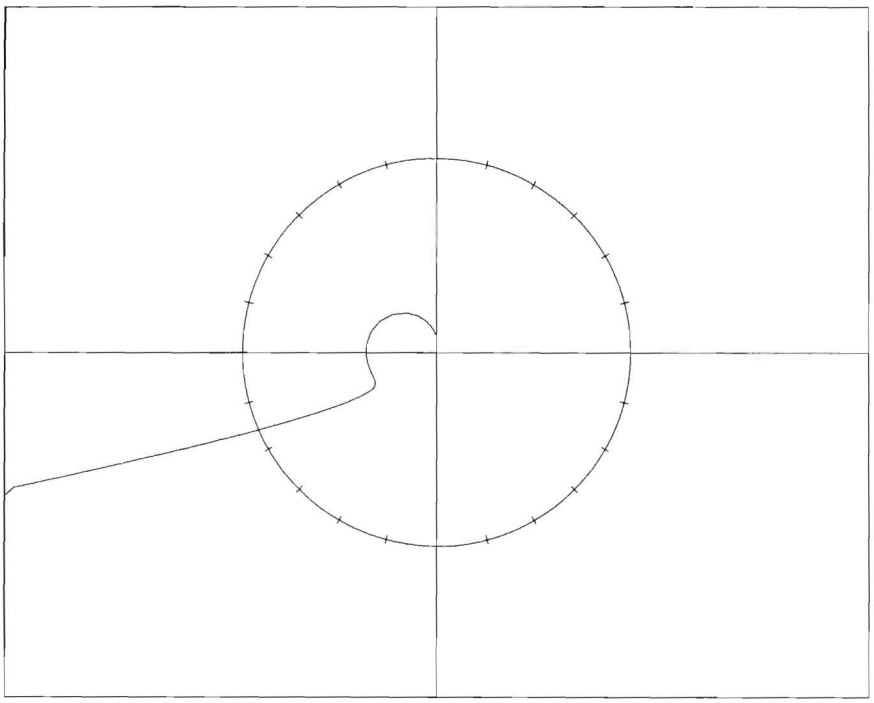

Figure 55. Nyquist Plot for DLG System with Configuration II Sampler Operating at 30 Samples/Second.

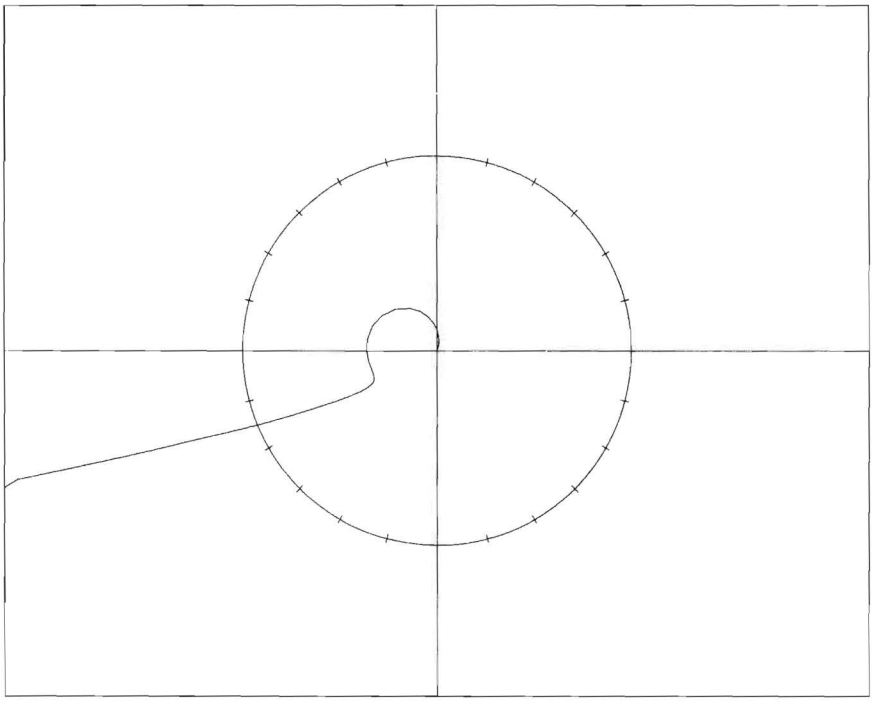

Figure 56. Nyquist Plot for DLG System with Configuration II Sampler Operating at 20 Samples/Second.

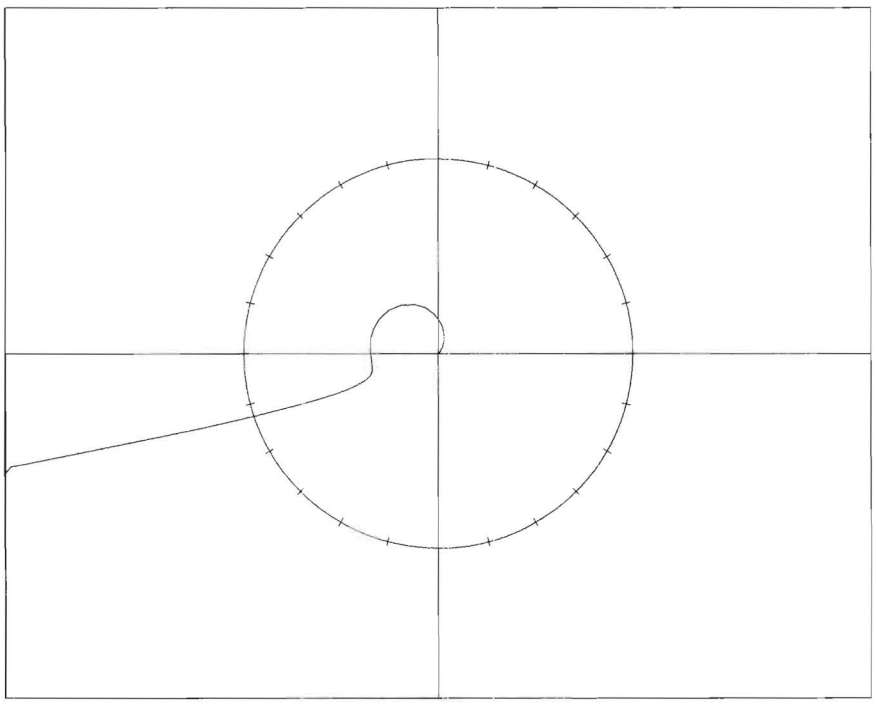

Figure 57. Nyquist Plot for DLG System with Configuration II Sampler Operating at 10 Samples/Second.

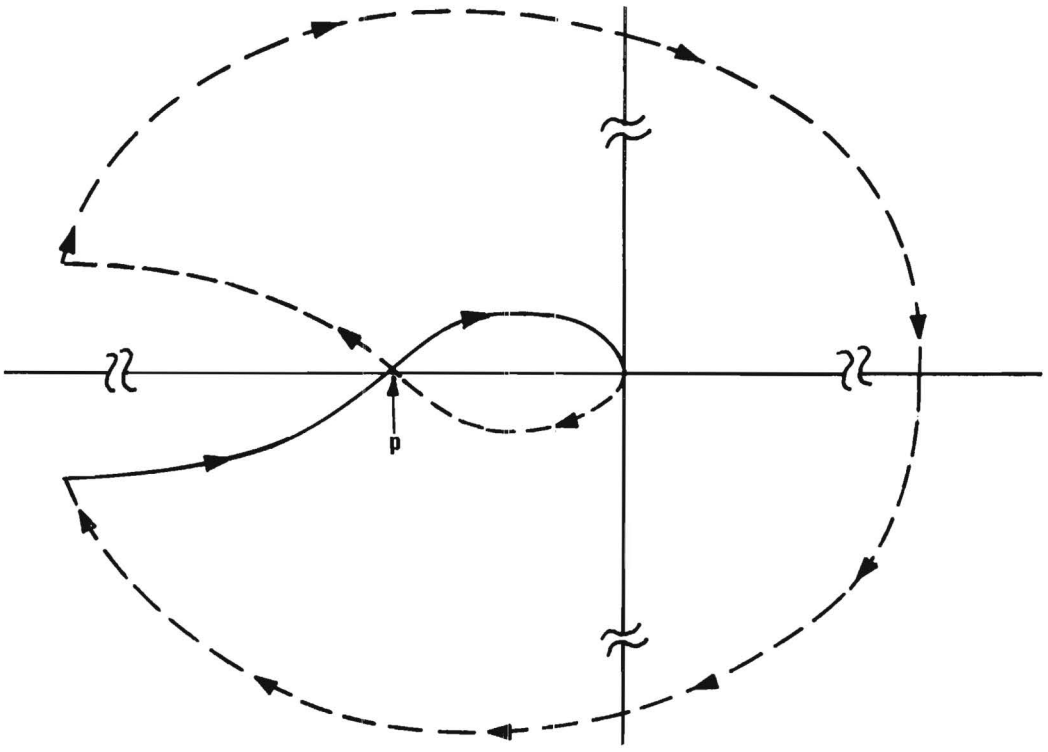

Figure 58. Nyquist Plot Closure for Configuration II Sampler.

The poles of $\left\{ \frac{1}{s} \cdot G_p(s) \cdot H(s) \right\}$ are found to be as follows:

$s_1 = -.70455 - j\ 1.431135$, $\quad s_2 = -.70455 + j\ 1.431135$,

$s_3 = -1.39551 - j\ 9.611223$, $\quad s_4 = -1.39951 + j\ 9.611223$,

$s_5 = s_6 = 0.$

The partial fraction expansion results in

$$\left\{ \frac{1}{s} \cdot G_p(s) \cdot H(s) \right\} = \left\{ \frac{.2500}{s^2} + \frac{1.1041}{s} \right.$$

$$+ \frac{(-.5689 - j\ .3874)}{(s + .70455 + j\ 1.431135)} + \frac{(-.5689 + j\ .3874)}{(s + .70455 - j\ 1.431135)}$$

$$\left. + \frac{(.01680 + j\ .005406)}{(s + 1.39551 + j\ 9.611223)} + \frac{(.01680 - j\ .005406)}{(s + 1.39951 - j\ 9.611223)} \right\} . \quad (40)$$

Taking the Z-transform of this expression and multiplying by $(\frac{z - 1}{z})$ gives the following for the Z-transform of the open loop transfer function for configuration III sampling.

$$OL(z) = \left\{ \frac{(.2500)T}{(z - 1)} + (1.1041)\ (1) + \frac{(-.5689 - j\ .3874)\ (z - 1)}{(z - e^{-[.70455 + j\ 1.431135]T})} \right.$$

$$+ \frac{(-.5689 + j\ .3874)\ (z - 1)}{(z - e^{-[.70455 - j\ 1.431135]T})}$$

$$+ \frac{(.01680 + j\ .005406)\ (z - 1)}{(z - e^{-[1.39551 + j\ 9.611223]T})}$$

$$\left. + \frac{(.01680 - j\ .005406)\ (z - 1)}{(z - e^{-[1.39551 - j\ 9.611223]T})} \right\} . \quad (41)$$

The Nyquist plots for configuration III sampling with sampling rates of 30, 20, and 10 samples per second are given in Figures 59, 60, 61, and the typical closure is given in Figure 62. The system is stable if the

Nyquist locus crosses the negative real axis to the right of the critical point. Inspection of Figures 59, 60, and 61 shows that the DLG system with configuration III sampling is stable for sampling rates of 30, 20, and 10 samples per second. Gain and phase margins are shown for the above sampling rates in Table XVI.

This study of the three versions of sampled-data DLG systems has been based upon fixed point (V/R = .25) analysis of the linearized model. The analysis results obtained are consistant with simulation results. It has been shown that sampling the sensor only (configuration I) results in an unstable guidance system. Sampling both the sensor and gyro output, as in configuration II or III, results in a stable, satisfactory system. Simulation studies show that configurations II and III give very similar performance; a design choice between the two should be based upon implementation considerations.

TABLE XVI

GAIN AND PHASE MARGINS FOR CONFIGURATION III SAMPLING

f_s	Gain Margin	Phase Margin (deg.)
10	3.9	50
20	4.9	50
30	5.4	45

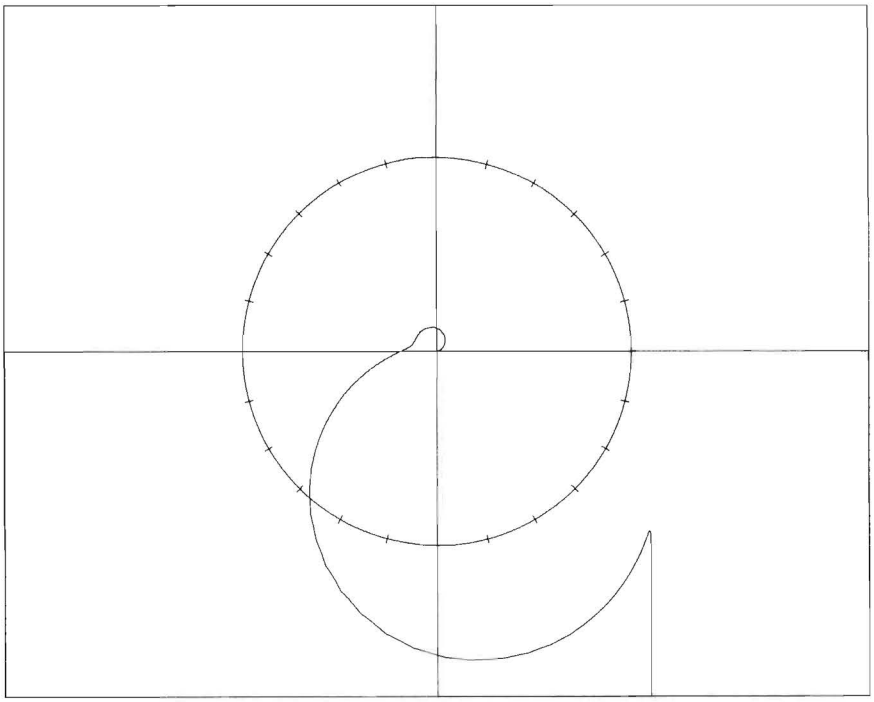

Figure 59. Nyquist Plot for DLG System with Configuration III Sampler Operating at 30 Samples/Second.

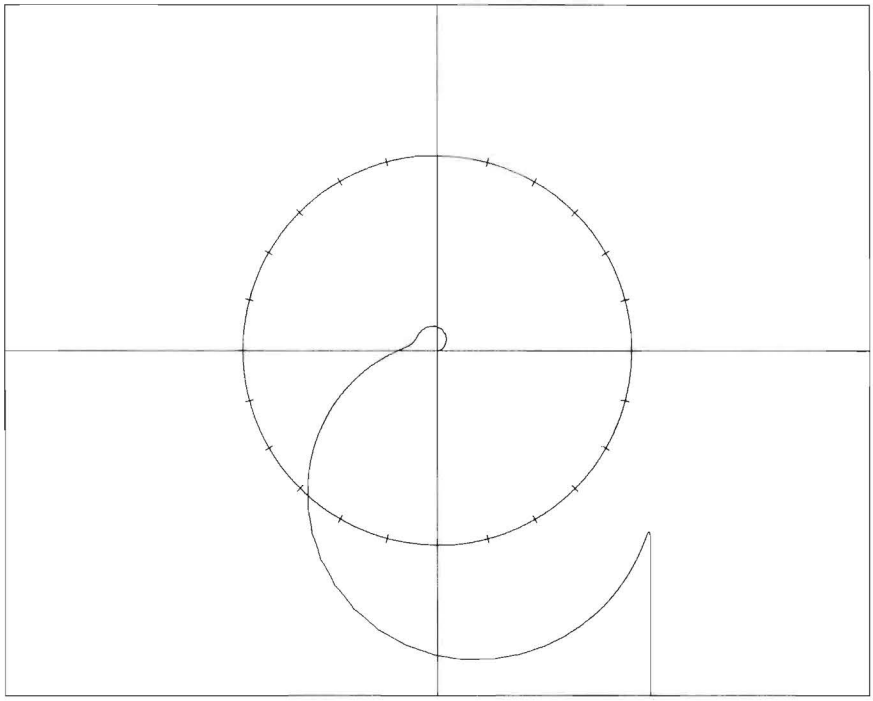

Figure 60. Nyquist Plot for DLG System with Configuration III Sampler Operating at 20 Samples/Second.

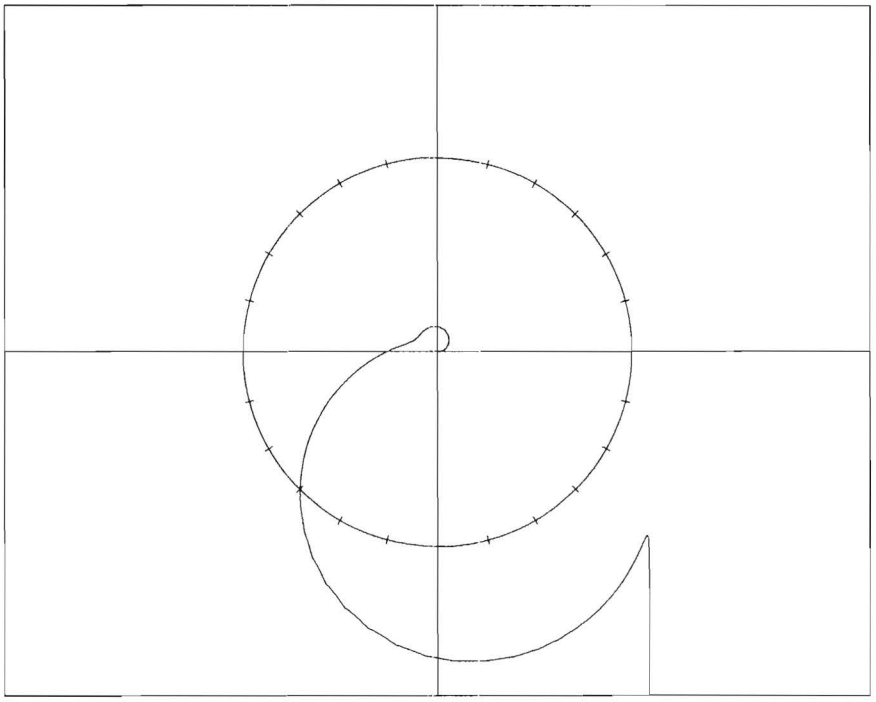

Figure 61. Nyquist Plot for DLG System with Configuration III Sampler Operating at 10 Samples/Second.

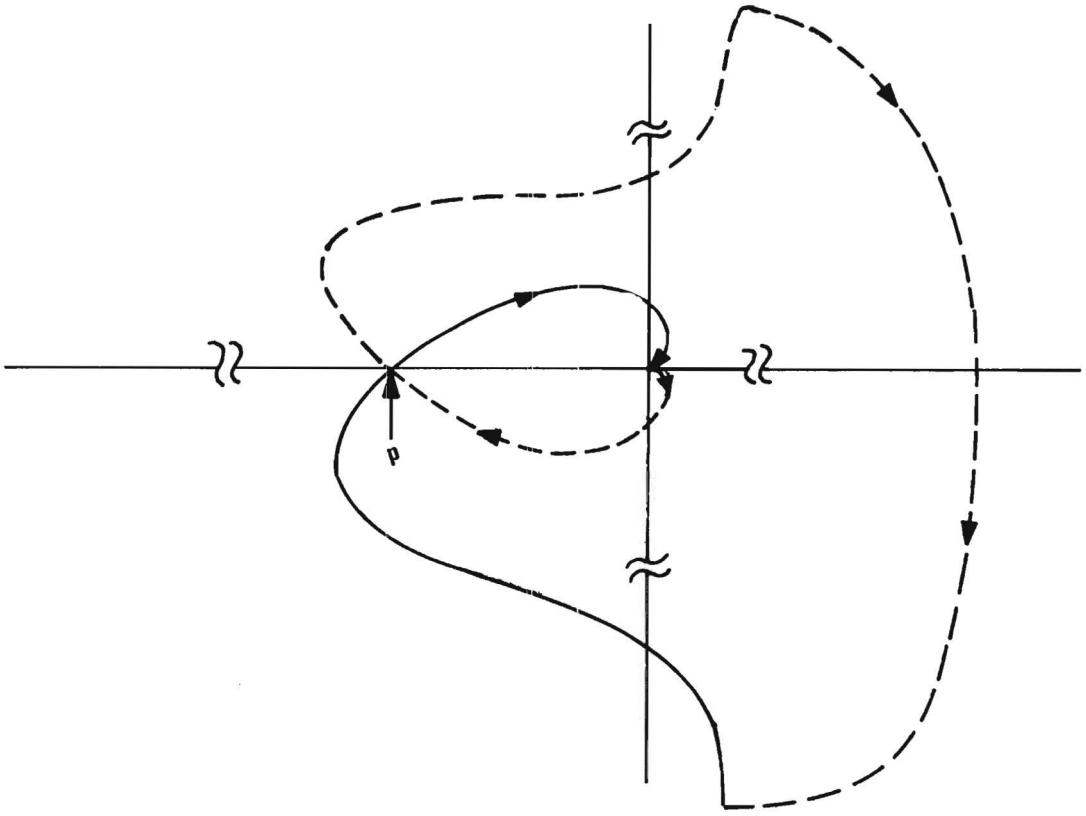

Figure 62. Nyquist Plot Closure for Configuration III Sampling.

Page intentionally left blank

VI. CONCLUSIONS

An investigation of techniques suitable for guidance of a small tactical missile for use against surface targets has been made. Most of the effort was devoted to analysis and study of Dynamic Lead Guidance (DLG). Theoretical areas investigated included (1) determination of satisfactory DLG parameters, (2) analysis of the required sensor characteristics, and (3) DLG performance with sampled (pulsed) data. A digital simulation was used to verify the theoretical results and to investigate other aspects of DLG. Performance characteristics studied with simulated flights included parameter variations, sensor characteristics (linearity, field-of-view, limiting, and bore-sight error), sampled data input, gyroscope gain, cross-feed between guidance channels, and gravity effects. Both constant-velocity and maneuvering targets were simulated.

Based on the investigations carried out the following conclusions are drawn:

(1) DLG is a satisfactory guidance technique for application to small tactical missiles for use against ground targets provided a satisfactory sensor can be developed.

(2) For a 1000 ft/sec missile operating against 100 ft/sec targets, a sensor with a field-of-view of approximately $\pm 10^{\circ}$ in each plane is required. The sensor output must be sensitive to the angle of the line-of-sight over the entire field of view. Any tendency towards saturation must not drop the equivalent gain below about 0.85.

(3) The system is not extremely sensitive to system gain (k_2), timelag constant (τ_L), or gyroscope gain (k_4). Simulation runs indicated satisfactory performance for $3 \leq \tau_L \leq 5$, $9 \leq k_2 \leq 12$, and $0.9 \leq k_4 \leq 1.1$.

(4) DLG performs satisfactorily for sampled data, but the sample-and-hold device must be located so that the gyro output as well as the LOS angle is included in the sampling process.

(5) There is no need to terminate guidance prior to intercept. DLG remains stable until the range closes to a "can't miss" value. Not having to terminate guidance is a distinct advantage since range information is not available in a semi-active system.

It is recommended that efforts be undertaken to develop a satisfactory strapdown sensor. The material presented in Section IV of this report should provide a basis for developing specifications for a sensor.

VII. REFERENCES

1. R. D. Wetherington, and J. L. Birchfield, "Techniques for Generating Guidance Signals from Body-Fixed Sensors," Georgia Tech Engineering Experiment Station, Interim Technical Report No. 1 on Project A-1164, Contract DAAH01-69-C-1390, dated 10 March 1970.

2. B. E. Thaler, and M. P. Pastel, Analysis and Design of Nonlinear Feedback Control Systems, McGraw-Hill, 1962.

3. J. C. Hsu, and A. U. Meyer, Modern Control Principles and Applications, McGraw-Hill, 1968.

4. J. DelToro, and S. R. Parker, Principles of Control Systems Engineering, McGraw-Hill, 1960.

5. B. C. Kuo, Automatic Control Systems, Prentice-Hall, 1962.

6. B. C. Kuo, Analysis and Synthesis of Sampled-Data Control Systems, Prentice Hall, 1963.

7. J. T. Tou, Digital and Sampled-Data Control Systems, McGraw-Hill, 1959.

8. E. I. Jury, Sampled-Data Control Systems, John Wiley & Sons, 1958.

Page intentionally left blank

VIII. APPENDICES

APPENDIX A

REVIEW OF GUIDANCE TECHNIQUES

In the search for guidance techniques which are well suited for use with strapped-down sensors in tactical missiles, a review of existing guidance techniques was made. Although the majority of the effort described by this report is concerned with a particular guidance scheme, Dynamic Lead Guidance (DLG), others such as the well known proportional and pursuit guidance techniques and some "optimal" schemes were given brief consideration. While several interesting papers on proportional navigation (or guidance) and on optimal guidance were found, nothing applying specifically to strap-down sensors was available. The following is a summary of the literature search for guidance techniques applicable to small tactical missiles.

This section contains a list of those journals in which pertinent papers were located; comments on each of those papers; and a detailed description of the papers most applicable to the problem of strap-down guidance for small homing missiles (anti-tank, etc.). The search was made using the Engineering Index (1965 - Mar. '70) and the Applied Science and Technology Index (1964 - May '70), using such key words as Proportional Navigation, Homing Guidance, Strapdown Systems, Tactical Missiles, Optimal Guidance, and Navigation. In some cases, references from primary papers (i.e., those papers located through the indices) are included in the listing.

A. Useful Periodicals

Articles from the following periodicals were reviewed.

Aeronautical Journal
AIAA Journal
AIAA-Simulation for Aerospace Flight Conference
Applied Optics
Astronautica Acta
Control Engineering
Electronics
Hydraulics and Pneumatics
Institute of Telecommunication Engineers Journal
Israel J. Technology
JACC

J. Aircraft
J. of the Astronautical Sciences
J. of Spacecraft & Rockets
Machine Design
Mech. Eng.
SIAM J. on Control
Space/Aeronautics
Sperry Engineering Review
Symp. on Ballistic Missile & Space Technology
Trans. on Aerospace & Electronic Systems (IEEE)

B. Results of the Open Literature Search

Of the thirty papers reviewed, the nine most applicable ones were copied for further study. This group includes one paper on the general problem of guiding tactical missiles, four papers on the development and comparison of guidance or navigation techniques commonly proposed for homing missiles, three papers on optimal guidance schemes (both deterministic and stochastic approaches), and one paper on miss-distance prediction.

Seventeen of the papers were found to be either not applicable to the tactical missile project (e.g., perturbation guidance for space rockets using large on-board computers); concerned only with the hardware of a specific system; limited to strictly inertial guidance (no homing sensor, etc.); or simply analysis of the kinematics of missile flight. Four of the papers were of the "news release" variety and were deemed useless.

1. Most Applicable Papers

"Guiding Tactical Missiles," by Guy Desloovere, Space/Aeronautics, Nov. '65, Vol. 44

The paper is an easy-to-read description of the elements of tactical missile systems with consideration of passive, semi-active, and active guidance; single and multiple sensors; homing guidance; and doppler radar. Pursuit and proportional navigation (guidance) methods are discussed with proportional navigation described in some detail as regards the effective navigation ratio (gain), noise sensitivity, and target discrimination.

"Steering a Tactical Air-to-Ground Missile," by Michael Davis in General Precision Aerospace TNB, Vol. 8, No. 1, 1965.

Definitions are given for guidance, navigation, steering, and flight control for missiles. In particular, the steering function is described as an equation, or law, that defines what attitude commands should be given to the flight control system to orient the velocity vector as commanded by the guidance law.

For an assumed stationary target (e.g., enemy radar sites), constant missile speed, and zero angle of attack (ideal flight control system), the paper investigates the following steering laws: Line-of-Sight (LOS), Deviated Line-of-Sight, Line-of-Sight Rate (proportional navigation), and Reference Line. Simplified equations of motion (planar) and lateral acceleration expressions are developed for each steering law.

LOS steering is shown to call for an infinite lateral acceleration immediately prior to impact; this results in a (small) miss-distance since a real missile cannot have infinite acceleration. Other than this final turn, the maximum acceleration is at the beginning of the trajectory. Deviated LOS steering is like LOS steering except that the missile is steered to maintain a constant bias angle between the velocity vector and the LOS in an attempt to compensate for moving targets. It also calls for infinite lateral acceleration near impact.

LOS Rate steering is probably the most frequently used steering law for homing type missiles. (It is also called Proportional Navigation.) For this type of steering, the rate of turn of the missile is made proportional to the rate of turn of the LOS (inertial); the constant of proportionality is called the navigation constant. Infinite acceleration is not commanded for this steering law; in fact, "LOS Rate steering has been proven to cause the minimum accelerations for use against a moving target" (probably for a constant velocity target and constant speed missile).

Reference Line steering corresponds to simply flying a straight line from the launch sight to the stationary target and uses deviation (and its derivative) from the line as feedback signals. One "reasonable" numerical case has shown Reference Line steering to result in higher initial lateral accelerations than LOS steering.

It is pointed out that the type steering law best suited for a given missile will depend upon the available hardware. For instance, LOS steering can use a fixed (bore-sight) tracker but LOS Rate steering requires either a stable platform tracker mount or a complicated computation of strap-down navigation on board the missile.

For pitch axis steering, a ballistic profile is suggested in order to maximize range capability. In choosing a steering law, one must also investigate the system response to noise, either natural or enemy counter-measures. Modern filtering techniques such as Kalman filtering and non-linear filtering can be used to reduce the miss distances when sufficient on-board computer capability is present.

"Homing Guidance by Proportional Navigation," by E. G. Solov in General Precision Aerospace TNB, Vol. 8, No. 1, 1965.

This paper derives a vector math model for the motion of a missile with proportional navigation and gives a stability analysis for a thruster (lateral acceleration controller) modeled with threshold and saturation effects.

The proportional navigation law is described by an acceleration command proportional to the cross product of the line-of-sight vector (body coordinates) and the missile angular velocity vector. An expression for the translational acceleration of the missile is derived and set equal to the commanded acceleration from the proportional navigation law. An assumption of roll-control decouples the equations of motion into two identical first-order differential equations.

It is shown that the navigation constant must be greater than two for stability even for ideal components. Realistic models for missile components are then inserted, including a nonlinear actuator model (thruster), and the stability analysis is continued using Routh's criteria and a root-locus plot. Expressions for the minimum stable values for the navigation constant in the presence of "realistic" component models are derived. It is noted that larger values of this gain (the navigation constant) make the system more sensitive to noise.

"Missile Guidance by Three-Dimensional Proportional Navigation," by F. P. Adler in Journal of Applied Physics, Vol. 27, No. 5, May '56.

This appears to be the first paper in the open literature which extends proportional navigation to three dimensions. Earlier papers treated only coplanar motion of the missile and target. As with many "first" papers, the development is not as clear as later papers on the subject; the resultant proportional navigation equation is the same as in Solov's paper discussed above.

The paper discusses the planar proportional navigation formulation key features and uses these features to develop three-dimensional proportional navigation. The resulting equations of motion are then linearized. Simulation has shown the linearized model to give results very close to those of the full nonlinear equations. Adler also shows that the navigation constant must be greater than two for bounded acceleration throughout the flight. An expression for the missile acceleration is given.

"Fundamentals of Proportional Navigation," by S. A. Murtaugh and H. E. Criel in IEEE Spectrum, Vol. 3, pt. 2, Dec. '66.

This paper defines the characteristics (LOS rotational rate, required velocity increment, initial acceleration, and effects of

gyro drift) of proportional navigation and several of its variations; application is made to a satellite interceptor. Simplified equations with closed-form solutions are used and most results are presented graphically.

"Optimum Intercept Laws for Accelerating Targets," by V. Garber, AIAA Journal, Vol. 6, No. 11, Nov. '68, pp 2196-8.

This paper uses functional optimization techniques to extend proportional navigation for better performance against an accelerating (maneuvering) target. Provisions are also made for offsetting the effects of drag and thrust. Unfortunately, the resulting feedback guidance law requires a continuous knowledge of time-to-go until impact as well as the target acceleration (and apparently predicted acceleration).

The paper states that proportional navigation can be shown to be the optimal guidance scheme for a quadratic performance index with the system modeled as point-mass vehicles and assuming a constant velocity (vector) target. Using that same performance index but allowing an accelerating target as well as drag on the interceptor missile, the paper derives the optimal feedback control.

In order to solve the optimization problem, the author uses an extension of the well-known linear system, quadratic loss optimization result to include non-homogeneous linear systems. The theoretical development is very similar to that of R. E. Skelton in a 1970 JACC paper.* Essentially, the effect of the non-homogeneous term (driving function) is to add a time-varying term to the feedback control which would be optimal for the homogeneous system. The time-varying term is found as a solution to a linear differential equation with final-value boundary conditions.

The optimal theory developed for the non-homogeneous system is then applied to the guidance problem for an accelerating target in a straight-forward manner. The resulting missile acceleration

*"Optimal Desaturation of Momentum Exchange Control Systems," by C. D. Johnson and R. E. Skelton, pp. 683-94 in preprints of 1970 Joint Automatic Control Conference, Georgia Tech, Atlanta, Georgia.

command is always finite, as in proportional navigation. It is interesting to note that the resulting optimal acceleration command for the missile can be expressed as

$$\underline{a}_m = \left[\frac{(t_f - t)}{\frac{1}{3}(t_f - t)^3 + 1/C_1} \right] \underline{S}\ (t,\ t_f)$$

where t = current time

t_f = final time (impact)

C_1 = design coefficient, and

$\underline{S}(t,t_f)$ = predicted miss distance based upon current missile velocity (coast-on-in) and target acceleration.

This expression of control acceleration as a direct function of predicted miss distance raises the possibility of using sophisticated stochastic prediction schemes (perhaps in a ground or aircraft computer) for the calculation of $\underline{S}(t,\ t_f)$.

Implementation of either available form of this guidance scheme requires a knowledge of the target acceleration vector (predicted all the way to impact) and the time until impact. Note also that the model assumed ideal sensors and actuators. The optimal solution implementation is probably too complex for small tactical missiles, but it can serve as a standard against which the performance of any proposed guidance scheme can be evaluated.

"Optimal Terminal Guidance of an Air-to-Surface Missile," by R. W. Rishel in Journal of Spacecraft & Rockets, Vol. 5, No. 6, June '68, pp 649-54.

This paper treats the guidance problem (in a plane) of an air-to-surface missile subject to gravity and to aerodynamic forces. Of key interest is the assumption of a noisy sensor (TV) for the homing seeker and random winds during flight. The equations of motion are derived and linearized, and a quadratic

performance index is chosen, and the Separation Principle of Joseph and Tou* is applied to allow separate optimization for control and estimation of unknown states. A section reviewing Kalman filter theory is included.

The resulting optimal control/estimator system is compared with both pursuit and proportional navigation and is shown to have little improvement in miss-distance statistics. It is pointed out that the large standard deviation in down-range position "corresponds to the fact, well known to guidance engineers, that accurate range information cannot be obtained from angular measurements."

"Application of Nonlinear Filter to Short Range Missile Guidance," by L. Teng and P. L. Phipps in Journal of the Astronautical Sciences, Vol. 15, No. 3, June '68, pp 138-147.

In contrast to Rishel's paper, this paper treats a nonlinear stochastic problem; however, rather than simultaneously attacking the optimal control (guidance) and estimation problems, the paper uses a standard navigation scheme such as proportional navigation and determines the best estimator (nonlinear) for the sensor/seeker system with the chosen navigation scheme. Simulation results are included.

Equations of missile motion are derived for both maneuvering and constant velocity targets. Both LOS and LOS Rate steering are described verbally and mathematically. Nonlinear stochastic filtering in the sense of Bellman is reviewed and applied to the guided homing missile problem to develop a Simulation Model Estimator, a Computer Analysis Model, and a Realistic Model Estimator (the latter is the most efficient estimator). The schemes derived in this paper require moderate-to-complex airborn computers and are perhaps applicable only to anti-missile-missiles for this reason. Many good references are given in the paper.

---

*P. D. Joseph and J. T. Tou, "On Linear Control Theory," Trans. AIEE, Part III, Vol. 80, No. 18, 1961.

"Final-Value Homing Missile Guidance," by M. J. Abzug, in Journal of Spacecraft and Rockets, Vol. 4, pp 279-80, Feb. '67.

This engineering note derives an expression for the miss-distance resulting if the missile control is cut off at any point in flight. This predicted error expression is then proposed for use in a "bang-off-bang" control law which simply applies a preset magnitude (of the required polarity) lateral acceleration whenever the predicted miss distance is larger than a preset tolerance.

The planar translational equations of motion are written in state variable form and the adjoint equation is used to write the final state (for zero control) in terms of current state and time-to-go. A bang-off-bang implementation of the guidance concept is compared by simulation with proportional navigation. Alternately, the new law (when linear) may be viewed as providing a correction to proportional navigation that accounts for the finite bandwidth of the missile acceleration control loop. The authors report improved miss distance over proportional guidance but the circumstances of the comparison are not clear. The "law" requires a knowledge of time-to-go.

2. Less Applicable Papers

"The Optimization of an Optical Missile Guidance Tracker," by I. J. Spire in Applied Optics, Vol. 8, p. 1365-71, July '69.

The article is concerned wholly with the optical system optimization. The seeker head is replaced with a human who tracks a flare on the back of a DART missile. "Consideration is not given here to the propulsion aspects, the mechanical and electronic elements of the guidance loop, or the transmission of steering information to the missile."

"A Comparison of Expected Flight Times for Intercept and Pure Pursuit Missiles," by L. L. Scharf, W. P. Harthill and P. H. Moose, IEEE Transactions on Aerospace and Electronic Systems, Vol. 5, pp 672-2, July '69.

The correspondence determines statistical expectation of

time-to-target (non-maneuvering; const. velocity) for two guidance schemes: pursuit and intercept. Results show little advantage in flight time for intercept method except for very small speed advantage of the missile. The author assumed random (equally likely over some angle) direction of motion for target vehicle and analytically expressed the expected value of the resulting time-to-intercept. The paper may be useful for a similar analysis of the Dynamic Lead Guidance or Proportional Guidance concepts.

"Application of Optimization Theory to the Design of a Missile Control," by Ralph R. Duersch, JACC, June 22-25, 1965, pp 483-98.

Optimal linear feedback guidance near thrust cutoff of a large booster is determined by linearization around predetermined optional trajectory in the paper.

"Guidance Concepts for Tactical Missiles," by Orval C. Sorensen, Sperry Engineering Review, Spring '64.

The article is relative to inertial platforms as opposed to homing guidance. The entire issue of the publication is devoted to Inertial Systems (including strap-down navigation).

"An Infrared Guidance Technique," by Lt. Col. S. Mishra, Institute of Telecommunication Engineering-Journal, Vol. 10, No. 5, 1964, pp 189-96.

This paper describes the principle of an IR guidance technique that avoids any focusing device. No equations are given; only bang-bang control is used; the guidance is within a cone from the target.

"Synthesis of a Guidance System for a Short-Range Infantry Missile," by John F. Muller, Journal of Spacecraft and Rockets, Vol. 6, No. 1, Jan. '69, p. 314-17.

This paper treats the anti-tank type missile but uses inertial guidance (apparently) with line of sight flight path. It does not appear to be a homing missile design.

"On Non-Zero Miss Distance," by A. G. Rawling, Journal of Spacecraft and Rockets, Vol. 6, No. 1, Jan '69, pp 81-83.

This paper is independent of the guidance scheme used. It treats only the miss distance equation after cessation of guidance when the missile is near the target and includes results which are usable with any navigation scheme.

"Analysis and Design of Missile and Aircraft Control Systems," by K. W. Han and G. J. Thaler, Journal of Aircraft, Vol. 4, No. 2, Mar-Apr '67.

The paper is an extension of the root-locus technique to handle more than one variable (parameter).

"Optimal Terminal Maneuver and Evasion Strategy," by Y. C. Ho, J. SIAM Control, Vol. 4, No. 3, 1966 (Aug), pp 421-8.

This is a treatise on stochastic differential games which is applicable only to much more sophisticated systems with missile and target using radar to observe the other and attempting to use computers to "out-guess" the opponent.

"A Look into Strap-Down Guidance Design," by D. D. Otten, Control Engineering, Oct-Nov '66, Vol. 13, pt. 2

This paper is concerned with navigation rather than guidance and the application is to boosters.

"The Maximization of the Range of a High-Lift, Low-Thrust Missile in Horizontal Flight," by Robert J. Stern, Astronautica Acta, Vol. 14, pp 119-130, 1969.

The paper looks at optional subarcs for missile intercept ignoring drag.

C. Conclusions

The literature search has yielded a wealth of information on proportional navigation and on other more theoretical guidance laws requiring various information such as range and time-to-go. The only papers located on strapdown

systems were relative to navigation for large booster rockets where the computerized function is purely navigation, separate from guidance calculations.

The guidance techniques proposed in the open literature can be categorized as (1) simple boresight schemes such as pursuit which are satisfactory for stationary targets but not for significant target motion, (2) the proportional navigation class schemes which require inertial-referenced information, and (3) complex schemes requiring range-to-go information. There is a noticeable absence of previous work with simple guidance schemes uitlizing body-fixed sensors which would be capable of reasonable performance against maneuverable ground targets such as trucks, tanks, etc.

The most promising such guidance scheme available is called Dynamic Lead Guidance (DLG). This scheme, similar in operation to the Proportional Lead Guidance scheme proposed by the Martin Co., obtains its "lead" with the use of passive circuitry.

APPENDIX B

Listing of FORTRAN program for simulating missile intercept for Dynamic Lead Guidance (DLG).

```
COMMENT INITIAL SETTING OF PARAMETERS
      PI = 3.141593
C * * * MISSILE LAUNCH PARAMETERS * * * * * * * * * * * * * * * * * * *
      XM = 0.                    - X COORDINATE, FEET
      YM = 0.                    - Y COORDINATE, FEET
      VM = 1000.0                -MISSILE VELOCITY,FT/SEC
      THET = 0.                  - LAUNCH ANGLE, RADIANS
C * * * TARGET LAUNCH PARAMETERS  * * * * * * * * * * * * * * * * * * *
      XT = 10000.                - X COORDINATE, FEET
      YT = 0.0                   - Y COORDINATE, FEET
      VT = 100.                  -TARGET VELOCITY, FT/SEC
      GAMT = PI/2. + THET        - LAUNCH ANGLE, RADIANS
      GTDEG = 0.0                - TURNING RATE, DEGREES/SEC
C * * * MISSILE PARAMETERS  * * * * * * * * * * * * * * * * * * * * * *
      AMAX = 10.                 - ACCELERATION LIMIT, G
      AKALF = 0.5                -AIRFRAME CONSTANT
      OMEGA = 10.0               - AIRFRAME NATURAL FREQ, RADIANS/SEC
      ZETAA = 0.2                - AIRFRAME DAMPING RATIO
C * * * SYSTEM PARAMETERS * * * * * * * * * * * * * * * * * * * * * * *
      TOUL = 5.0                 - TIME CONSTANT FOR F OF THETA
      OMEG1 = 1.                 - LEAD-LAG FREQ NO 1
      OMEG2 = 1.                 - LEAD-LAG FREQ NO 2
      BK2 = 12.0                 - NOMINAL SYSTEM GAIN
      BK3 = 1.
      BK4 = 1.0                  - GYRO OUTPUT MULTIPLIER
      SENSLP = 1.0               - SENSOR SLOPE
      LIMMPU = 10                - LIMIT OF MISSED PULSES
      FOV = 1.0                  - FIELD OF VIEW
      SIGLNL = .99               - SENSOR LINEARITY LIMIT
      SAMPER = .001              - SAMPLING PERIOD, SEC
      SMPLPR = 0.0               - SAMPLING PROBABILITY FACTOR
C * * * SIMULATION PARAMETERS * * * * * * * * * * * * * * * * * * * * *
      GBIAS = 0.0                - GRAVITY BIAS
      DELT = 0.001               - STEP SIZE, SEC
      TPRT = 0.1                 - PRINTOUT INTERVAL, SEC
```

```
C * * * * CALCULATED PARAMETERS AND INITIALIZATION OF VARIABLES * * * * *
      BK1 = OMEG2/OMEG1
      SIGM2 = 0.
      SIGM3 = 0.0
      SIGLIM = SENSLP*SIGLNL
      ISAM = 1
      IMISPU = 0
      ISATFG = 1
      ERRS = 0.
      SIGMS = 0.
      SAMTIM = SAMPER
      GDTMAX = (32.2*AMAX)/VM
      ERRSOL = 0.
      GMTDT = GTDEG*PI/180.0
      GMTDGR = GAMT*180.0/PI
      TLIM = 0.0
      T = 0.0
      LINE = 0
      GAMM = THET
      FTHET = THET
      COMAND = 0.
      GAMDTC = 0.
      GAMDDT = 0.0
      GAMDT = 0.0
      TLIM = TLIM - DELT/2.0
      AKA1 = OMEGA**2
      AKA2 = 2.0*ZETAA*OMEGA
      RSQ = 1.0E20
      IFCOLL = 1
      IRNPU = 0
  730 FORMAT(36H0 TARGET OUTSIDE FIELD OF VIEW AT T=,F7.3)
  731 FORMAT(28H  SENSOR ENTERING SATURATION)
  732 FORMAT(27H  SENSOR LEAVING SATURATION)
  733 FORMAT(22H  PULSE MISSED AT T = ,F7.3)
C * * * * * * * * * * * * * * * * * * * * * * * * * * * * * * * * * * * *
```

```
COMMENT BEGIN MAIN LOOP
   10 RLAST = RSQ
C * * * * * * * * * * * * * * * * * * * * * * * * * * * * * * * * * * * *
COMMENT GEOMETRY CALCULATIONS
      DELY = YT - YM
      DELX = XT - XM
      IF (DELX) 21,22,23
   21 SIGR = PI + ATAN(DELY/DELX)
      GO TO 24
   22 SIGR = PI/2.0
      IF (DELY .LT. 0.0) SIGR = -SIGR
      GO TO 24
   23 SIGR = ATAN(DELY/DELX)
   24 CONTINUE
      SIGM = SIGR - THET
      IF (T .LT. TLIM) GO TO 120
C * * * * * * * * * * * * * * * * * * * * * * * * * * * * * * * * * * * *
COMMENT MAIN PRINT ROUTINE
      ALOSDG = (180./PI)*SIGM
      L1 = MOD(LINE,40)
      L2 = MOD(L1,5)
      IF (L1) 26,25,26
   25 CONTINUE
      WRITE(6,700) VM,VT,SENSLP,OMEG1,BK1,OMEGA,GMTDGR,SIGMNL,OMEG2,
     1       BK2,ZETAA,GTDEG,FOV,TOUL,BK3,AKALF,SMPLPR,SAMPER,GBIAS,BK4
  700 FORMAT(8H1 VM   =,F7.1,8X,5HVT  =,F7.1,6X,8HSENSLP =,F7.3,5X,      700_0
     1       7HOMEG1 =,F6.2,7X,5HBK1 =,F7.2/8H OMEGA =,F7.1,6X,          700_1
     2       7H GAMT =,F7.1,6X,8HSIGLNL =,F7.2,5X,7HOMEG2 =,F6.2,7XY     700_2
     3       5HBK2 =,F7.2/8H ZETAA =,F7.2,6X,7HGMTDT =,F7.2,8X,          7_0_3
     4       6HFOV  =,F7.2,5X,7HTOUL  =,F6.2,7X,5HBK3 =,F7)2/8H AKALF =, 700_4
     5       F7.2,6X,7HSMPLPR=,F7.2,6X,8HSAMPER =,F7.3,5X,7HGBIAS =,     700_5
     6       F6.2,7X,5HBK4 =,F7.2)                                       700_6
      WRITE(6,704)
  704 FORMAT(132H0  T      GCL-GAM     T COLL     THETA     GAMDTC     GAMDT
     1     GAMM        XM        XT        YM        YT        A     EMSDST   E
     2STTIM LOS-D)
```

```
   26 IF (L2 .EQ. 0) WRITE(6,706)
  706 FORMAT(1H )
      LINE = LINE + 1
C*****************************************************************
COMMENT   ESTIMATE MISS DISTANCE AND TIME TO GO BASED UPON FROZEN VELOCITIES.
      XTMXM = XT - XM
      YTMYM = YT - YM
      DXTMXM = VT*COS(GAMT) - VM*COS(GAMM)
      DYTMYM = VT*SIN(GAMT) - VM*SIN(GAMM)
      TMTOGO = (XTMXM*DXTMXM + YTMYM*DYTMYM)/(DXTMXM*DXTMXM + DYTMYM*DYT
     1MYM) * (-1.)
      ESTTIM = TMTOGO + T
      EMSDST = SQRT((XTMXM + DXTMXM*TMTOGO)**2. + (YTMYM + DYTMYM*TMTOGO
     1)**2.)
COMMENT        END ESTIMATES
C   * * * * * * * * * * * * * * * * * * * * * * * * * * * * * * * * * *
COMMENT    CALCULATION OF COLLISION PATH STEERING ANGLE
      IF(IFCOLL.NE.1) GO TO 115
      CB = XM - XT
      CC= YT - YM
      IF((ABS(CB)).LE.1.0) GO TO 105
      IF((ABS(CC)).LE.1.0) GO TO 110
      CA = (CB*SIN(GAMT) + CC*COS(GAMT))*VT/VM
      TEMP1 = CB * CB + CC * CC
      TEMP2 = CA * CB / TEMP1
      TEMP3 = SQRT(TEMP2**2 + (CC *CC - CA * CA)/TEMP1)
      SINGAM = TEMP2 + TEMP3
      IF((CC/(VT*SIN(GAMT)-VM*SINGAM)) . LE. 0.) GO TO 10
      SINGAM = TEMP2 - TEMP3
  100 GAMCOL = ASIN(SINGAM)
      TCOLLC = -1*(CC/(VT*SIN(GAMT)-VM*SINGAM))
      GO TO 115
  105 GAMCOL = ACOS(VT*COS(GAMT)/VM)*CC/ABS(CC)
      TCOLLC = -CC/(VT*SIN(GAMT)-VM*SIN(GAMCOL))
      GO TO 115
```

```
  110 GAMCOL = ASIN(VT*SIN(GAMT)/VM)
      TCOLLC = CB/(VT*COS(GAMT)-VM*COS(GAMCOL))
COMMENT     END OF COLLISION GUIDANCE CALCULATION
  115 CONTINUE
      TCOLLC = T + TCOLLC
      ACCEL = VM*GAMDT/32.2
      GAMDIF = GAMCOL - GAMM
      WRITE(6,710) T,GAMDIF,TCOLLC,THET,GAMDTC,GAMDT,GAMM,XM,XT,YM,YT,
     1ACCEL,EMSDST,ESTTIM,ALOSDG
  710 FORMAT(1H ,F5.2,2X,F8.4,3X,F7.3,4E10.3,4(2X,F7.1),F6.1,2X,F7.1,2X,
     1F7.3,1X,F5.1)
      IF (IRNPU .GT. 0) WRITE(6,712) IRNPU
  712 FORMAT(1H+,5X,1H*,I1)
      IRNPU = 0
      TLIM = TLIM + TPRT
  120 CONTINUE
C * * * * * * * * * * * * * * * * * * * * * * * * * * * * * * * * * * * *
COMMENT SIMULATION OF MISSILE CONTROL SYSTEM
C*****SENSOR SIMULATOR**************
  205 SIGMIN = SIGM
      XSIG = ABS(SIGMIN)
      IF(XSIG.LT.SIGLNL) GO TO 225
      IF(ISATFG.NE.1) GO TO 210
      ISATFG = 0
      WRITE(6,731)
  210 CONTINUE
      IF(XSIG.LT.FOV) GO TO 215
C****MISSED PULSES INCREMENT MISSED PULSE INDEX AND HOLD OR ZERO SIGM**
      WRITE(6,730)T
      IMISPU = IMISPU + 1
      IF(IMISPU.LT.LIMMPU) GO TO 232
      SIGM0 = 0.
C*******GO TO ACQUISITION MODE
      WRITE(6,710) T,GAMDIF,TCOLLC,THET,GAMDTC,GAMDT,GAMM,XM,XT,YM,YT,
     1ACCEL,EMSDST,ESTTIM,ALOSDG
      GO TO 990
```

```
  215 IMISPU = 0
      IF(SIGMIN.GT.0.) GO TO 220
      SIGM1 = -SIGLIM
      GO TO 230
  220 SIGM1 = SIGLIM
      GO TO 230
  225 SIGM1 = SIGMIN*SENSLP
      IF(ISATFG.NE.0) GO TO 230
      ISATFG = 1
      WRITE(6,732)
  230 CONTINUE
      SIGM0 = SIGM1 + SIGM2 + SIGM3
  232 CONTINUE
      THETPR = BK4*THET                                          - TEST POSITION
C*************END OF SENSOR SIMULATOR$   OUTPUT IS SIGM0**********
      SIGMS = SIGM0
      SIGMSS =SIGMS
      THETP2 = BK4*THET
      SIGRPR = THETPR + SIGMS
      FTHET = FTHET + DELT*(BK3*THETP2 - FTHET)/TOUL
      ERR = SIGRPR - FTHET
      IF(SAMTIM.LT.SAMPER) GO TO 305
      ERRS = ERR
  235 SAMTIM = DELT/2.0
      ISAM = ISAM + 1
  305 CONTINUE
      SAMTIM = SAMTIM + DELT
      COMAND = COMAND + BK1*(ERRS-ERRSOL)+DELT*(BK1*OMEG1*ERRSOL-OMEG2*C
     1OMAND)
      GAMDTC = BK2 * COMAND
      ERRSOL = ERRS
      GAMDDT = GAMDDT*(1.0 - AKA2*DELT) + AKA1*(GAMDTC - GAMDT)*DELT
      GAMDT = GAMDT + GAMDDT*DELT
      XGAM = ABS(GAMDT)
      IF (XGAM .LE. GDTMAX) GO TO 320
      GAMDT = (XGAM/GAMDT)*GDTMAX
```

```
  320 CONTINUE
      GAMM = GAMM + GAMDT*DELT
COMMENT       GRAVITY EFFECT
      VX = VM*COS(GAMM)
      VY = VM*SIN(GAMM) - 32.2*GBIAS*DELT
      GAMM = ATAN(VY/VX)
      THET = GAMM + AKALF*GAMDT
C * * * * * * * * * * * * * * * * * * * * * * * * * * * * * * * * * * * *
COMMENT INCREMENT VARIABLES
      T = T + DELT
      XM = XM + VM*COS(GAMM)*DELT
      YM = YM + VM*SIN(GAMM)*DELT
      XT = XT + VT*COS(GAMT)*DELT
      YT = YT + VT*SIN(GAMT)*DELT
      GAMT = GAMT + GMTDT * DELT
      RSQ = (XT - XM)**2 + (YT - YM)**2
      IF (RSQ - RLAST) 10,400,400
  400 CONTINUE
C * * * * * * * * * * * * * * * * * * * * * * * * * * * * * * * * * * * *
COMMENT COMPUTE MISS DISTANCE AND STOP
      TI = (XT - XM) / (VM*COS(GAMM) - VT*COS(GAMT))
      YIM = YM + VM*SIN(GAMM)*TI
      YIT = YT + VT*SIN(GAMT)*TI
      AMSDST = YIM - YIT
      XM = XM + VM*COS(GAMM)*TI
      YM = YIM
      WRITE(6,720) T,XM,YM,AMSDST
  720 FORMAT(14H0INTERCEPT AT ,F6.3,11H SEC. XM = ,F8.1,7H, YM = ,F8.1,
     118H, MISS DISTANCE = ,F7.3)
  990 CONTINUE
      STOP
      END
```

APPENDIX C

Listing of subroutines for plotting Bode and Nyquist plots on CALCOMP plotter.

```
      DIMENSION TT(3) /0.05,0.0333,0.1 /
         DIMENSION IBUF(10000)
      COMPLEX W,Z,AR(210),ONE,Z1,Z5,Z6,Z4
         CALL PLOTS(IBUF(1),10000,2)
COMMENT    DLG SYSTEM   CASE 1 VOR =.25                SAMPLED DATA ANALYSIS
      C1 = -.050846
      C2 = -.436108
      C3 = -.934310
      C4 = -.259522
      C40 = 2.3434
      C5 = .617760
      C50 = -21.5308
      C6 = .576074
      C60 = 23.3875
      ONE = CMPLX(1.,0.)
      OMEG1 = 1.E-5
         L = ALOG10(OMEG1)
         OMEG1 = 10.**L
      DO 300 J = 1,3
      T = TT(J)
      Z1 = (1.,0.)
      Z4 = CMPLX(EXP(-C40*T),0.)
      Z5 = CMPLX(EXP(-C50*T),0.)
      Z6 = CMPLX(EXP(-C60*T),0.)
      DO 200 I =1,201
         X = (I - 1)*(0.05)
         W = CMPLX(0.,OMEG1*((10.0)**(X/2.5)))
      Z = (ONE + W)/(ONE - W)
      AR(I) = C1*T*T*(Z+Z1)/(2.*(Z-Z1)*(Z-Z1)) + C2*T/(Z-Z1) + C3
     1   + C4*(Z-Z1)/(Z-Z4) + C5*(Z-Z1)/(Z-Z5) + C6*(Z-Z1)/(Z-Z6)
      WRITE(6,20) Z, AR(I)
   20 FORMAT( 1H , 4E17.6 )
  200 CONTINUE
      CALL BODE(OMEG1,AR)
      CALL NYQIST(2.25,AR)
  201    CONTINUE
```

```
      WRITE(6,40)
   40 FORMAT(1H0)
  300 CONTINUE
      STOP
      END



      SUBROUTINE BODE (OMEG1,AR)
      COMPLEX AR(210)
COMMENT  ***** ESTABLISH ORIGIN
      CALL PLOT(0.,-5.2,3)
      CALL PLOT(1.,0.,-3)
      CALL PLOT(0.,-4.,3)
COMMENT  ***** DRAW PERIMETER OF GRAPH
      DO 10 I = 1,2
      CALL PLOT(0.,4.,2)
      CALL PLOT(10.,4.,2)
      CALL PLOT(10.,-4.,3)
   10 CALL PLOT(0.,-4.,2)
COMMENT  ***** DRAW VERTICAL GRID LINES
      DO 50 I = 0,3
      A = I
      DO 50 J = 2,10
      B = J
      X = 2.5*A + 2.5*ALOG10(B)
      CALL PLOT(X,-4.,3)
      CALL PLOT(X,4.,2)
   40 CALL PLOT(X,-4.,2)
   50 CONTINUE
COMMENT  ***** DRAW HORIZONTAL GRID LINES
      DO 60 I = -3,3
      A = I
      CALL PLOT(0.,A,3)
      CALL PLOT(10.,A,2)
   60 CALL PLOT(0.,A,2)
```

```
COMMENT  ***** LABEL HORIZONTAL LINES ON LEFT SIDE OF GRAPH
      DO 70 I = -4,4
         A = I
      IF(I.LT.0) CALL NUMBER(-.7,A-0.1,.21,10.*A,0.,-1)
      IF(I.EQ.0) CALL NUMBER(-.28,A-0.1,.21,0.,0.,-1)
      IF(I.GT.0) CALL NUMBER(-.49,A-0.1,.21,10.*A,0.,-1)
   70 CONTINUE
         CALL SYMBOL(-1.,-1.43,.21,14HMAGNITUDE (DB),90.,14)
COMMENT  ***** LABEL HORIZONTAL LINES ON RIGHT SIDE OF GRAPH
         CALL NUMBER(10.30,3.9,.21,0.,0.,-1)
         CALL NUMBER(10.30,1.9,.21,-90.,0.,-1)
         CALL NUMBER(10.30,-0.1,.21,-180.,0.,-1)
         CALL NUMBER(10.30,-2.1,.21,-270.,0.,-1)
         CALL NUMBER(10.30,-4.1,.21,-360.,0.,-1)
         CALL SYMBOL(11.5,-1.1,.21,11HPHASE (DEG),90.,11)
COMMENT  ***** LABEL VERTICAL LINES ON BOTTOM OF GRAPH
      DO 80 I = 0,4
         A = (10.**I)*OMEG1
         B = ALOG10(A)
         NDEC = -B
      IF(NDEC.LE.0) N = 1 - NDEC
      IF(NDEC.GT.0) N = 1 + NDEC
      IF(NDEC.LE.0) NDEC = -1
         CALL NUMBER(I*2.5-N*0.125,-4.37,.21,A,0.,NDEC)
   80    CONTINUE
         CALL SYMBOL(2.42,-4.88,.21,23HFREQUENCY (RADIANS/VEC),0.,23)
         J = 3
COMMENT  ***** PLOT GAIN
      DO 100 I = 1,201
         X = .05*(I-1)
         Y = 2.*ALOG10(CABS(AR(I)))
      IF (Y.GT.4.) Y = 4.
      IF(Y.LT.-4.) Y = -4.
         CALL PLOT(X,Y,J)
  100    J = 2
         J = 3
```

```
COMMENT  ***** PLOT PHASE
      DO 110 I = 1,201
         X = .05*(I-1)
COMMENT     APPROXIMATE FOR REAL( ) MAGNITUDE BELOW 1.E-30
      RR = REAL(AR(I))
      IF (ABS(RR).LT.1.E-30) RR = 1.E-30
      Y = 1.27324*ATAN2(AIMAG(AR(I)),RR) + 4.0
      IF (Y.GT.4.) Y = Y - 8.0
         CALL PLOT (X,Y,J)
  110    J = 2
         CALL SYMBOL(X+0.1, Y, 0.14, 1HP, 0., 1 )
         CALL PLOT(13.,-6.,3)
         CALL PLOT(13.,-6.,999)
         RETURN
      END
```



```
      SUBROUTINE NYQIST(R,AR)
      COMPLEX AR(210)
      PI = 3.1415926
      CALL PLOT(0.,-5.2,3)
      CALL PLOT(1.,0.,-3)
      CALL PLOT(0.,-4.,3)
      DO 10 I = 1,2
      CALL PLOT(0.,4.,2)
      CALL PLOT(10.,4.,2)
      CALL PLOT(10.,-4.,2)
   10 CALL PLOT(0.,-4.,2)
      CALL PLOT(5.,0.,-3)
      CALL PLOT(-5.,0.,3)
      CALL PLOT(5.,0.,2)
      CALL PLOT(0.,-4.,3)
      CALL PLOT(0.,4.,2)
      CALL PLOT(R,0.,3)
```

```
      THET = 0.
      DELTH = PI/180.
  100 THET = THET + DELTH
      X = R*COS(THET)
      Y = R*SIN(THET)
      CALL PLOT(X,Y,2)
      IF(THET .LT. 2.*PI) GO TO 100
      DELTH = PI/12.
      THET = 0.
  101 THET = THET + DELTH
      X = (R-.05)*COS(THET)
      Y = (R-.05)*SIN(THET)
      CALL PLOT(X,Y,3)
      X = (R+.05)*COS(THET)
      Y = (R+.05)*SIN(THET)
      CALL PLOT(X,Y,2)
      IF(THET.LT.2.*PI) GO TO 101
      J = 3
      DO 150 I = 1,201
      X = R*REAL(AR(I))
      Y = R*AIMAG(AR(I))
      IF(ABS(X) .GT. 5.) X = SIGN(5.,X)
      IF(ABS(Y).GT.4.) Y = SIGN(4.,Y)
      CALL PLOT(X,Y,J)
  150 J = 2
      CALL SYMBOL(-1.26,-4.5,.21,12HNYQUIST PLOT,0.,12)
      CALL PLOT(7.,-6.,999)
      RETURN
      END
```

UNCLASSIFIED

Security Classification

DOCUMENT CONTROL DATA - R & D

(Security classification of title, body of abstract and indexing annotation must be entered when the overall report is classified)

1. ORIGINATING ACTIVITY *(Corporate author)*
Georgia Institute of Technology
Atlanta, Georgia

2a. REPORT SECURITY CLASSIFICATION
Unclassified

2b. GROUP

3. REPORT TITLE
Techniques for Generating Guidance Signals from Body Fixed Sensors

4. DESCRIPTIVE NOTES *(Type of report and inclusive dates)*
Final Technical Report, 10 April 1969 to 9 February 1971

5. AUTHOR(S) *(First name, middle initial, last name)*
Holland, L.D., Wetherington, R. D.

6. REPORT DATE	7a. TOTAL NO. OF PAGES	7b. NO. OF REFS
9 February 1971	128	8

8a. CONTRACT OR GRANT NO.	9a. ORIGINATOR'S REPORT NUMBER(S)
DAAH01-69-C-1390	Final Technical Report
b. PROJECT NO. 1M262301A204	Project A-1164
c.	9b. OTHER REPORT NO(S) *(Any other numbers that may be assigned this report)*
d.	

10. DISTRIBUTION STATEMENT
Distribution of this document is unlimited.

11. SUPPLEMENTARY NOTES	12. SPONSORING MILITARY ACTIVITY

13. ABSTRACT

The feasibility of using a relatively simple guidance technique and a strap-down sensor for guidance of a small tactical missile has been investigated. The principal method investigated was Dynamic Lead Guidance (DLG). Theoretical analyses were carried out to determine workable system parameters, to determine the required sensor characteristics, and to investigate the performance of DLG for sampled data input. Simulation runs were used to examine the dependence of system performance on the sensor characteristics, sampled data operation, cross-feed between channels, gyro gain, and gravity bias. Both constant velocity and maneuvering targets were simulated.

Dynamic Lead Guidance was found to be a practical technique provided a strap-down sensor with the proper characteristics can be developed.

14 KEY WORDS	LINK A		LINK B		LINK C	
	ROLE	WT	ROLE	WT	ROLE	WT
Intercept						
Missile Guidance						
Dynamic Lead Guidance						
Simulation						
Strapdown Seekers						
Body-Fixed Sensors						